POPULATION INVERSION IN HOLLOW CATHODE, PULSED AND POSITIVE COLUMN, DISCHARGES.

by

Colin Sidney Willett, B.Sc*, Grad. Inst. P.

A thesis submitted for the degree of
Doctor of Philosophy of the University of London

Department of Physics,
Royal Holloway College,
Englefield Green,
Surrey.

Department of Physics,
University of York,
Heslington,
York.

December, 1966.

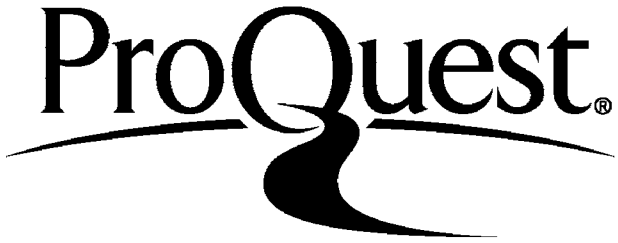

Abstract

Firstly, a survey is given of excitation processes occurring in gas discharges, together with an analysis of selective excitation processes in gaseous optical masers.

Hollow cathode discharges have been investigated as excitation media for gas lasers.

Evidence is given for the establishment of a relationship between the 632.8nm helium-neon laser discharge and transition 'weak to strong' discharges. An optimum electron temperature for oscillation on the 632.8nm line is indicated.

In a pulsed helium-iodine discharge, oscillation is reported on four new laser transitions, one an intercombination transition. Simultaneous oscillation for the first time is reported on hyperfine components of the ionised iodine lines at 703.3, 658.5, 612.7, 606.9, 576.0 and 567.8nm. Hyperfine intervals of the $6p'\ ^3D_1$ and $6s'\ ^3D_1$ levels have been established, giving agreement between calculated and observed hyperfine components of lines at 658.5, 606.9 and 576.0nm. These levels are shown to be strongly perturbed.

An anomalous behaviour is reported on hyperfine oscillations on the 658.5nm line, which can be attributed to non-equilibrium in the population of hyperfine sublevels of the $6s'\ ^3D_1$ level, due to pressure/current changes.

Results support the proposal that charge transfer is the selective excitation mechanism in the helium-iodine laser.

Contents

Note regarding sections, diagrams, references etc.

Sections. Each chapter is divided into sections and sub-sections referred to thus:- 2.2, 3.3.1 etc. without the words chapter or section etc.

Equations. These are numbered serially within each chapter and are quoted in parenthesis thus (2.1), (4.16) without the word chapter.

Diagrams and Tables. These are collected at the ends of the chapters, (apart from Fig. 3.3), and referred to as Fig. 1.2, 4.3, Table 6.1 etc.

References. These are numbered serially in each chapter, are collected at the end of the thesis and tabulated under each chapter.

Nomenclature. The following summarises the notation used throughout the text where an explanation is not given.

General.

α,	gain coefficient (cm^{-1})
A_{21},	Einstein A coefficient, transition 2 $\longrightarrow$ 1
D,	diameter of discharge tube
$\triangle$ E,	energy discrepancy in electron volts
e,	electronic charge
eV,	electron volt
E,	electric field strength
f,	frequency of oscillation
g_1, g_2,	statistical weights levels 1 and 2
g_o,	fractional gain $(distance)^{-1}$ at line centre
G,	carrier gas atom
h,	Planck constant

K,	change in propogation vector of incident electron
k,	Boltzmann constant
K.E,	kinetic energy
λ_c,	atom mean free path
λ_e,	electron mean free path
λ_o,	wavelength at line centre
Λ,	diffusion length of container.
m,	mass of electron
M,	mass of atom
n,	rate of excitation of level
N_e,	electron concentration
N_1, N_2,	atom density levels 1 and 2
ν,	frequency of transition
p,	gas pressure
r_c,	critical radius, (Bates and Damgaard) at which potential is within 1 per cent of asymptotic form.
R,	radius of discharge tube
R_i, R_f,	initial and final state wave functions
T,	absolute temperature
T_e,	average electron temperature
τ,	radiative lifetime.
v,	velocity
V,	potential in volts
σ,	standard deviation
δ,	difference in phase from maximum intensity

Spectroscopic, and collisional notation.

Electron, e

Neutral atom, O; excited atom, O'; metastable atom, O^m.

Ion, 1; excited ion, $1'$.

Photon, ϕ

(Example of collision reaction, (ref. 2(11)), $10/01'/01\phi$, indicating spark line enhancement.)

He^*, Ne^*, metastable helium and neon atom respectively.

H', excited helium atom.

Neutral line, — I; ionised line, — II.

Wavelengths given in nanometres (nm) and microns without the prefix λ .

CHAPTER 1

Introduction

This thesis covers work carried out in the period 1963 to 1967, and includes part of one of the most fertile, and probably the most rapidly moving period in Physics, which followed the demonstration of optical maser action in ruby by Maiman (1) in 1960. In the wake of this demonstration has followed the observation of harmonic generation, stimulated Raman emission, and non-linear effects produced by the extremely large intensity of this optically pumped solid state optical maser.

With less spectacular results than those shown by the ruby laser, the gaseous optical maser was developed in 1961 by Javan, Bennett and Herriott (2). In lieu of the megawatt power capabilities of their forerunner, the gaseous optical maser possesses virtues of spectral purity, beam directionality and spatial coherence enormously superior to those of the solid state laser. At present, continuous oscillation has been achieved in gas lasers in neutral, singly and doubly ionised species, on over 100 transitions ranging from the near ultra-violet into the middle infra-red and beyond. As well as continuous operation, oscillation on over 700 transitions has been observed under transient or pulsed conditions at peak powers of up to 200kW.

Although much of the work on lasers has been technological, the borderline between technology and pure physics has been such that an increased understanding of atomic physics has followed each technological advance. Perhaps more important, one has been shown glimpses

of what one does not know, in an area where the physicist, chemist, electrical engineer and spectroscopist can meet, converse, and all contribute.

Because of 1) the rapidity with which advances have been made in this newly risen field of Optical Physics, and 2) the competitiveness of the work, publications have often been incomplete or fragmentary. This has necessitated the rapid assimilation of new ideas and techniques, and has stimulated throughout the search for clarifying links with other, and earlier work.

Up to now, work in this new area has led to striking advances. A consolidation period would appear now to be required, in which a better understanding is sought of the processes which one so successfully manipulates. With the sophisticated experimental techniques now available, it would seem an appropriate time to repeat a number of experiments, conducted - with limited techniques - during the 1930 to 1950 period in the background area of Optical Physics.

1.1 The problems dealt with in this work.

The work covered in this thesis can be divided into four main sections.

In the first section, Chapters 2 - 4, following the general considerations and oscillation requirements of Chapter 1, effort has been directed towards analysing a number of gaseous optical masers and classifying the atomic processes that occur in them. It is only at this point that the major selective excitation processes are becoming discernable.

In the second section, covered in Chapter 5, accounts are given of the experiments carried out on hollow cathode discharges during the first part of the project. At the commencment of the work this type of discharge had not been used as an optical maser medium, and it was considered that its use might yield information on the importance of resonant energy transfer and molecular processes in achieving population inversion.

Throughout the development of gaseous optical masers and in the literature reports of 'enhancement' in inert gas-vapour discharges (see Chapter 2), the exact part played by helium is not clear. In this project, this led to,

(i) a study of certain aspects of the helium-neon laser, (Chapter 6), and

(ii) experiments being carried out on a helium-iodine system operating under pulsed conditions (Chapter 7).

1.2 General Consideration

Except in some cases where large optical gains are realised, optical masers have generally been used as oscillators and not amplifiers. Basically a maser oscillator differs little from those proposed by Schawlow and Townes (3), and consists of an optical resonator which supports the oscillation frequency and provides the positive feedback necessary for the build up of oscillations from spontaneous emission into the particular resonator mode, and the maser medium which provides the population inversion necessary for maser action.

1.3 Oscillation requirements

A gaseous discharge medium supplies the stimulated emission to build up coherent oscillations from the usual dominant spontaneous emission on a transition. If the gain on one pass between the resonator mirrors is sufficient to compensate for the loss, the intensity in the resonator mode increases until stimulated emission builds up and competes with spontaneous emission for atoms whose centre frequencies are within a natural line width of the mode (4).

The requirements for oscillation were first put forward by Schawlow and Townes (3), in which they equated the power produced by stimulated emission in the cavity mode to the rate at which energy decayed. The same result is obtained by equating the gain and loss per unit length. The gain by stimulated emission, and loss to absorption, and its dependence on line shape, is calculable using classical methods. In most cases of low pressure maser systems the primary source of line broadening is the thermal motion of the atoms.

Following the treatment of Mitchell and Zemansky (5), when the natural line width and pressure broadening $\ll$ Doppler width, the expression for the fractional gain/unit distance (g_o) at the centre of a Doppler broadened line is given by:

$$g_o = (\ell n 2/\pi)^{1/2} (g_2 A_{21}/4\pi)(N_2/g_2 - N_1/g_1)(\lambda_o^2/\Delta\nu_D) \qquad \ldots\ldots (1.1).$$

It is evident from (1.1) that to obtain gain $N_2/g_2 - N_1/g_1 > 0$, this imposes limitations on the lifetime requirements of the levels suitable for cw maser operation. The most favourable case occurs when only the upper

state is excited, and the lower level is only populated by radiative cascade in the maser transition.

The density of the lower state satisfies the equality

$N_1 = -R_1 N_1 + A_{21} N_{21}$, where R_1 represents the total decay rate of the lower transition. A steady state solution exists so that $N_2/g_2 > N_1/g_1$, if the total decay rate of the lower state obeys the inequality, $R_1 > A_{21}(g_2/g_1)$. For obtaining maser oscillation this condition is not sufficient; enough inversion must exist so that the optical gain in a single pass exceeds the losses per single pass; for small losses the oscillation condition becomes

$$((g_1/g_2)N_2 - N_1) > \frac{\ell_{loss}}{\ell} \frac{\Delta\nu_D}{\lambda_o^2} \frac{4\pi}{g_2 A_{21} (\ell n 2/\pi)^{1/2}} \quad \ldots\ldots (1.2).$$

The steady state populations are determined by the lifetimes (τ_1) and (τ_2) of the levels and the rate of excitation (n_1) and (n_2) to these levels, or

$$((g_1/g_2)n_2\tau_2 - n_1\tau_1) > \frac{\ell_{loss}}{\ell} \frac{\Delta\nu_D}{\lambda_o^2} \frac{4\pi}{g_2 A_{21}(\ell n 2/\pi)^{1/2}} \quad \ldots\ldots (1.3).$$

It can be seen from (1.3) that even if the lifetimes and statistical weights are favourable, population inversion cannot be achieved unless the excitation rate to the upper level is sufficient.

Of considerable importance, are the lifetimes τ_1 and τ_2 of the two maser levels. In a gaseous discharge environment it is the effective lifetimes which determine the oscillation and gain conditions. These effective lifetimes can differ appreciably from purely radiative ones, due to the combined processes of spontaneous decay, resonance trapping and inelastic collisions, (4).

For a consideration of the determination of effective lifetimes the reader is referred to "Measurement of Excited State Relaxation Rates", by Bennett et al. (7).

This thesis will now be confined to a treatment and observations on the way in which population inversion is realised in a discharge.

CHAPTER 2

Selective excitation processes in gas discharges

2.1 Theoretical treatment

A number of analytical studies of population inversion in gaseous discharges have been made, (Ward (1), Javan (2), Fabrikant (3) and Basov et al. (4)).

In all cases, the studies start with assumed cross-sections for electronic, or collisional and de-excitation processes, and an assumed Maxwellian electron energy distribution.

Little practical benefit has ensued from these calculations and the degree of agreement with experimental studies has not instilled confidence in this approach to the complex processes of the laser system, in which one plays off one non-thermal equilibrium process against another in order to achieve population inversion. Since such calculations up to 1962 (5), had not even enabled advance predictions of transitions on which oscillation could be obtained, it has become clear that more data on collision cross sections of all types is required. Also the assumed universal applicability of Maxwellian electron energy distributions to discharges needs to be determined, before any theoretical treatment of collective discharge processes is more than mere exercise.

It is possible, however, to understand in a qualitative way the operation of gaseous discharge optical masers by considering the dominant

processes that have been used, and those that appear to be used, to produce population inversion.

Fig. 2.1, and 2.2, show schematically the very general 4 and 3 level situations obtained in cw gas laser systems, for neutral and ion lasers respectively.

Transition probabilities

Theoretical calculations of pure radiative transition probabilities have been made by Bates and Damgaard (6) using the Central Field approximation. For atomic systems with single electrons outside closed electron shells, the method of Bates and Damgaard yields results in extremely good agreement with experiment, and in closer agreement than results calculated from the more complex Hartree-Fock differential equations.

Inelastic collisions

Theoretical treatments of elastic and inelastic collisions have been made by Massey and Burhop (7), Townsend (8), and Mott and Massey (9); and a treatment of inelastic collisions between heavy particles has been made by Bates (10). Full reviews of these theoretical treatments, together with experiments are given in the work of Hasted (11), (12), McDaniel (13); and in Massey (14). and Bates and McCarrol (15).

A number of predominant collision mechanisms have been observed in maser systems thus far; these include:

(1) Atom-atom, atom-ion excitation transfer
(2) Charge transfer,
(3) Atom-molecule, and
(4) Electron impact collisions.

2.2 Resonant excitation energy transfer

Collision processes of the type

$$X' + Y \longrightarrow X + Y' \pm \Delta E \quad (0'0/00') \qquad \ldots\ldots (2.1)$$

in which energy is transferred from the state X' of one atom to another Y' have been studied theoretically by Massey and Burhop (7).

Theory and experiment (16) shows that this type of collision:-

(a) is highly resonant for near exact energy coincidence, with a cross section larger than 100×10^{-16} cm^2; with ΔE of the order of a few kT, cross sections of approximately 10^{-16} cm^2 are realised. For $\Delta E \gtrsim 0.1$ eV the cross sections are negligible as shown in Fig. 2.3 (after Mott and Massey).

(b) has a larger cross section when the Wigner Spin Rule is obeyed, than when spin is not conserved. However, this rule is not always obeyed.

2.3 Charge transfer

Represented in its simplest form by a collision of the type

$$X^+ + Y \longrightarrow X + Y^+ \mp \Delta E \quad (10/01) \qquad \ldots\ldots (2.2)$$

ΔE as in (2.1) is the change in energy during the collision.

The energy dependence of the cross-section for a particular charge transfer reaction depends markedly on the magnitude of ΔE, as discussed in Massey's (11), (17) near - adiabatic hypothesis. The cross section for a collision in which an electronic transition occurs, is small at gas kinetic collision velocities unless $|\Delta E|$ is small. This is because the gradual collision enables the atomic electrons to change with the varying conditions.

As the relative velocity rises, the cross section increases and reaches a maximum when the time of interaction (a/v) is comparable with the time of transition $h/|\Delta E|$, where a is the range over which the interaction occurs, and v is the relative velocity of the interacting particles.

Thus $a\ |\Delta E|\ /hv \approx 1;$ ..... (2.3)

when $|\Delta E|$ is small or zero, the maximum cross section occurs at low energy. $|\Delta E|$, however, is a function of the separation of the colliding particles, and it is customary to use $|\Delta E_{\infty}|$, the value of $|\Delta E|$ at infinite separation. ΔE can also be dominated by Coulomb or polarisation forces and corrections must be made to give a mean energy defect averaged over the interaction path (18).

The probability for excitation decreases rapidly as v decreases, so that for low energies, the cross section is small unless ΔE is resonant.

For a resonant reaction, the magnitude of the cross section, evidenced by 'enhancement' or preferential excitation appears to be dependent on the type of level excited and not simply on the energy defect. Duffendack and Thomson (19) found that transitions from triplet levels of the spark spectrum of copper were enhanced in neon more than transitions from singlet levels, although some singlet levels were closer to the neon ion ground state than triplet levels, (as shown in Fig. 2.4), in a near resonant collision of the type

$$Ne^{+}\ (^{2}P_{3/2}) + Cu(^{2}S_{1/2}) \longrightarrow Ne\ (^{1}S_{o}) + Cu^{+}(^{3}P) + \Delta E \quad (10/01') \quad ..... (2.4).$$

Similarly, Duffendack and Thomson observed the $10/01'/01\phi$ process in gold and silver, in a helium arc; in each of these cases there is a predominance of triplet enhancement in accordance with the Wigner Spin Rule. In the case of silver, although transitions are enhanced from triplet levels within 0.1eV of the helium ion ground state, other transitions from levels approximately 2eV away are also enhanced.

Gran and Duffendack (20) have observed similar enhancements in the s, p, f and d levels in the ion spectrum of lead, but in which the Wigner Spin Rule is not obeyed.

Non resonant collisions

According to (2.3), the maximum cross sections will occur at high energies for non-resonant collisions; Lipeles et al. (21), however, have recently reported that in their studies of optical excitation with low energy ions large maximum cross sections of the order of 10^{-16} cm^2 are observed at low energies, contrary to expectation. These observations can be reconciled with (2.3) by noting that in general the energy levels of the molecular complex formed during the collision are strongly dependent on the internuclear separation. Thus according to Lipeles et al. the relative velocity (v) and the interaction range are functions of the internuclear separation.

Summary

It can be seen that in charge transfer collisions, the energy discrepancy need not be as small as that required for the realisation of large cross sections in atom-atom resonance energy transfer collisions.

2.4 Atom-molecule collisions, dissociative excitation transfer.

These collisions, which have not been studied extensively, take the form

$$M' + AB \rightarrow \quad M + A' + B \ (\text{or } B') \qquad \ldots\ldots (2.5).$$

In this type of collision more than two atoms are involved, so that a description of the reaction is not simple, and theoretical explanations based on the interaction curves become too complicated for even the simple case involving a diatomic molecule. For this reason no quantitative theory exists, though it is possible to discuss the collision qualitatively.

It is assumed that relatively long range interactions between M' and AB cause vertical transitions between the ground state and excited, repulsive states of AB'. AB' then dissociates to give, in general, one excited atom and one ground state atom. Since each state of the products A' and B, or A' and B' will correlate with several repulsive AB' curves, and since three atoms are involved, there is no strong resonance requirement. Cross sections of approximately 10^{-15} cm^2, with ΔE of 1-2 eV have been noted by Bennett (22).

If the products of the dissociative excitation transfer are diatomic radicals they may have rotational and vibrational as well as electronic excitation, and population inversion in rotational/vibrational levels can result (23).

2.5 Electron impact

In a gaseous discharge several collision mechanisms are present. Electron impact collisions upon atoms are by far the most common. Not all of the collisions lead to changes of state. For population inversion to occur, the inelastic collisions are of primary interest, and electron impact excitation has yielded more laser oscillations than any other selective excitation process.

The cross section Q_{12} for excitation from the ground state (1) to an excited state (2) by electron impact is given by the Born approximation (22), (24) as

$$Q_{12} \propto \int_{K_{min}}^{K_{max}} \left| \int \psi_1 e^{ikz} \psi_2^* d\tau \right|^2 k dK \qquad \ldots\ldots (2.6),$$

where the incident electron energy $\gg E_n$, and E_n is the excitation energy threshold,

$$Q_{12} \propto \left| \int \psi_1 \psi_2^* z d\tau \right|^2 \qquad \ldots\ldots (2.7).$$

The term on the right hand side of the proportionality in (2.7) is proportional to the electric dipole matrix element for a radiative transition between an excited state and the ground state. To a first approximation, at electron energies where electron exchange can be neglected,

$$Q_{12} \propto A_{21} \qquad \ldots\ldots (2.8)$$

where A_{21} is the Einstein transition probability.

This $Oe/O'e$ process has its onset at the threshold energy, and is either non-resonant or broadly resonant up to approximately 100 - 150 volts, (or 10 times the excitation potential). After passing the maximum, the probability curves fall away slowly.

The above only holds for excitation of atoms for which spin-orbit coupling is negligible. For heavier and more complex atoms L-S coupling is not a good approximation, and j-j coupling is obeyed.

Electron exchange collisions

Electron exchange collisions can also result in excitation in which spin multiplicity is changed. Except in heavy atoms, transitions involving a change of multiplicity are dominated by electron exchange. Such collisions are very important close to threshold in the case of transitions involving no change in the azimuthal quantum number; and have excitation functions with much sharper maxima than for optically allowed transitions. Fig. 2.5 (after Bennett (22)) gives a qualitative illustration of the energy dependence of inelastic excitation cross sections for (a) optically allowed transitions and (b) for excitation between levels of the same parity.

Ionisation by electron impact.

Calculations for ionisation using the Born approximation quantum theory are similar to those for excitation, and yield similar curves to

those of excitation by electron impact (Kieffer and Dunn (25)). Above threshold the ionisation function increases linearly with energy to a maximum several times the ionisation energy and then falls off gradually above this.

Apart from work on helium and nitrogen, the review article of Kieffer and Dunn shows that little work has been published on ionisation into excited final states. It is of some relevance to ion lasers to know if ionisation functions exhibit resonances.

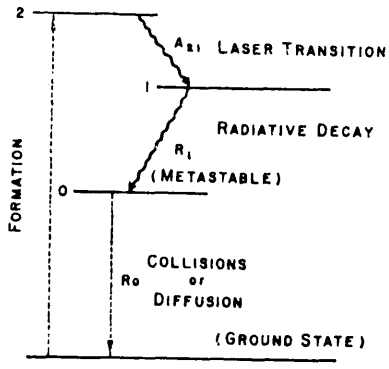

Ideal four-level system representative of most cw gas lasers.

Fig. 2.1

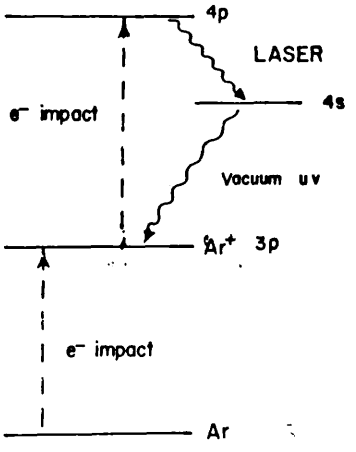

Three-level excitation model proposed by Gordon to explain the behavior of the small-bore cw Ar^+ laser characteristics.

Fig. 2.2

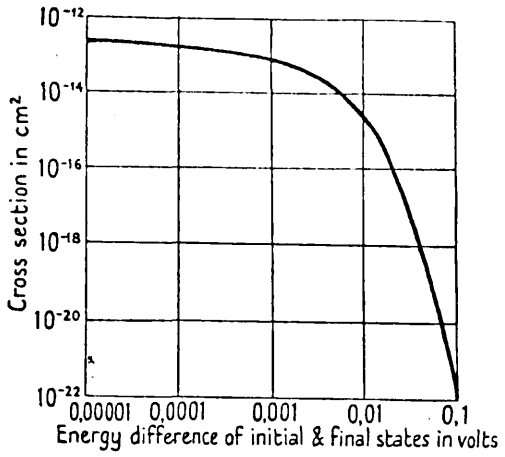

Fig. 2.3

Calculated cross-section for transfer of charge between two atoms as a function of the resonance defect ΔE.

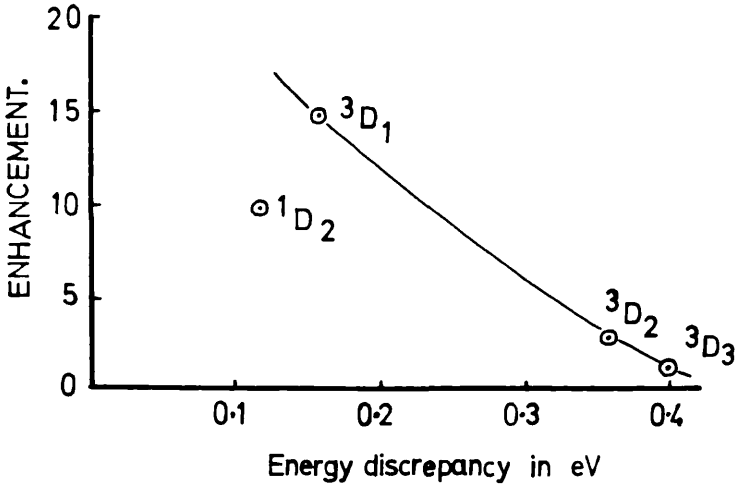

Fig. 2.4

Curve showing the relation between the relative enhancement of the d^9s copper levels and the energy discrepancy with neon ions.

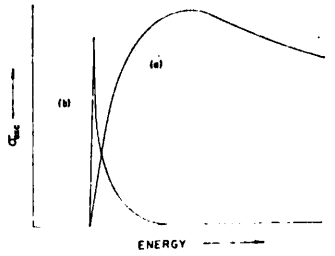

Fig. 2.5

Qualitative illustration of the energy dependence of inelastic electron excitation cross sections for optically allowed transitions (a) and for excitation between levels of the same parity (b). The low-energy region (b) is compatible with the stepwise excitation process

CHAPTER 3

Excitation processes in discharges used as optical maser media

Introduction

The possibility of the use of a gas discharge to obtain a non-equilibrium population distribution necessary to support optical maser oscillation was recognised by several people. According to Schawlow, this possibility was first pointed out by W. S. Boyle in 1958. However, achievement of a negative temperature state was reported in the Soviet Union by Butayeva and Fabrikant in 1957 (1) in a mixture of a metal vapour and a buffer gas. An earlier claim for the formulation of maser theory by Fabrikant as early as 1951 cannot be substantiated (2).

The first specific proposals were published in 1959 by Sanders (3), (4) and Javan (5). Javan (6), using rf excitation was the first to realise oscillation in a gas discharge.

Since the first proposals, all the following methods of excitation have been used in successful optical maser oscillators:-

(a) the glow discharge, including

  (i) the negative glow and

  (ii) the positive column regions

(b) rf excitation

(c) hollow cathode discharges

(d) pulsed positive column discharges.

3.1 The glow discharge

There have been a number of excellent analyses of the glow discharge which include those of von Engel (7), Francis (8), Brown (9) and Parker (10). Since an analysis of this discharge seems to cover most aspects of laser discharges, including those of the hollow cathode and pulsed afterglow discharges, on which a considerable amount of work was carried out in the work reported here, an abbreviated qualitative description of salient parts of the glow discharge in a gas at low pressure will be given.

Fig. 3.1 (after von Engel (7)) shows the spatial distribution of dark and luminous zones, the electric field, space charge densities $\rho+$ and $\rho-$, and current densities in a glow discharge at a pressure 0.1 - 1 torr.

3.1.1 The negative glow.

The negative glow is the first large bright luminous region, going from the cathode to the anode, that occurs in the glow discharge. If a plane cathode is mounted in a large spherical bulb and rotated with respect to a fixed anode, the negative glow region swings round as if fixed to the cathode surface, the positive column merely fills the remaining space between the Faraday dark space and the anode. This indicates the beam like nature of the negative glow. Whereas the positive column is affected by the dimensions of the discharge vessel, the negative glow is not.

Consider an electron emitted from the cathode, for example by a positive ion impinging on the cathode. Initially the electron is in a region of high field strength and is rapidly accelerated away from the cathode. At first it has insufficient energy to excite or ionise; further from the cathode, though the field is weaker, the electron ionises more efficiently and strong electron excitation of the gas takes place.

Near the boundary between the cathode dark space and the negative glow, the electric field is very weak, and only the fast electrons which have not lost energy by inelastic collisions will be able to ionise in that region. Although a small group of fast electrons reaches the edge of the negative glow, the majority of the electrons have energies only slightly above that required to ionise the gas. This group loses its energy by inelastic collisions as it enters the weak field region of the negative glow. In the middle of the glow there are many more slow electrons than fast.

Table 3.1

Electron Velocity Distribution

Helium ($p = 1$ torr, $j = 2 \times 10^{-5}$ A cm^{-2})

Electron Energy (eV)	0.6	7.3	25
N_e (cm^{-3})	4.10^9	5.10^7	5.10^6

Table 3.1 gives an electron velocity distribution in a discharge in helium, (after Pringle and Farvis (11)).

Since the slow electrons have energies below the ionisation maximum (7) but above or at the excitation maximum, they experience many exciting collisions and produce the negative glow. The electron concentration in the negative glow has been shown to be approximately 20 times larger than in the positive column (12). When the electron energy is sufficiently small, recombination with positive ions takes place.

With increasing ~~field~~ distance from the boundary fewer fast electrons are found and less light is emitted. Further on, the field increases slowly, recombination decreases and the Faraday dark space develops until the electrons have again sufficient energy to excite and ionise the gas; the uniform positive column or the first striation then commences.

The extent of the negative glow has been shown by Brewer and Westhaver (13) for various gases and values of cathode fall to be equal to the range of the electrons. Hurt (14) found that emission from atomic species occurs on the cathode edge of the negative glow region with molecular emission from species further into the glow.

For more specific details of processes leading to atomic and molecular species and the excitation processes with the negative glow, the reader is referred to 3.5, 'The similarities of the afterglow of a pulsed discharge and the negative glow region'.

3.1.2 The positive column

The axial component of the electric field, as shown in Fig. 3.1, is constant at any point, and the densities of positive ions and electrons

are equal. In the positive column, due to the smaller mobility of the positive ions, most of the current is carried by electrons. Von Engel (7) has shown that the uniform appearance of the glow is due to the random velocity (V) of the electrons acquired by numerous elastic collisions in the field, and not from the drift velocity (V_d) in the field direction.

V_d/V is usually < 0.1 for $E/p < 20$ volt cm^{-1} $torr^{-1}$ (7).

In the steady uniform positive column the electric field has such a value that the number of electrons and ions produced is equal to the loss of charge to the walls. The elementary theory of the positive column gives a good quantitative description of the relation between the axial and radial electric field, the pressure, the tube radius and the nature of the gas. The approach is usually to derive the radial distribution of charge concentration by equating the ionisation rate and the diffusion loss, then to calculate the electron temperature (T_e), assuming a Maxwellian distribution of the electrons, necessary to maintain the rate of ionisation.

A theoretical treatment of the electron temperature in the positive column in mixtures of atomic gases has been given by Dorgelo, Alting and Boers (15), in an extension of the Schottky theory which applies only to the range where diffusion is a dominant process. They assume that electrons have a Maxwellian energy distribution and that ions are produced only by direct electron collisions with gas molecules, and are destroyed at the walls.

If q_1 is the number of ions of gas 1 formed per cm^3 per sec. and is given by

$$q_1 = \alpha_1 N_e \qquad \ldots\ldots (3.1)$$

where N_e is the electron concentration and α is the number of ions sec^{-1} electron^{-1}, then an equation analogous to Schottky's is derived:-

$$kT_e/e\left(\left(d^2N_e/dr^2 + 1/r\,\frac{dN_e}{dr}\right) + \left(\frac{\alpha_1}{b_1} + \frac{\alpha_2}{b_2}\right)\right)N_e = 0 \qquad \ldots\ldots (3.2)$$

where b_1 and b_2 are the ion mobilities of the gas components.

The solution is a zero order Bessel function, having the boundary condition $N_e = 0$ at the wall, where $r = R$, leading to

$$\frac{\alpha_1}{b_1} + \frac{\alpha_2}{b_2} = \frac{kT_e}{e}\left(2{\cdot}4/R\right)^2 = \frac{2}{3}\bar{V}\left(2{\cdot}4/R\right)^2 \qquad \ldots\ldots (3.3)$$

where $e\bar{V}$ is the mean electron energy. In general

$$\alpha = ap^{m/e}\cdot\, 4/\sqrt{\pi}\left(2kT_e/m\right)^{3/2}\left(1 + 1/2\, e/k\, V_i/T_e\right)e^{-eV_i/kT_e} \qquad \ldots\ldots (3.4)$$

where V_i is the ionisation potential of the gas.

(3.4) shows that the rate of ionisation depends strongly upon V_i/T_e. For an easily ionisable gas or vapour such as argon or mercury, T_e will be low. Reasonable agreement was obtained between calculated values of T_e, for mixtures of neon-mercury and neon-argon and the results from probe measurements, by Dorgelo, Alting and Boers (15).

In typical low pressure positive columns T_e is between 0.1 - 10 eV. In narrow bore discharge tube systems, as used for gas lasers, E/p can be as much as 50 V cm^{-1} $torr^{-1}$, and T_e can be as large as 20 eV (16). In bores below 5mm, the electron temperature rises rapidly in both glow discharges and rf discharges (17). In this region the Schottky theory

of the positive column is not expected to be valid, as the electron mean free path can be comparable to the diameter of the discharge tube, and as an extended negative space charge sheath develops on the side walls and reflects electrons back into the plasma.

At low values of pR the sheath takes control of the radial motion of charges and the above theory does not apply. It is in this region and below that laser discharges are operated, and the assumed Maxwellian electron energy distribution is questionable, - see Chapter 6.

3.2 rf discharges

The early work on laser excitation was concentrated on systems which had special advantages. The most widely used was that of rf excitation. This method of excitation was chosen because it avoided (i) contamination and destruction of the internal cavity mirrors then used, and (ii) gas clean up that occurs with internal electrodes.

3.2.2 General considerations

The following gives a physical picture with maximum insight into the physical processes occurring in the rf discharge with minimum recourse to Diffusion theory.

Ionisation, the necessary condition for obtaining a discharge in a gas subject to alternating fields, differs from ionisation in steady dc fields, in the following ways:

(i) the field reverses periodically, thus charges may not be swept out of the volume on to the walls or electrodes (18), losses are reduced and a sustained discharge can be maintained with low electric fields.

(ii) secondary charged particles released from the walls do not contribute to the growth of a discharge unless they are emitted when the direction of the electric field is favourable.

(iii) alternating discharges can be maintained in insulating vessels, with the static fields set up by the drifting of ions and electrons, controlling the equilibrium density of ionisation in the discharge volume.

(iv) the maximum kinetic energy in the oscillatory motion of an electron at the minimum electric field intensities needed for breakdown corresponds to approximately 10^{-3} eV (Brown (19); this is insufficient to give gas breakdown, and sufficient energy can be acquired only by an electron experiencing collisions. A free electron in an oscillatory electric field oscillates in phase with the field, so that the average power gained from the field is zero. In a collision an electron can have its orderly oscillatory motion changed to random motion, and it can gain energy from the field. The kinetic energy lost by an electron in an elastic collision, is more than replaced by the gain in energy due to its change of phase. The energy of the electrons, therefore, increases until it is enough to enable the electrons to excite or ionise, when they lose large amounts of energy.

Following Francis (18), the factors which influence the breakdown field (E) and the subsequent current and ion density of a fully developed plasma are:-

(a) the gas pressure, p (torr), and consequently the mean free path λ_e(cm) of the electrons, and the frequency ν , (equal to V/λ_e sec^{-1}, with which they hit gas atoms and molecules.

(b) the frequency f, and wavelength λ of the applied electric field E.

(c) the dimensions of the containing vessel, the length d (cm) in the direction of the electric field and the perpendicular width of radius R (cm).

The following sets of conditions, determine the physical processes occurring in the discharge:-

1. Very low pressures (10^{-2} torr or less) $\lambda_e \geq$ d, R.

The electrons hit the walls of the containing vessel more often than they hit molecules or atoms. The secondary effects at the walls then affect the maintenance of a discharge or the breakdown of a gas.

2. Medium or high pressures.

(a) $\lambda_e <$ d, R; low frequency, $\nu \gg$ f

The electrons make many collisions for each field oscillation, and drift as a cloud in phase with the field.

If the frequency (f) is high, the amplitude of oscillation is low and can be less than d, or R; charged particles formed by ionising collisions in the gas are lost by diffusion to the walls.

If the frequency (f) is low, the amplitude of oscillation is high and electrons are driven into the walls of the tube in each half cycle. Secondary wall processes are then essential to maintain the discharge.

(b) $\lambda_e < d, R$; high frequency, $\upsilon \ll f$

The electrons make many collisions with atoms or molecules, and make many small amplitude oscillations between collisions. They remain essentially stationary and spread out only by diffusion.

3. Very high frequency, (microwave frequencies)

$$\lambda_e \lesssim d, R$$

The electrons are not under the influence of the electric field, but are subject to the standing oscillatory electromagnetic wave determined by the frequency of the field, the excitation and the geometry, that is by the cavity properties.

The situation in 2b, $\lambda_e < d, R$, high frequency $\upsilon \ll f$ is applicable to rf excited laser discharges, where R = 5 - 10mm, pressures are approximately at 1 torr, and λ_e is about 1mm, for electrons of 16 eV in helium, (Ward (20)). Diffusion theory can be used to determine the breakdown of the gas and the maintenance of the discharge.

Limits of the Diffusion theory.

Certain basic assumptions are made in calculations of breakdown as a balance between ionisation rate and loss of electrons by diffusion.

At low frequency, dimensions of containing vessels are small compared with the wavelength of the electric field and the uniform field assumption is very good.

At high frequency, there is a limit to the size of the discharge tube consistent with the uniform field assumption of the diffusion theory.

The limit is when the size of the discharge tube is equal to a single loop of a standing wave of the electric field.

The relation between the parallel plate separation (L), the wavelength (λ), and diffusion length Λ may be written (19) as

$$\lambda/2 = L = \pi\Lambda \qquad \ldots\ldots (3.5)$$

or $$p\lambda = 2\pi(p\Lambda) \qquad \ldots\ldots (3.6).$$

The diffusion length Λ of a containment vessel is determined by the dimensions of the vessel and can readily be calculated from

$$1/\Lambda^2 = (\pi/d)^2 + (2.405/r)^2 \qquad \ldots\ldots (3.7)$$

where r is the radius and d is the length of the vessel.

The first term is the contribution due to diffusion to the end walls, and the second, diffusion to the side walls.

Diffusion theory also does not apply when the electron mean free path λ_e becomes comparable to the size of the tube.

In the limit, this occurs when $\lambda_e = \Lambda$.

The probability of collision P_m is equal to $1/(p\ \lambda_e)$, therefore

$$P_m = 1/p\Lambda \quad , \text{ or } \quad p\Lambda = 1/P_m \qquad \ldots\ldots (3.8)$$

The value of P_m is not constant but depends on the electron energy. From measured values of P_m it is therefore possible to calculate the limit for use of the Diffusion theory.

Average electron energy

The variation of electron temperature (T_e) with frequency has been studied by von Engel and Harris (21). Fig. 3.2 (after von Engel and Harris) shows that at low frequency the modulation is 100 per cent. At high frequency the mean energy is high for the same field.

3.3 The Hollow Cathode Discharge. (H.C.D.).

General description

This type of discharge, although often called a Schuler discharge, was first developed and used by Paschen (22).

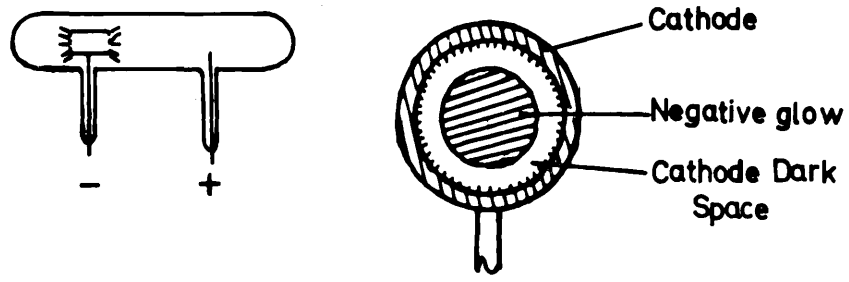

Fig. 3.3 Typical Hollow Cathode discharge configuration

If a dc voltage of more than 1 KV is applied to a simple discharge tube containing an inert gas as shown in Fig. 3.3a then at a pressure which depends on the cathode diameter and the carrier gas, but at approximately 1 - 20 torr, an intense glow concentrates inside the cylindrical cathode, Fig. 3.3b.

The brightness of the discharge depends in rather a critical manner on the carrier gas pressure. If the pressure is reduced beyond the optimum of 1 - 3 torr, the brightness falls until at a critical point

the discharge inside the cathode quenches and forms a diffuse discharge. It is then characterised electrically by a high resistance and low current.

When the current is a few milliamperes only a small inner portion of the cathode is covered with a glow. As the current is increased, the glow extends to cover the whole surface of the cathode without any increase in the sustaining voltage (V_s) across the tube. Any further increase in current now leads to an increase in V_s as the anomalous cathode potential fall develops, as in the abnormal glow discharge.

The intensity of the light emitted from the discharge is many times greater than that from the positive column of a glow discharge. Measurements of the electric field in the glow, made by Schuler (23), show that it is less than in the positive column, but similar to that in the negative glow region of a glow discharge.

When the light emitted by the discharge is examined, it is found to consist of spectrum lines of the carrier gas and also of the material of which the cathode is made. As the electric field in the discharge is small when operated under normal conditions, the emission lines are almost entirely free from Stark broadening; further, if the cathode is cooled the Doppler width of the lines can be reduced and fine lines obtained, (Tolansky (24)). Roessler and de Noyer (25) have reported line widths of less than 0.01 cm^{-1} in a liquid helium cooled H.C.D.

Excitation theories

A number of theories have been suggested to account for the interaction of the double cathode phenomenon of the high current, high electron density, H.C.D., the occurrence being due to:-

(a) a reduction of the positive space charge in front of the cathode, or increase in ionisation in the cathode dark space due to electrons coming from opposite sides of the cavity (26) (27), (28).

(b) an increase in ion density and radiation from high quantum states in the nearly field free negative glow region (28) (25).

(c) more efficient geometric use of (i) ions (ii) photons or (iii) metastable atoms, in causing secondary emission of electrons from the cathode (25), (27), (29), (30).

(d) the presence in the cathode region of a large number of sputtered metallic atoms which may influence the secondary processes at the cathode, and in the volume of the discharge (31), (32).

In spite of the wide usage of the H.C.D. little experimental verification, apart from the work of Little and von Engel (26), has been forthcoming to show the validity of the above statements.

Sputtering action

As stated previously, spectra of the cathode material are observed, as well as that of the inert, or molecular carrier gas used, from the plasma of the H.C.D.

The cathode material is sputtered by positive ions which can have energies corresponding to the full cathode fall of a few hundred volts impinging on the cathode (33), and is excited in the negative glow plasma. The majority of particles ejected from the cathode according to von Hippel (34) are atomic. However, Honig (35) has shown thatwhen 600 eV positive ions of argon bombard a silicon carbide cathode, ion species Si^+, SiC_2^+, Si_2C^+ and $Si_2C_2^+$ are emitted in measurable quantities. Wehner and co-workers (35) - (39), have determined sputtering yields for low energy, 100 - 600 eV inert gas ions, and have found that there is a periodic dependence on atomic number, similar to the reciprocals of the heat of sublimation. Peaks in yield occur at manganese, copper, silver and gold in the periodic table.

The exact mechanism of the sputtering process is not yet fully understood, but the accepted explanation is that:

(i) momentum is transferred from the incident ion to the cathode surface, and atoms, ions, and molecules are emitted with varying velocities from the cathode, (Townes, (40)).

(ii) evaporation of atoms occurs under the ion bombardment.

Use as a spectroscopic source

Because of the sputtering action, and low electric fields away from the cathode edge of the negative glow, the H.C.D. has been used extensively as a source of line spectra of most of the elements (24), and is only surpassed by the atomic beam and the laser in the production of spectra having small line-widths. Its main advantage over other

types of discharge source is in exciting the high melting point metals, for which the sputtering action can produce the necessary atomic vapour without the necessity for high temperature (41).

Effect of carrier gas

The type of spectra emitted is affected considerably by the carrier gas.

Helium produces more 'spark' spectra than any of the inert gases. It is believed that this is due to its high excitation and ionisation potentials. Helium is also a less effective sputterer than other gases, (Stocker (42)), so that the cathode material vapour pressure is low, and Penning type collisions are likely to predominate over electron excitation/ionisation collisions. The low electric fields in the H.C.D. also make it a favourable source for the excitation of spark spectra with the excitation limited by charge transfer ($10/01'$), or ($10^*/1'0$) collisions (Sawyer (43)).

The type of excitation produced is not only a function of the excitation potentials of the carrier gas. Mitchell (44) found that argon gave arc-like spectra, but xenon gave more ion spectra, using an ion cathode, although the excitation potential of xenon is less than that of argon. Examination of the data given in (43) shows that there is a maximum of excitation observed in a H.C.D., explainable as resulting from the ($10/01'$) process, which with helium as a carrier gas, appears more probable than a metastable - metastable collision process, in the excitation of metal spectra.

3.4 Pulsed discharges

Pulsed gas discharges were first used as laser excitation sources by Boot and Clunie (45), who obtained oscillation in the near infra-red in the afterglow of a high pressure, high-current, pulsed discharge. This means of excitation has enabled lasers to be developed working up into the triply ionised species under pulsed conditions, and has led subsequently to the rapid development of high power cw and the new transient laser systems.

Excitation processes at breakdown

If a high potential is applied to a discharge tube via internal electrodes, in parallel with a capacitor, the gas breaks down at a particular voltage. This voltage depends on the gas pressure and the separation between the electrodes, i.e. E/p. Plots of the variation of breakdown voltage with pressure and separation of the electrodes, form the familiar Paschen breakdown curves. Provided the electric field is uniform and the pressure-electrode separation (pd) is less than 150 torr cm, Paschen's Law is obeyed.

At breakdown the current rises rapidly to a value determined by the resistance in the circuit and the finite power of the source. After the initial rapid rise in current, the electric field falls until the current reaches a particular value, after which the maintaining potential is independent of the current. The current then decays exponentially according to the time constant of the circuit. In such a discharge the current density can approach 300 Amp cm^{-2}, as a result of the considerable ionisation that occurs.

The normal capacitor discharge is not a versatile discharge as far as analysis of a discharge is concerned, since it is not possible to isolate processes which occur in the afterglow of the initial breakdown pulse, from those which occur during the decaying current pulse. By use of a delay line, however, in conjunction with a thyratron switch and a pulse transformer, as shown in Fig. 7.2 it is possible to produce quasi-cw rectangular discharge current pulses of up to 100 msec duration.

In the pulsed positive column discharge the electric and spectral properties are determined by the dimensions of the discharge tube, and the emissive properties of the cathode.

To the writer's knowledge no electron energy distribution determinations have been made in a pulsed discharge, but it is believed that the average electron energy is high because of the large E/p at breakdown, of the order of 200 V cm^{-1} $torr^{-1}$, and during the large sustaining period, when the ratio of the electron drift velocity to random velocity $V_d/V \longrightarrow$ 0.2 - 0.3 in some gases. The results of Cheo and Cooper (46) on pulsed carbon dioxide and nitrogen laser discharges show that electrons are of high energy only during the time to gas breakdown.

Beyond breakdown, Breusava (47) has shown that in the case of all the gases she investigated, the large electric field decayed at a rate determined by the diameter of the discharge tube; the initial voltage drop being steeper in the smaller discharge tube. The time of decay of the large electric field was approximately 25 microseconds from initial breakdown of the gas.

Excitation processes in the afterglow of a pulsed discharge.

It is instructive to consider afterglow processes in helium, since helium is commonly used as a buffer gas, and since it is mainly with helium that second kind collisional energy transfer processes, producing population inversion, have been postulated for laser systems.

In the afterglow of a pulsed discharge in helium, there is a sharp increase in intensity, in atomic spectra 5 - 10 microseconds after cessation of the pulse, with the peak intensity varying with the particular excited level (48). Biondi and Holstein (49) have found that visible line spectra are emitted from high level states n = 3, 4, 5 and 6 all within 1.5 eV of the helium atomic ionisation potential. They also determined that the square root of the radiation intensity emitted from the afterglow followed closely the decay of electron density, indicating that the emission was by a recombination process. This was subsequently verified by microwave studies made by Anderson (50).

The most important deionisation processes in helium are stated by Pakhomov et al. (48) to be:-

$$He^+ + 2e \longrightarrow He' + e \qquad \ldots\ldots (3.9),$$

(The process $He^+ + e \longrightarrow He'$, has a much lower recombination rate than (3.9), (Loeb (51).)

and

$$He_2^+ + e \begin{cases} \nearrow He' + He \longrightarrow 2He + h\nu & \ldots\ldots (3.10a) \\ \searrow He_2' \longrightarrow He_2'' + h\nu & \ldots\ldots (3.10b). \end{cases}$$

Processes 3.9 and 3.10a lead to de-excitation with the production of atomic lines and process 3.10b to the appearance of molecular bands.

Pakhamov has shown that at discharge wall temperature of 77°K the intensity of the afterglow of molecular helium bands is low, so that reaction (3.10b) is negligible.

After all current has ceased, the flux of energetic electrons is nearly zero, and the remaining electron density is composed of free electrons produced by reactions of the type:-

(a) below 5 torr

$$He^* (2^3S) + He^* (2^3S) \longrightarrow He_2^+ + e \quad \ldots\ldots (3.11)$$

and (b) above 5 torr

$$He^* (2^3S) + He^* (2^3S) + He \longrightarrow He_2^+ + He + e \quad \ldots\ldots (3.12).$$

Electrons, atomic and molecular ions are therefore present for recombination to occur.

Additional processes producing molecular ions and electrons (51) are the:

Hornbeck - Molnar process

$$He + (e + \rangle 23 \text{ eV and } \langle 24.2 \text{ eV}) \longrightarrow He^* + e \quad \ldots\ldots (3.13)$$

$$He^* + He \longrightarrow He_2^+ + e + K.E. \quad \ldots\ldots (3.14)$$

and the Holt - Biondi process

$$He^+ + 2He \longrightarrow He_2^+ + He + K.E. \quad \ldots\ldots (3.15)$$

(which occurs at higher pressures).

The dissociation energy of He_2^+ is between 2.2 and 3.1 eV (51). To account for the dissociative-recombination $He_2^+ + e \longrightarrow He' + He$, where He' is an excited state of helium (n = 3, 4, 5 or 6), the molecular helium ion He_2^+ cannot be in its lowest energy state, but must be an excited

molecular ion, which lies within 1.5 eV of the atomic ionisation potential of helium, and not at 24.5 - (2.3 or 3.1) eV.

The He' from recombination and dissociation is excited to within 0.5 - 0.3 eV of the helium ionisation potential, the reaction being

$$He_2^{+'} + e \longrightarrow He' (>23 \text{ eV}) + He \quad \ldots\ldots (3.16).$$

Further, following Loeb (51), to account for this reaction, the $He_2^{+'}$ in its excited vibrational state must last long enough to recombine with helium atoms, at collision frequencies of 10^7 - 10^8 sec. This means that the excited vibrational He_2^+ ions can suffer approximately 10^6 collisions without losing their energy of vibration. Studies of such vibrational states excited to within 0.3 eV of the atomic ionisation potential indicate that the chance of energy loss is of the order of 10^{-5} per collision. This means that the excited helium molecular ion is metastable ($He_2^{+*'}$). This process, according to Biondi (52) has been established 'beyond any question', by the observed Doppler broadening of the atomic lines from He'. However, it is now questioned, following the work of Ferguson et al. (53).

The overall process, therefore in the afterglow of a pulsed helium discharge is one of de-excitation of $He^*(2^3S)$ atoms by double impact or triple impact depending on the pressure as in (3.11) or (3.12), giving

(a) metastable molecular helium ions ($He_2^{+*'}$)

(b) excited helium atoms, excited to within 0.3 - 0.5 eV of the helium ion ground state.

This is just the energy range in which selective excitation occurs in

helium-mercury and helium-iodine lasers, and in which a decay interval similar to the decay of excited helium atomic levels is observed. More recent work by Collins and Robertson (54), on a flowing helium afterglow, has shown at extremes of high ionisation and low neutral density, that it is collisional-radiative recombination of He^+, that determines the rate of atomic spontaneous emission in the 50-250μsec period in a helium afterglow and that the rate of emission follows that of He^+ and not He_2^+, even at pressures as high as 20 torr.

3.5 Similarity of the negative glow of the glow discharge and the afterglow of a pulsed discharge.

Anderson (55) has shown that the negative glow of a pulsed discharge can be quenched by the application of microwave radiation. More important, he found that emission from the anode side of the negative glow was quenched, while that on the cathode side was enhanced. These results suggest that recombination is the important process deep in the negative glow, since this is the only process leading to the formation of radiative states that would be affected by the microwaves.

Hurt (14) in investigations on the negative glow has found that emission from atoms peaked on the cathode side of the glow, with the peak for molecular emission, ten times greater than in the positive column, occurring towards the anode side. To account for the molecular emission in the negative glow, Emeleus and Duffendack (56) proposed a three body collision

$$He^*(2^3S) + 2He \longrightarrow He_2\,(2^3\Sigma\,) + He \qquad \ldots\ldots (3.17).$$

Using a flowing helium afterglow, Collins and Hurt (57) determined that the observed molecular emission was definitely the result of recombination of the molecular ion. They found that the molecular emission had the same pressure dependence as the molecular ion, which was very different from the pressure dependence of the atomic ion or the He (2^3S) metastable.

As in the helium afterglow, molecular emission is enhanced at higher pressures in the negative glow. Above several torr, the molecular ion is the dominant ion, (Kerr (58), Hornbeck and Molnar (59), Phelps and Brown (60)). Another striking similarity between the afterglow and the negative glow molecular emission is that the relative intensities of molecular bands are the same, indicating that excited molecules are formed by the same process in the two cases.

Recent work by Ferguson, Fehsenfeld and Schmeltekopf (53), (briefly mentioned in 3.4) on flowing helium afterglows appears to confirm the conclusions reached by Collins and Robertson (54) on the mechanism producing the atomic emission in the helium afterglow. They appear to show conclusively that:

(i) the atomic emission is due to collisional recombination of the atomic ion by the $He^+ + 2e \longrightarrow He' + e$, process (3.9) of Pakhomov et al. (48).

(ii) the molecular emission in the late afterglow is due to collisional-radiative recombination of the He_2^+ ion.

If this is the case, the presence of the highly excited metastable molecular helium ion, necessary to explain the process established 'beyond any question' by Biondi is questionable. It is hopedthat the situation will be made clearer in the near future following further flowing afterglow experiments.

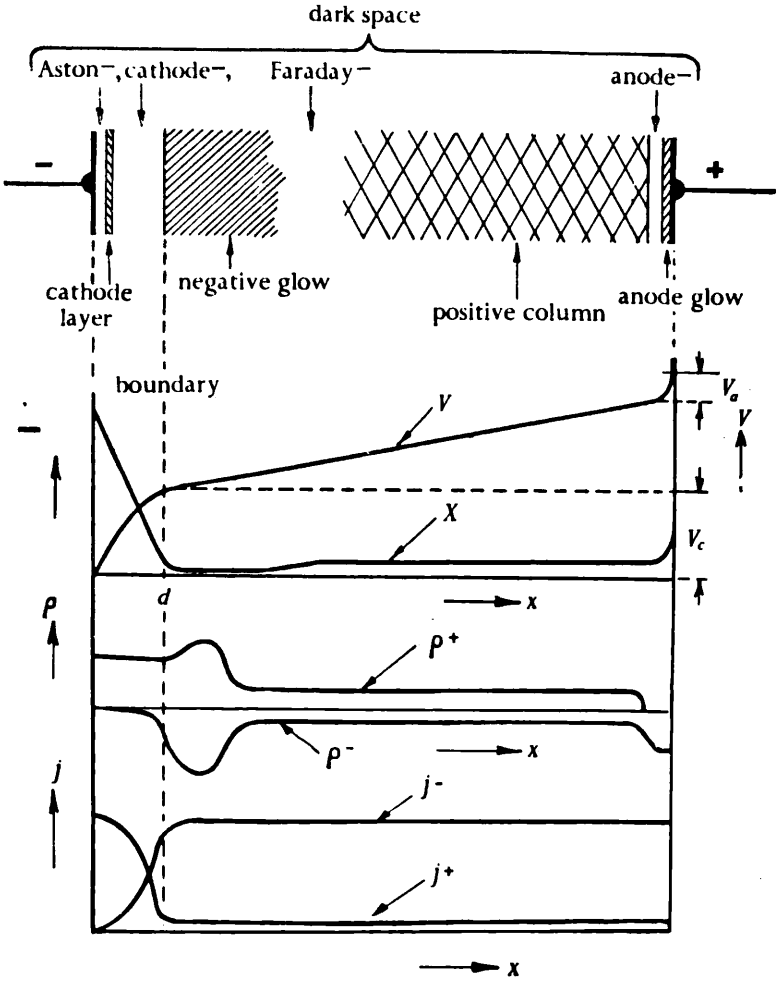

Fig. 3.1

Spatial distribution of dark and luminous zones, electric field X, space-charge densities ρ^+ and ρ^-, and current densities j^+ and j^- in a glow discharge (schematically).

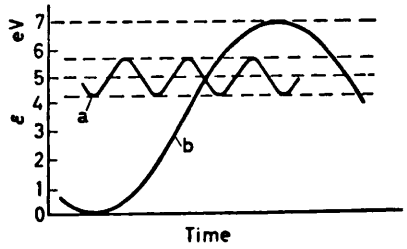

Fig. 3.2

Variation of the average electron energy with time, in helium at $X/p \sim 0{\cdot}6$ *V/cm mm Hg: (a) high frequency; (b) low frequency.* (From A. VON ENGEL and W. L. HARRIES

CHAPTER 4

Specific Oscillator Systems

Introduction

In this chapter, particular systems have been chosen for analysis to illustrate the selective excitation processes discussed under the six headings in Chapter 2.

4.1 Atom-atom, excitation transfer collision masers

There have been four successful masers in which population inversion has been produced predominantly by excitation transfer collisions. These are the helium-neon, mercury-zinc, helium-krypton and neon-xenon systems.

4.1.1 Helium-Neon System

The first laser oscillation, on five transitions in the near infra red in neon was obtained by Javan (1) in 1961. The five transitions are between the 2s and 2p levels of levels in neutral neon.

It can be seen from Fig. 4.1 that there is an energy coincidence between the helium (2^3S) metastable level, and the four neon 2s levels. A similar energy coincidence exists between the helium (2^1S) metastable level and the four neon 3s levels.

Fig. 4.2 shows in detail the energy coincidences for the helium (2^3S) metastables at 19.8 eV above the ground state.

As stated in section 2.1, large collision cross sections are observed for collisions of the type $A^* + B \longrightarrow A+B(\text{excited}) + \Delta E$ ..... (4.1) where ΔE is less than a few kT and where the Wigner Spin Rule is not violated (2).

All the Ne 2s energy levels are within 1247 cm^{-1} of the He (2^3S) level, so that resonant energy transfer is to be expected between the helium (2^3S) metastable atoms and neon ground state atoms, resulting in excitation to the 2s levels and de-excitation of the helium metastable atoms.

The reaction is:-

$$He^* (2^3S) + Ne \longrightarrow Ne (2s_{3,4,5}) + He (^1S_o) + \Delta E \text{ .... } (4.2).$$

The $2s_{3,4,5}$ levels correspond to the $^3P_{o,1,2}$ levels respectively in LS notation, so that spin conservation is obeyed in this reaction. The $2s_4$ level is optically connected to the ground state via a strong far UV transition so that a large electron impact cross section for the reaction

$$Ne + (e + K E) \longrightarrow Ne (2s_4) + e \text{ ..... } (4.3)$$

results in selective excitation of the $2s_4$ level occurring.

Assuming that the neon pressure is high enough for radiation trapping of the far UV photons to occur the $2s_4$ level population is maintained and can decay only radiatively to the 2p state.

Lifetime considerations

The effective lifetimes of the 2s levels of neon have been measured by Bennett (3) and of the 2p levels by Bennett (4), Klose (5), Landenburg (6) and Griffiths (7).

Table 4.1 gives the effective lifetimes from ref. (3) of the two states. The 2s values correspond to 1 torr of neon.

Table 4.1 Radiative lifetimes for the 2p and 2s (Paschen notation) levels of neon, in nanoseconds.

$2s_2$	$2s_3$	$2s_4$	$2s_5$	$2p_1$	$2p_2$	$2p_3$	$2p_4$	$2p_5$	$2p_6$	$2p_7$	$2p_8$	$2p_9$	$2p_{10}$
96	160	98	110	8	10	13	12	11	13	13	16	17	20

The effective lifetimes differ appreciably from the purely radiative ones exhibited by an isolated atom and given by the method of Bates and Damgaard (8), since collisional de-excitation rates can be comparable to radiative decay rates at pressures of a few torr.

From lifetime considerations alone, given sufficient excitation of the 2s levels, it should be possible to obtain population inversion on all of the thirty allowed 2s - 2p transitions, and thus oscillation should be obtainable in a pure neon discharge. Although oscillation on 2s - 2p transitions was first observed in a mixture of helium and neon, oscillation has since been reported in pure neon by Bennett (9) and Chebotayev (10).

Assuming that the electron energy distribution was Maxwellian, Javan (11) calculated that the reaction

$$e + Ne^{*}(1s) \longrightarrow Ne(2p) + e \qquad \ldots\ldots (4.4)$$

and resonance trapping of the 2p —— 1s photons were second order processes, and that inversion would not be upset between the 2s and 2p levels.

At high pressures these second order processes were subsequently found to be of considerable importance, necessitating operation at low pressures, —— where the assumption of a Maxwellian electron distribution is questionable.

The addition of an impurity (argon) to reduce the Ne (1s) metastables, did not achieve the effect desired by reducing this second order process, as the upper state population rate was reduced. (Argon was an unfortunate choice in this respect as it has a high ionisation efficiency.) The addition of hydrogen or oxygen, by Chebotayev (10) in later work using hollow cathode discharges has enabled oscillation in neon on a number of 2s - 2p transitions to be obtained, by reducing the Ne (1s) metastable concentration.

Noting the resonant energy transfer process of (4.2), Javan (12), suggested using a helium-neon mixture in which oscillation in the discharge afterglow might be observed.

Experimental studies by Javan and Bennett (13) showed that in neon the 2s levels decayed with a time variation similar to the $He(2^3S)$ metastables, and laser oscillation was subsequently observed in the afterglow at five wavelengths (in microns):-

1.1180	$(2s_5 - 2p_9)$;	1.1523	$(2s_2 - 2p_4)$;
1.160	$(2s_2 - 2p_3)$;	1.199	$(2s_3 - 2p_2)$;
1.207	$(2s_5 - 2p_6)$.		

The strongest oscillation occurred on the $2s_2 - 2p_4$ transition. This was contrary to expectation as selective excitation of the $2s_2$ level is not expected in collisions with $He(2^3S)$ metastables since the Wigner Spin Rule is violated, —— the $2s_2$ level in LS coupling being a singlet ($^1P_1$) level.

The reaction $He(2^3S) + Ne \longrightarrow Ne(2s_2) + He + \Delta E$ ..... (4.5)

was therefore apparently of greater importance than (4.2).

ΔE is only 313 cm^{-1} for the $2s_2$ level, and 468 cm^{-1} for the $2s_3$ level, so that it appears that the smaller energy discrepancy is more important than the spin conservation requirement, unless LS coupling fails in the Ne(2s) level.

The $2s_2$ level is strongly optically connected to the ground state, so that a large cross section for direct excitation from the ground state is to be expected in the reaction:

$$e + Ne \longrightarrow Ne(2s_2) + e \qquad \text{..... (4.6).}$$

Studies by Bennett (14) have shown that not only are reactions (4.5) and (4.6) of equal importance for the optimum pressures used in the infra-red, rf helium-neon laser (P_{He} approx. 1 torr, P_{Ne} approx. 0.1 torr) but that reaction (4.6) was enhanced by the presence of helium. Evidently the presence of helium enables a higher electron concentration to be obtained without a decrease in electron temperature. An explanation of this is proposed in Chapter 6. Cw oscillation has been obtained now on 25 of the 30 possible transitions between the 2s and 2p levels of neon.

Inverse radial dependence of gain.

Gain measurements on the 1.1523 micron line by Bennett (9) showed that the single pass gain varied inversely as the discharge tube diameter, for diameters ranging from 7 - 30 mm. A similar radial gain relationship has been obtained on the 2.02 and 3.5 micron lines in xenon, and on the optically pumped cesium transition at 7.182 microns (15).

Bennett (15) has shown that the only mechanism which yields a $1/r$ gain dependence in the helium-neon laser is that of atom-atom collisional de-excitation of the metastable/quasi-metastable Ne(1s) levels. A dominant loss mechanism dependent on diffusion to the walls (usually assumed), results in a $1/r^3$ dependence. Using known diffusion constants and estimated cross-sections for helium-neon collisions, a transition from a collision to diffusion limited case, should occur at a bore of approximately 5 mm, within a factor not greater than 3.

In all treatments, the radial dependence of the electron temperature, and its effect on the selective excitation of the upper maser level has been neglected; this is considered in Chapter 6.

Attempts to increase the atom-atom collisional relaxation rate of the Ne(1s) level bottleneck by the addition of argon has led only to a reduction in gain, and it has been presumed that the Penning type reaction

$$He\ (2^3S) + \overset{Ar}{\cancel{Ne}} \longrightarrow \quad Ar^+ + He + e \qquad \text{.....(4.7),}$$

resulting in the destruction of $He(2^3S)$ metastables, is large compared with $He(2^3S) + Ne \longrightarrow Ne(2s_2) + He + e$ of (4.5).

The presence of even small quantities of argon in a glow discharge has been shown by Dorgelo, Alting and Boers (16) to reduce the electron temperature, so that as well as destroying $He(2^3S)$ metastables, the rate of production of triplet metastables and $Ne(2s_2)$ atoms by high energy electrons will be reduced, and lower gain will ensue.

The addition of hydrogen, which is known from the dispersion work of Ladenburg, and Dorgelo (17) to be effective in destroying Ne(1s) metastables has been used as a successful relaxation constituent in a neon maser during the last year by Chebotayev (10), but as yet there have been no reports of the addition of hydrogen to a helium-neon system. The cross section of 6.1×10^{-16} cm^2, (Benton (18)) or 1.7×10^{-16} cm^2 (Jesse and Sadauskis (19)) for the destruction of $He(2^3S)$ by hydrogen molecules is comparable to that of 6.6×10^{-16} cm^2 (Benton and Robertson (20)) for their destruction by argon atoms, so that unless the electron temperature is maintained, little benefit will result from the addition of hydrogen.

The gain measurements of Bennett (14), which proved that a practical amount of gain was obtainable by direct electron impact excitation on the $2s_2$ level of neon, led to an investigation of other pure noble gas systems, and to obtaining oscillation subsequently in them. The addition of helium to the other noble gas systems, where resonant energy transfer processes do <u>not</u> occur with helium metastables, has also resulted in increased gain.

<u>Oscillation in the visible.</u>

Rigden and White (21) observed that the $3s_2 - 2p_4$ transition at 632.8nm in neon was strongly enhanced in a discharge in a helium-neon mixture and concluded that selective excitation was occurring through the reaction

$$He\ (2^1S) + Ne \longrightarrow Ne\ (3s_2) + He + \Delta E \qquad \ldots\ldots(4.7).$$

This was not the first observation of selective excitation of the $3s_2$ level of neon, as enhancement on the vacuum UV transition $3s_2 - 2p^6\ {}^1S_0$

at 60.004nm in neon in a condensed discharge in a helium-neon mixture, had previously been reported in 1938 by Suga (22). Suga concluded that resonant energy transfer from helium (2^1S) metastables to neon ground state atoms was responsible for the enhancement.

Figure 4.3 gives the energy coincidences for helium (2^1S) metastables in neon and shows that the $3s_2$ level of neon lies 386 cm^{-1} (approximately 2 kT) above the singlet helium metastable level and is further from it than the $3s_3$ or the $3s_4$ levels. The $3s_2$ level is a singlet level, so that spin is conserved in reaction (4.7) involving the singlet helium metastable and a ground state neon atom. Unlike reaction (4.5) in which the Wigner Spin rule is not obeyed, in this case the larger energy discrepancy appears to be of less importance than spin conservation. However, there are additional reasons for the selective excitation of the neon $3s_2$ level. The $3s_2$ level is optically connected to the ground state by the strong vacuum UV transition at 60.004nm and has a large cross-section for electron impact excitation, in a similar way to the $2s_2$ level of neon.

The reaction,

$$e + Ne \longrightarrow Ne\ (3s_2) + e \qquad \ldots\ldots\ (4.8).$$

can therefore be as important in selectively exciting the $3s_2$ level, as reaction (4.6) is in exciting the $2s_2$ level of neon. It subsequently appears that direct electron impact excitation of the $3s_2$ level is comparable to the resonant energy transfer process of (4.7).

Although oscillation could not be obtained in the large bore discharge tubes used for the first infra-red masers, Rigden and White (21) were successful in obtaining cw operation at 632.8nm on the $3s_2 - 2p_4$ transition in neon by utilising smaller bore tubes and different optimum pressures. In this operation at 632.8nm, it has not been possible to determine with any certainty that a resonant energy transfer process is actually involved in the selective excitation of the $3s_2$ level.

The lifetime of the He(2^1S) metastables is very short under the operating conditions of the 632.8nm helium-neon laser, so that enhancement is not observed in the afterglow (Suzuki (23)), and it has not been possible to use the elegant time-resolved coincidence technique of Bennett (14) to determine if the 632.8nm spontaneous emission has the same decay rate as the He(2^1S) metastable decay rate.

Inverse radial dependence of gain

Rigden and White (24) have shown that oscillation on the 632.8nm transition exhibits a similar inverse radial gain dependence to that of the 1.1523 micron maser. As well as increasing the diffusion loss of Ne (1s) metastables, a reduction in the bore of a discharge tube results in an increase in the electron temperature, so that the contribution to upper level population by direct electron impact excitation can assume greater significance.

Additional laser transitions from the 3s levels in Neon.

Oscillation from the $3s_2$ level to other 2p levels has now been observed, by suppressing the strong 632.8nm ($3s_2$ - $2p_4$) transition, on seven other lines. There are two omissions, $3s_2$ - $2p_9$ and $3s_2$ - $2p_{10}$. At the time of writing, although transitions from the $3s_{3,\ 4\ \text{and}\ 5}$ to the 2p group have been shown by Zarowin and Schiff (25) to show some gain, oscillation has still to be reported on them.

Bloom et al.(26) were the first to report oscillation from the $3s_2$ to the 3p levels, ($3s_2$ - $3p_4$) at 3.39 microns. The gain on this transition (more than 20 db per metre) is sufficient to saturate the medium, and can prevent oscillation at 632.8nm by depleting the population of the common $3s_2$ upper level.

Although oscillation has not been obtained on the $3s_{3,\ 4,\ \text{and}\ 5}$ levels to the 2p levels, oscillation between the $3s_4$ and $3s_5$ levels and the 3p group have been observed (Patel et al.(27).

Resonant energy transfer between He(2^1S) metastables and the 4f levels in neon, which lie approximately 4 kT above the metastable level, is also considered responsible for selectively populating the 4f levels and so enabling oscillation to be obtained on six 4f - 3d transitions at 1.8 microns (28).

4.1.2 Mercury - Zinc System

Before oscillation at 1.1 microns in neon had been reported, Ablekov et al.(29) reported obtaining considerable gain in a mercury-zinc discharge

at 636.2nm, corresponding to the $4\ ^1D_2 - 4\ ^1P_1$ transition in zinc. The selective excitation mechanism proposed being

$$Hg\ (7\ ^3S_1) + Zn \longrightarrow Hg + Zn\ (4\ ^1D_2) - \Delta E \quad \ldots\ldots (4.9)$$

where $\Delta E = 133\ cm^{-1}$.

Mercury atoms in the $7\ ^3S_1$ state act as donors in a resonant energy transfer process with ground state zinc atoms to give excitation to the $4\ ^1D_2$ level of zinc, 133 cm^{-1} above the $7\ ^3S_1$ state. Decay of the lower $4\ ^1P_1$ level takes place through UV radiation at 213.8nm. The lifetimes of these levels are in the ratio of $2.5 \times 10^{-8}/1.7 \times 10^{-9}$ and so satisfy the oscillation lifetime requirement.

In spite of the reported optical amplification of 10 at 636.2nm oscillation has not been reported in this system. It would appear that the earlier experimental results were misinterpreted.

(Private Communication, Prokhorov (1964), work is about to recommence on this system; no reply given to query about oscillation.)

4.1.3 Helium-krypton and neon-xenon systems

Oscillation in the visible was obtained in the afterglow of pulsed helium-krypton and neon-krypton discharges by Dana and Laures (30) in 1964.

In each case, helium and neon are buffer gases at high pressures (3 to 10 torr) and only small quantities (10^{-4} - 10^{-2} torr) of krypton and xenon are necessary to sustain oscillation.

The excitation mechanisms, in which spin is conserved, are:

$$He\ (2^3S) + Kr^+(^2S_{1/2}) \longrightarrow He(^1S_o) + Kr^+\ (6s\ ^4P) + \Delta E \quad (4.10),$$

$$Ne\ (1s) + Xe^+(^2S_{1/2}) \longrightarrow Ne(^1S_o) + Xe^+\ (7s\ ^4P) + \Delta E \quad (4.11).$$

The He (2^3S) metastable level is approximately 2000 cm^{-1} (0.25 eV) above the Kr^+ ($6s\ ^4P$) levels and resonant energy transfer occurs between the helium and krypton levels. The Kr^+ ($6s\ ^4P$) levels decay in transitions having strong oscillator strengths predicted on the basis of LS coupling, and oscillation can be obtained.

Similarly, in the neon-xenon mixture, resonant energy transfer occurs between the Ne (1s) levels and the $7s\ ^4P$ levels of singly ionised xenon. ΔE is approximately 1200 cm^{-1} (0.15 eV) and population inversion occurs in the afterglow between the $7s\ ^4P$ and $5d'\ ^2S$ levels, and the $6p\ ^4P$ and $6p\ ^4D$ and $5d'\ ^2S$ levels, and the $6p\ ^4P$ and $6p\ ^4D$ levels. Oscillation occurs only in the afterglow as stated, with spontaneous emission lasting 25 - 30 microseconds. It will be noted that the above reactions for an atom-ion collision are resonant with energy discrepancies of up to 0.25 eV, so that the requirement for resonance involving ions is not as restrictive as for resonant atom-atom collisions in which ΔE must be of the order of a few kT, presumably because polarisation occurs during the collision.

The lower laser levels for the reported lines in krypton are the upper levels for laser lines reported in pure krypton by Bridges and Chester (31) so that rapid depopulation of the lower levels can occur. Oscillation on the lower level laser lines obtained in low pressure pulsed krypton discharges (31) was not observed in the high pressure helium-krypton discharges of Dana and Laures, so that the selective excitation appears almost certainly to be of a collisional type.

The strongest lines in both krypton and xenon obey the selection rules $\Delta J = \Delta L = 0$.

4.2 Charge transfer collision masers

A number of successful lasers have been observed in which the selective excitation of the upper laser level appears to be through a charge transfer, or electron exchange collision.

In only two cases has the mechanism producing population inversion been reasonably determined as being due to a charge transfer collision.

These two are the helium-iodine and helium-mercury systems.

4.2.1 Helium-Iodine System

The first laser in which charge transfer was proposed as the selective excitation process, was the helium-iodine system reported by Jenson and Fowles (32).

Oscillation was obtained by them in the afterglow of a pulsed helium-iodine discharge, from three levels in singly ionised iodine, within 0.51 eV of the helium ion ground state. The proposed upper state populating mechanism was:-

$$He^{+}\ (^{2}S_{1/2}) + I\ (^{2}P_{3/2}) \longrightarrow He\ (^{1}S_{o}) + I^{+}(6p^{3'}) + \Delta E \quad \ldots\ (4.12),$$

where ΔE was between 0.21 - 0.51 eV.

The 6p levels which were preferentially excited are all triplet levels. Although there are singlet levels which lie closer to the helium ion ground state than the triplet levels, oscillation does not occur on transitions from them. Fowles and Jenson (33) suggested that this was a case in which the Wigner Spin selection rule applies. There is a triplet level, however, neglected by Fowles and Jenson which is within 0.2 eV of the helium ion

ground state from which there is a strong analogous laser transition in isoelectronic doubly ionised xenon, yet oscillation is not observed from this triplet ($6p'\ ^3F_3$) level.

Typical operating conditions were a few torr of helium and 0.2 torr vapour pressure of iodine, in a 5mm diameter, 1.2m long, cold cathode pulsed discharge. Oscillation was also observed on two transitions in a neon-iodine discharge when rf excitation was used together with high current pulses. These two transitions have analogous laser transitions in singly ionised chlorine and doubly ionised xenon, and the selective excitation is extremely likely to be by a two stage, electron impact, typical ion laser process.

A full analysis of this system is given in Chapter 7, together with results obtained in research undertaken on this system.

4.2.2 Helium-Mercury System

Laser action in gaseous ions was first observed in ionised mercury, by Bell (34), who obtained oscillation in the afterglow of a pulsed helium-mercury discharge, on green (567.7nm), orange (615.0nm), and a number of infra-red transitions in singly ionised mercury.

Since the first reported oscillation, oscillation has been reported at other wavelengths, with other inert gas-mercury mixtures, and in pure mercury by a number of workers (35) - (39).

The following three selective excitation mechanisms have been suggested for this high gain, (greater than 20 per cent/metre) system.

(1) Bloom, Bell and Lopez (35) suggested that direct electron impact excitation from the ground state populated the upper laser levels of the 567.7 and 615.0nm transitions. They accounted for the hollow beam formation which they observed, under certain excitation conditions, and the ability to change from oscillation at one wavelength to another by apparently minor changes in their pulse rise time and current, as being due to changes in the electron energy distribution. Fig. 4.4 shows the transitions first observed by Bloom, Bell and Lopez (35).

(2) Dyson (40) has shown fairly conclusively that in the case of the 615.0nm line, the selective excitation in his discharge system was that of charge transfer involving the helium ground state ion, the reaction suggested being

$$He^{+}(^{2}S_{1/2}) + Hg(^{1}S_{o}) \longrightarrow He(^{1}S_{o}) + Hg^{+}(7^{2}P_{3/2}) + \Delta E \quad \ldots\ldots \quad (4.13)$$

where $\Delta E = 0.15$ eV, with a cross-section of 1.3×10^{-14} cm^2 comparable to the Penning ionisation cross section for $He(2^{3}S)$ + Hg of 1.40×10^{-14} cm^2.

(3) Suzuki (41), using a time resolved spectroscopic gating technique, showed that the intensity of the 615.0nm line was proportional to the product of the densities of metastable helium and metastable mercury atoms in the discharge system that he was using. He concluded that the selective excitation mechanism was that originally proposed by Paschen (42) to explain enhancement of the 615.0nm line observed in a helium-mercury hollow cathode discharge:-

$$He^{*}(2^{3}S) + Hg^{*}(^{3}P) \longrightarrow He + Hg^{*}(7^{2}P_{3/2}) + (e + KE) \quad \ldots\ldots (4.14).$$

An estimate of this cross section is approximately 10^{-14} cm^{2}. Fig. 4.5 shows the energy relation between the metastable states of mercury and helium.

The excitation conditions used by Suzuki and Dyson differed. Dyson used a discharge tube of 2.3 cm bore and Suzuki one of 6mm bore, so that differences in results might be expected. Although Suzuki used short excitation pulses of 0.5 microseconds which are considered not to give large metastable concentrations (Hasted (43)), his selective excitation is still attributed to metastable-metastable collisions.

According to Bridges and Chester (44), Bell and Bloom have recently obtained oscillation at 479.7, 567.7 and 615.0nm in a pure mercury discharge (as yet unpublished), so that it is evident that a number of selective excitation processes are involved in the mercury systems, which include charge transfer, direct electron impact excitation and metastable-metastable collisional energy transfer.

Further evidence that electron impact excitation is of considerable importance in the helium-mercury system, is that oscillation has now been observed in other Group 2a elements, - cadmium and zinc - on identical transitions to those on which oscillation is observed in mercury. On only a few of these transitions in cadmium or zinc does collisional energy transfer appear likely.

Given in Appendix 4.1 are the equivalent laser transitions in zinc, cadmium and mercury, together with lists of the neutral and ionised levels involved in the laser transitions. Indicated also, are the possible metastable-metastable, ion-atom, resonant type collisions responsible for the selective excitation.

4.3 Atom-molecule lasers.

At least four gas systems have exhibited maser action on dissociation by collisions with metastable atoms of another gas. These include:-

(a) Ne - O_2 ; Ar - O_2, He or Ne - CO or CO_2, He or Ne - NO or N_2O giving oscillation in atomic oxygen at 844.6nm (Patel et al. (45, 46)).

(b) He or Ne - CO or CO_2, giving oscillation in neutral atomic carbon in the infra-red (45, 46).

(c) He - SF_6, or SF_6 giving oscillation in neutral atomic sulphur (45, 46).

(d) Argon - Br_2, giving oscillation at 844.6nm, in an unknown species, most likely atomic bromine (45, 46).

4.3.1 Ne - O_2, Ar - O_2 Systems

It is only in these two masers that a quantitative description can be given of the excitation process involved, as collision cross sections are known only for energy transfer from neon or argon metastables to oxygen. For a comprehensive account of these systems the reader is referred to Patel (47).

The pertinent energy levels of neon and argon, the oxygen molecule and atomic oxygen are shown in Fig. 4.6 after Bennett et al. (48). Maser action is obtained at 844.6nm on the $3p\ ^3P_2 \longrightarrow 3s\ ^3S_1$ transition of atomic oxygen.

In the Ne - O_2 maser, collisions of oxygen molecules with neon metastables, result in molecular dissociation, leading to ground state (2^3P) and excited (3^3P) oxygen atoms being produced.

Radiative decay occurs from the 3^3P level to the 3^3S level, and then to the atomic ground state giving radiation at around 140.0nm. The radiative lifetime of the $3\ ^3P_2$ level is approximately 3×10^{-8} sec, and the $3\ ^3S$ level approximately 10^{-9} sec, so that the transition probabilities are suitable for oscillation. The low atomic ground state oxygen population ensures that radiation trapping does not limit this system as it does in other atomic systems.

The excitation process is:-

$$Ne^* (^3P_1, ^3P_o) + O_2 \longrightarrow O\ (3p\ ^3P) + O\ (2^3P) + Ne \quad \ldots\ldots (4.15).$$

The Ar - O_2 system is slightly different from that of Ne - O_2, in that it involves a two step process leading to the preferential excitation of the 3^3P level of atomic oxygen. Argon metastables have insufficient energy to give direct excitation to the 3^3P level, but are efficient in giving dissociation to the metastable 2^1S and 2^1D levels, as follows

$$Ar^*\ (1s) + O_2 \longrightarrow O^*(2^1S, 2^1D) + O(3^3P) + Ar \quad \ldots\ldots (4.16),$$

or

$$\longrightarrow O^*(2^1D) + O^*(2^1D) + Ar \quad \ldots\ldots (4.17).$$

The second reaction giving one excited and one ground state atom is the more usual form of dissociative energy transfer.

The metastable oxygen atoms are then excited by electron impact to the 3^3P level, resulting in population inversion occurring. The operating conditions for both systems are slightly different, but result in similar population inversions.

4.4 Electron Impact, - Pure noble gas masers

It was the gain results of Bennett (9) on the $2s_2 - 2p_4$ transition in neon at 1.1523 microns which showed that a practical amount of gain was obtainable in a system that relied on electron impact excitation alone for selective excitation.

Subsequently Patel et al. (49) have produced cw maser oscillation on 14 noble gas transitions, and have extended cw operation out to 133 microns in the noble gases; most of the transitions being in neon.

4.4.1 Neutral lasers

The electron configuration of neon, argon, krypton and xenon are similar; the ground state is $(np)^6$, where n = 2, 3, 4 and 5 respectively. In each gas, there are strongly allowed optical transitions from the levels in the higher $(np)^5$ ms and $(np)^5$ md configurations, and so the main excitation occurs through reactions of the type,

$$e + (np)^6 \longrightarrow (np)^5 \text{ ms} + e \qquad \ldots\ldots (4.18)$$

$$\text{and } e + (np)^6 \longrightarrow (np)^5 \text{ md} + e \qquad \ldots\ldots (4.19)$$

where m = n + 1, n + 2 etc as shown in Fig. 4.7.

For the pressures at which these masers are operated (P_{Ne} 0.01 - 0.2 torr, in up to 40mm bore tubes), the strongly allowed UV transitions to the ground state are radiation trapped, and the s and d states can only decay through transitions to the lower lying excited p states. These are marked as MASER in Fig. 4.7.

The radiative lifetimes of levels $(np)^5$ mp configurations are of the order of 10^{-8} sec due to transitions of the type mp - (n + 1)s. Thus these levels are suitable laser levels and population inversions can occur between the s and p, and the d and p levels.

In spite of this, it is found that more maser transitions are observed in neon and argon from transitions between the higher lying s, p, d and f levels, than between the s and p, and the d and p levels.

It is only in the case of the 5s - 4p transitions, where the He (2^1S) metastables are considered responsible for selectively exciting the 5s level, that the populating mechanism is known. The only explanation seems to be that a large part of the excitation to the high lying states arises from cascade transitions, or through electron-ion recombination.

As stated in section 4.1.1, it has been found that the addition of large quantities of helium to an rf discharge in xenon increased the optical gain on a number of transitions (Patel et al. (50)), but particularly at 2.026 and 3.508 microns. This increase in gain has been attributed to an increased electron density, or an increased temperature, or both. Aisenburg (51). using a multi-probe technique, has observed an increase in the electron density but no appreciable change in the electron.

temperature when helium was added to an rf discharge in xenon under lasing conditions.

In a dc discharge in xenon the addition of helium only results in a slight increase in gain, and at the higher currents necessary, cataphoresis occurs and the gain is greatly reduced (Bridges, (52)).

4.4.2 Ion lasers.

Oscillation in gaseous ions was first observed by Bell (34) in singly ionised mercury, in the afterglow of a pulsed, high current discharge. Whilst investigating the effect of noble gas buffers on the visible mercury laser ion lines, oscillation was observed in singly ionised argon. Even small traces of argon were sufficient in which to sustain oscillation (Bridges (53), Convert et al. (54) (55)).

Unlike the afterglow oscillation in mercury, oscillation in argon was observed during the excitation pulse. Quasi-cw operation, longer than any time constants of reasonable atomic processes was reported in ionised argon by Bennett et al. (56) who obtained output powers of watts for about a millisecond.

By utilising small bore tubes, giving increased current density, cw operation was achieved by Gordon et al. (57) on most of the strong singly ionised argon, krypton and xenon lines.

Oscillation has now been obtained in over 20 elements on over 250 transitions, in singly, doubly and triply ionised species, extending over the UV, visible and IR regions of the spectrum (Cheo and Cooper (58), Bridges and Chester (59)).

The selective excitation in the majority of these transitions is by electron impact, and is characterised by two types of process,

(i) the sudden perturbation process of Bennett et al. (56)

(ii) the two step process of Gordon et al. (60).

(i) Sudden perturbation process

This first process has been used to interpret pulsed low pressure discharges, in which there is a preponderance of p - s and p - d laser transitions. Bennett (56) has shown that the sudden perturbation process results in mainly excited states in the ion core having the same parity as the ion ground state. Having the same parity as the ion ground state, radiative decay can occur to lower levels which can be relaxed by strong vacuum UV transitions to the ground state. This populating mechanism only appears dominant in pulsed discharges with high E/p, and short pulse duration.

The sudden perturbation treatment has been extended to higher degrees of ionisation than the first, in which this process must occur with excitation, not from the neutral ground state, but from the ion ground state of the preceding degree of ionisation. This interpretation has been borne out by the observations of Cheo and Cooper (61), who report that doubly ionised lines only appear after saturation of the singly ionised lines, consistent with a two step process.

(ii) Two-step process

This process was proposed to explain the small bore cw argon ion laser, and is a two stage process:

$$Ar\ (3p^6) + e \longrightarrow Ar + (3p) + 2e \quad \ldots\ldots (4.20),$$

$$\text{then } Ar^+(3p) + e \longrightarrow Ar^+ (4p) + e \quad \ldots\ldots (4.21).$$

The evidence to support this process is that the spontaneous emission rate of the upper argon ion levels varies as the square of the discharge current.

Another two step process has been proposed by Bennett and Lichen (62), which is as follows

$$Ar\ (3p^6) + e \longrightarrow Ar^* (3p^5\ 4s) + e \quad \ldots\ldots (4.22),$$

$$\text{followed by } Ar^* (3p^5\ 4s) + e \longrightarrow Ar^+ (4p) + 2e \quad \ldots\ldots (4.23).$$

In this process, the first step produces metastable argon atoms in the $3p^5\ 4s$ level; the second electron impact produces the selective excitation to the Ar^+ (4p) level.

4.4.3 Transient Lasers

The first transient laser was reported by Fowles and Jenson (63) who observed a high gain laser transition $6p\ 7s\ ^3P_1 - 6p^2\ ^1D_2$ at 722.9nm in the spectrum of neutral lead. The lower laser level has the same configuration as the lead ground state, and is metastable. The laser transition is also forbidden for electric dipole radiation in LS coupling, though it is observed as a fairly intense line in the arc spectrum of lead.

Transient oscillation has also been reported by Piltch et al. (64) in neutral manganese, and recently oscillation has been observed in neutral atomic copper vapour at 510.54nm (58 db/m, 2 kW peak power) and at 578.213nm (42 db/m, 0.6 kW peak power), by Walter et al. (65).

Physical properties of the new transient lasers

All the transient lasers are typified by the lead and copper systems, the energy level diagrams of which, laser transitions and excitation paths are shown in Figs. 4.8 and 4.9 and are characterised by the following:

(a) the upper laser level is a resonance level, having an opposite parity to the ground state, with the excitation provided by electron-atom collisions.

(b) the lower laser level is metastable having the same parity as the ground state.

(c) the transition probability of the laser transition is smaller than that of the excitation transition (approximately 10^8 sec^{-1}), but larger than the relaxation transition (approximately 1 sec^{-1}).

Experimental conditions

(i) To obtain sufficient vapour pressure of suitable elements high temperatures have been used in the lasers reported so far. The temperatures used have ranged from 800°C in the case of lead to 1500°C in the case of copper, giving vapour pressures of 0.1 to 0.3 torr.

(ii) Carrier gases of helium or neon at pressures of 1 - 3 torr, enable the discharge to be carried from the electrodes to the metallic vapour region, and prevent metallic vapour from being deposited on the Brewster angled windows.

(iii) The pulse rise time has to be shorter than the radiative lifetime of the laser transition to enable sufficient population inversion to build up. To achieve this, the pulse excitation has taken the form of a simple capacitor discharge through internal electrodes, or by the discharge of a delay line, charged to about 7.5 kV through a spark gap in series with the discharge tube.

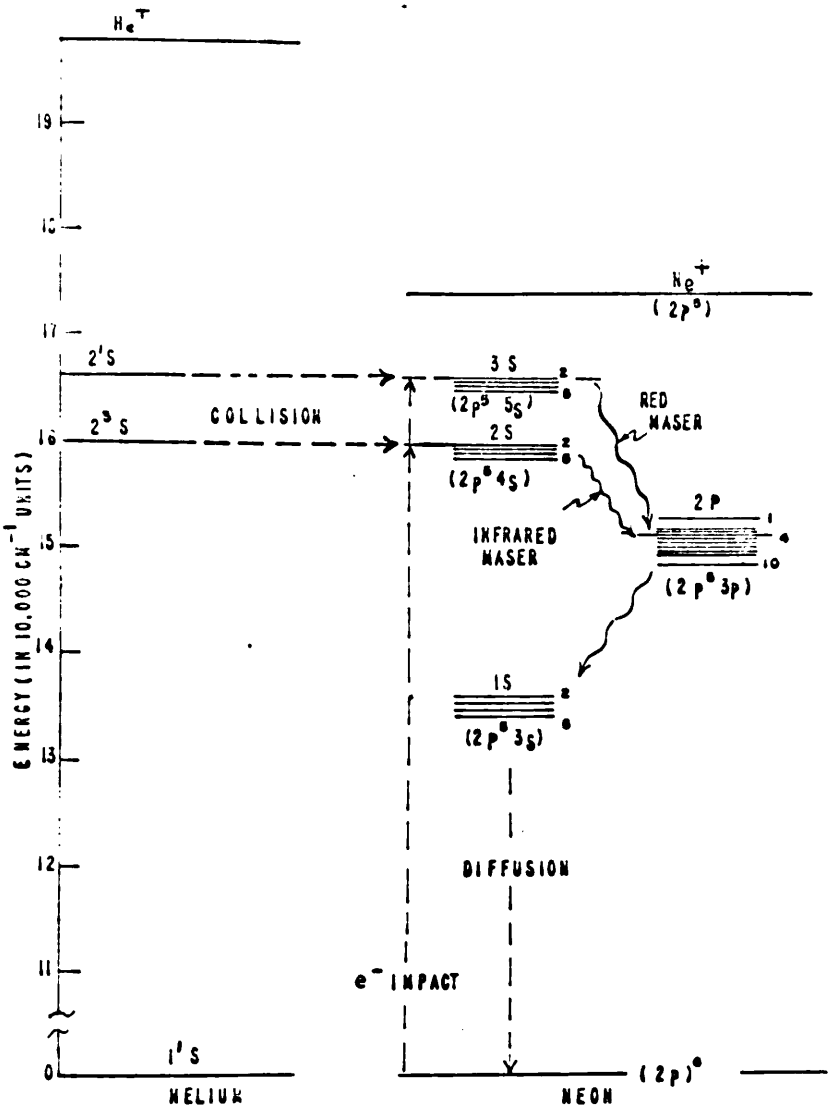

He-Ne energy levels. The dominant excitation paths for the red and infrared maser transitions are shown.

Fig. 4.1

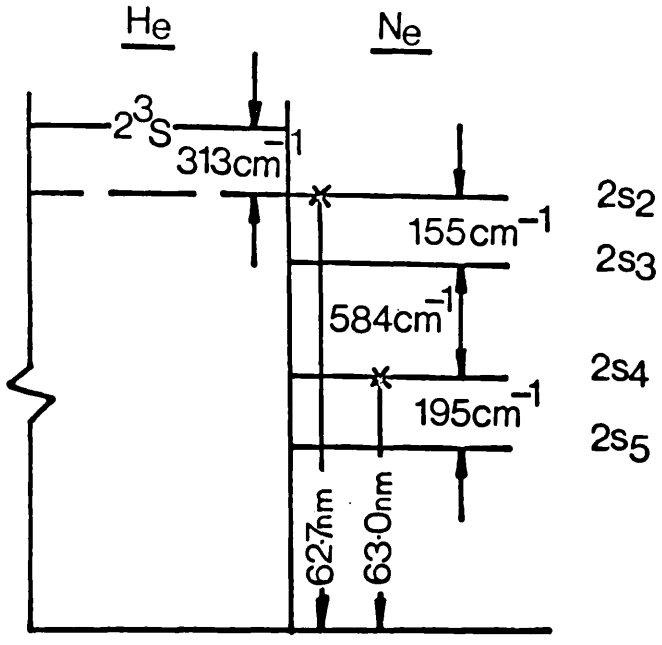

Fig. 4.2

Helium (2^3S) metastable energy level coincidences in Neon.

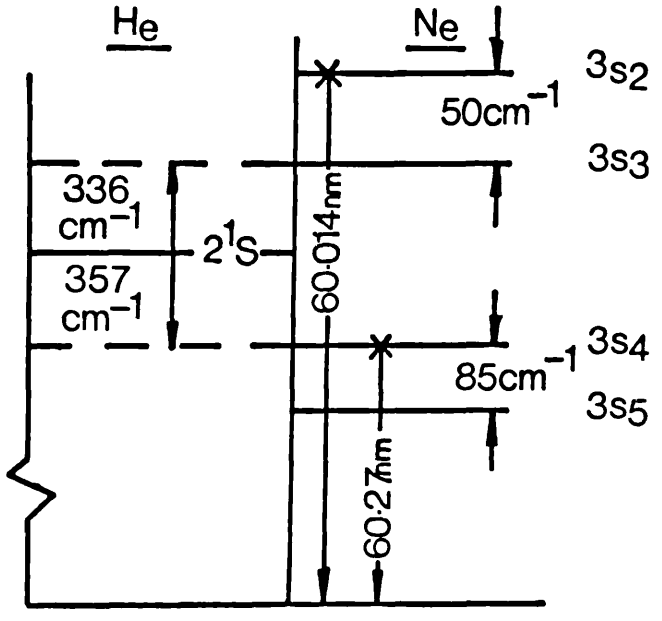

Fig. 4.3

Helium (2^1S) metastable energy level coincidences in Neon.

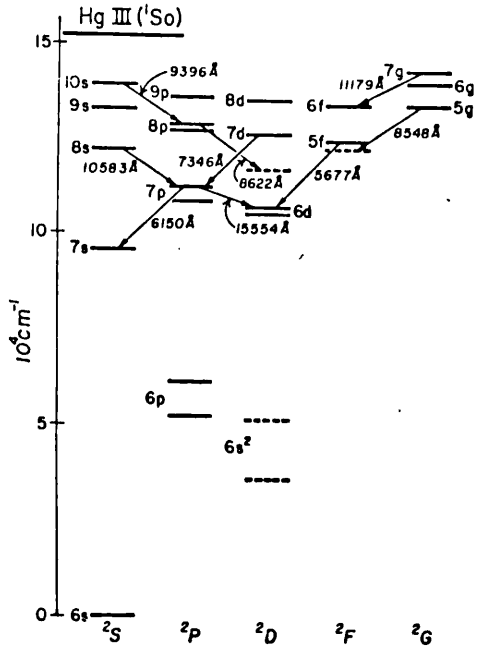

Fig. 4.4

Partial energy level diagram of Hg II showing laser transitions, (after Bloom et al.(35)).

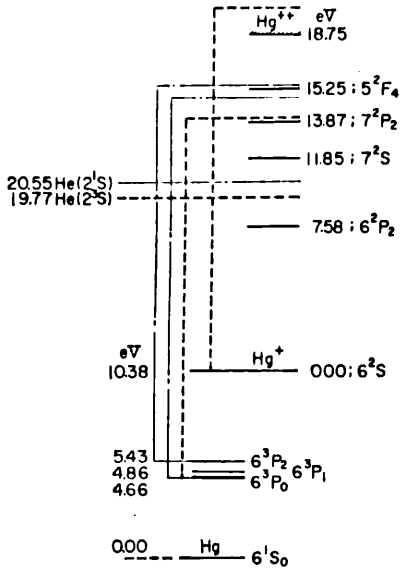

Fig. 4.5

Energy relation between states of mercury and metastable states of helium,(after Suzuki,(41).

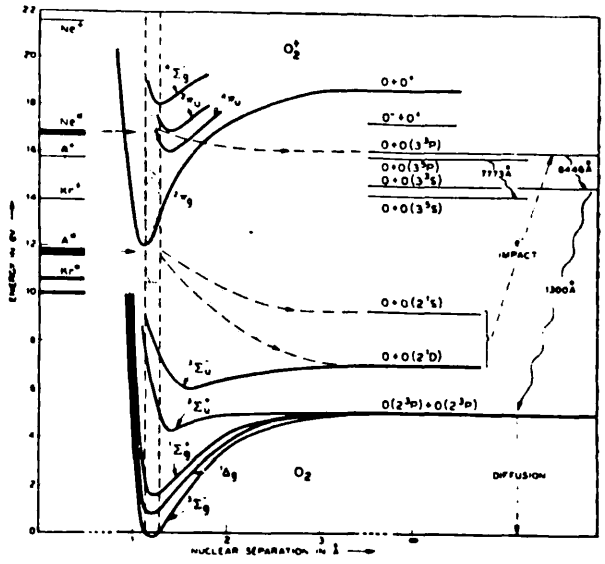

Fig. 4.6

Energy levels[69] pertinent to the neon–oxygen and argon–oxygen masers.[8] The dominant excitation paths in these two systems are indicated by the arrows.

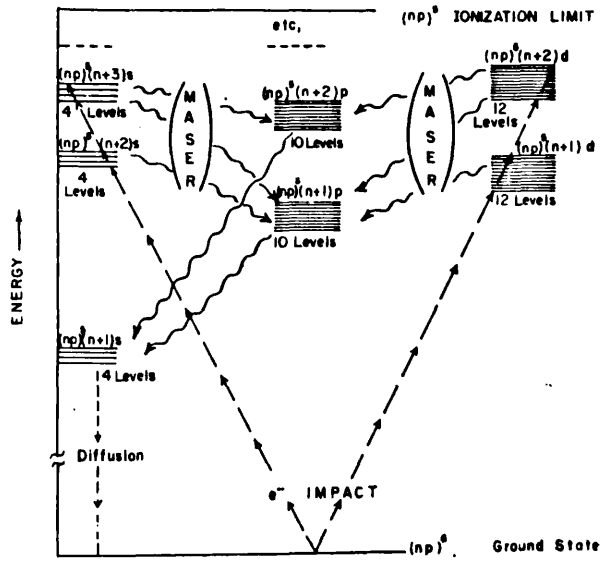

Fig. 4.7

Schematic indication of electron configurations pertinent to the pure neon, argon, krypton, and xenon masers. The dominant excitation paths are indicated by the arrows.

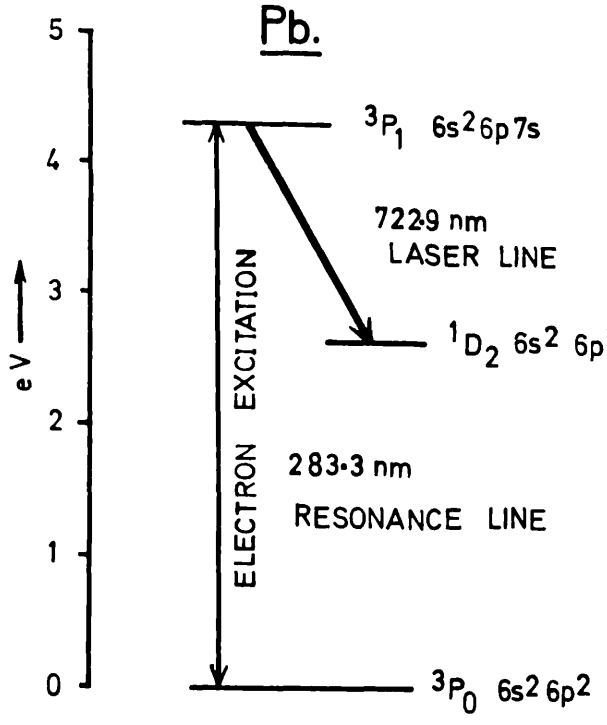

Fig. 4.8

Energy level diagram for the lead laser.

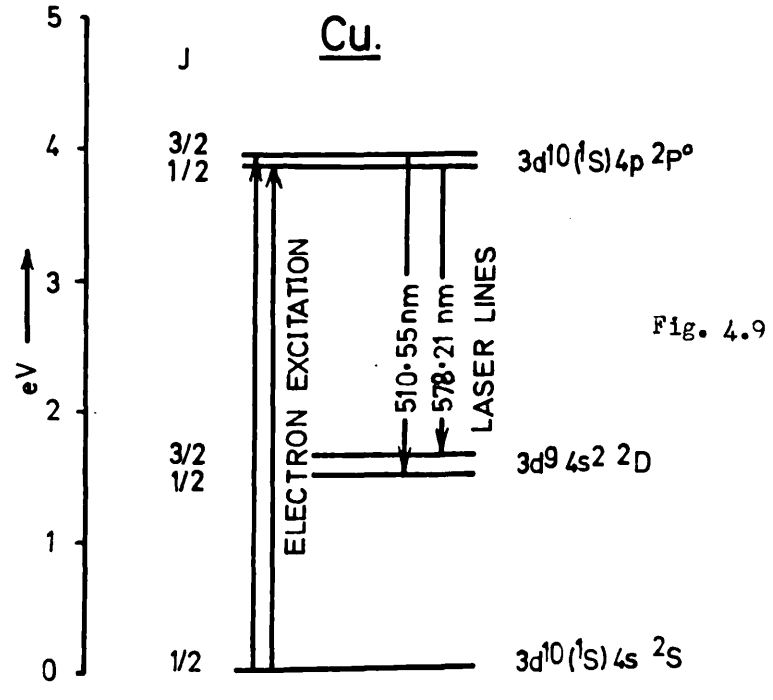

Fig. 4.9

Energy level diagram for the copper laser.

CHAPTER 5

Population Inversion in the negative glow plasma of a Hollow Cathode Discharge

Introduction

The resonant, atom-atom, energy transfer process, in 1963 believed to be the predominant selective excitation process in the helium-neon laser, indicated that this process would be the sort of process to seek for other laser systems.

The negative glow Hollow Cathode Discharge (H.C.D.) has the following properties which made it worthy of consideration as a laser medium.

(a) Atom-atom processes

The literature indicated that atom-atom collisional processes were of considerable importance, in the low-field, electron-beam maintained plasma of the H.C.D.

(b) Narrow line-width

Under suitable conditions, the H.C.D. can give extremely narrow lines, having been used extensively for hyperfine structure analysis by Schuler (1), Tolansky (2) and Roesler and De Noyer (3). The fractional gain in a laser (g_o) is inversely proportional to $\Delta\nu_D$, assuming the line is Doppler broadened (Heavens (4)), as is shown by (1.1). Considerable advantage is, therefore, to be expected in using a source that provides narrow emission lines.

(c) Electron concentration

The electron concentration is larger in the negative glow-region of a glow discharge than in the positive column, and is larger by two orders of magnitude in the H.C.D. (Badareu and Wachter (5)). Further, it is believed that a non-Maxwellian electron energy distribution biased to high energies occurs in the H.C.D. at the cathode edge of the negative glow plasma, (Francis (6)).

(d) Radiant intensity

The radiant intensity in the H.C.D. is many times larger than that in the positive column of the glow discharge. (Popovici and Somesan (7)).

(e) Sputtering mechanism

The sputtering action of the H.C.D. provides an atomic vapour of the material of which the cathode is constructed, without the need for high temperatures to provide sufficient vapour pressure in which to obtain laser oscillation. By a suitable choice of cathode material and carrier gas, population inversion through resonant energy transfer collisions appeared possible. This, in 1963 would have extended laser investigations into the non-gaseous elements, and possibly into shorter wavelengths than were then available. (Pulsed oscillation has now been obtained in non-gaseous elements by Bell et al. (8); Piltch et al. (9); and Silfvast et al. (10) using high temperature techniques.)

(f) Molecular processes

The negative glow of a glow discharge is a recombination-dominated plasma, (Hurt, (11)). Molecular processes are of considerable importance in such a plasma and are therefore of interest in basic laser studies.

(g) Plasma uniformity

No striations or instabilities have been reported in electron-beam maintained, field free plasmas, and the same is to be expected in the H.C.D. (Birger-Persson (12)).

5.1 Specific systems

The H.C.D. was investigated as a means of obtaining population inversion and cw laser oscillation in:

(1) metallic elements which have low vapour pressures and high melting points.

(2) the ion species of a gas mixture.

(3) pure neon; or in a helium-neon mixture, at low pressure at 632.8nm.

5.1.1 Population inversion in metal vapours

Resonant energy transfer reactions of the type

$$M + G^{*} \longrightarrow M' + G \pm \Delta E \qquad \ldots\ldots (5.1)$$

where M here indicates a metal atom, and G a carrier gas atom, were considered, for $\Delta E < \pm$ 0.1 eV, in which large cross sections for energy transfer occur (see Fig. 2.4 from Mott and Massey (13)).

Suitable combinations were determined, of the inert gases helium, neon and argon, and of elements from which cathodes or cathode liners could be

made and in which close energy coincidences occurred between metastable levels of the inert gas and the cathode element.

The metastable levels of the inert gases are higher than the ionisation potentials of other elements, so that reaction (5.1) becomes the familiar Penning reaction:-

$$M + G^{*} \longrightarrow M^{+'} + G + (e + \Delta E)\ (00'/1'0e) \qquad \ldots\ldots (5.2).$$

In this reaction an electron is available to remove any excess potential energy and resonant restrictions are not as stringent as for non-ionising, atom-atom excitation transfer collisions.

Assuming that particular levels would be selectively excited by this process, with ΔE of the order of a few kT, transitions were determined from Atomic Energy Levels (14) and examined for laser suitability. Possible resonant energy combinations of the inert gases and mercury, with various cathode materials are given in Appendix 5.1.

Because of the high sputtering yield of neon (15) and information available on the concentration of neon metastables in a H.C.D. (16), combinations of neon and cathode materials were given special attention.

Figs. 5.1 - 5.3 show electric dipole radiation transitions with suitable lifetimes for the upper and lower levels in which the upper level has a close energy coincidence with a neon 1s metastable level.

The neon-aluminium combination was chosen for experimental studies for the following reasons: (i) transition probabilities are calculable for ionised aluminium with sufficient accuracy using the Bates and Damgaard Central Field approximation, and (ii) neon can give a high sputtering yield of aluminium.

5.1.2 Population inversion in gas mixtures

Consideration of the report of population inversion in a mercury-zinc system (later unsubstantiated) by Ablekov et al. (17), and various aspects of the operating conditions of the helium-neon positive column and rf excited lasers led to an examination of the H.C.D. as an excited medium for gas, and gas mixture lasers. Three systems were examined:-

(i) helium-mercury;

(ii) helium-iodine; and

(iii) helium-neon; and neon; at low pressures.

In both mercury and iodine, the spectrum lines show extensive hyperfine structure, and it was of considerable interest to examine such structure during laser oscillation.

(i) Helium-mercury

Laser oscillation was first observed in the ion species, in mercury, in a mixture of helium and mercury under pulsed excitation conditions by Bell (18). Oscillation occurred on two visible lines and on a number of lines in the infra-red. The behaviour of the laser output was such to indicate that saturation was not occurring so that cw operation might be possible in a suitable source.

During an experiment designed to determine if mercury was an effective carrier gas in producing sputtering and to check whether the Al II line at 390.0nm (see 5.8.3.) was enhanced in a H.C.D. with a carrier gas other than neon, it was necessary to identify strong spectrum lines in the region of 400nm.

In this identification it was found that the strong lines originated from highly excited mercury ion levels, above the levels from which laser transitions occur. It was a small step then to check for the lines on which oscillation had been obtained in the range 300 - 800nm, in the H.C.D. spectrum. In this range, all the lines on which oscillation had been obtained under pulsed conditions were observed in the H.C.D., with intensities comparable with those of Hg I lines. A later literature search revealed that these lines had been observed and examined by McLennon (19), Naudé (20), and Mrozowski (21) in a H.C.D. in mercury and helium-mercury mixtures. In view of this, a number of experiments were carried out to see if it was possible to maintain a plasma in a long metal hollow cathode, with a length of greater than one metre, necessary for obtaining a practical amount of gain.

Studies were also made of multi-cathode hollow cathode discharges.

(ii) Helium-iodine

Pulsed laser oscillation was first obtained by Fowles and Jenson (22), on 12 visible and near infra-red lines in the neutral and ion spectrum of iodine. Oscillation occurred only in the afterglow.

In studies of halogen excitation using argon, neon and helium, Berezin and Yanovskaya (23) observed that the intensity of certain ionised iodine lines was considerably enhanced when a helium-iodine mixture was excited in a H.C.D. Three of the lines λs 498.6, 521.6 and 540.7nm which were found to be enhanced in the wavelength range 440.0 - 570.0nm (Table 7.1), have exhibited pulsed laser oscillation. The maximum intensity of these ionised lines in the H.C.D. occurred at a pressure of 17 torr.

The high pressure operation of the H.C.D. of Berezin and Yanovskaya and the relatively high pressure of operation (a few torr of helium) of Fowles and Jenson, indicated that the helium-iodine system was almost certainly a resonant collisional system with atom-atom, atom-ion, or atom-molecule collisions being responsible for the selective excitation of the upper laser levels. Since the upper laser levels, with one exception, are within 0.51 eV of the helium ion ground state, Fowles and Jenson suggested that the selective excitation was one of the charge exchange type (10/01'). The high gain in this system does suggest that the excitation is via a resonant process. However, energy transfer processes have only been considered resonant when the energy discrepancy is less than 0.1 eV, and large collision cross sections are, by the Massey 'near-adiabatic hypothesis', not expected for slow ions.

Dr. R. Stebbings (private communication) has shown that a large collision cross-section occurs in the slow molecule, $O^+ + N_2$ collision but only when resonance is obtained. Presumably polarisation or Coulomb forces, which could account for the large $\triangle E$ for resonant ion-atom collisions, are not relevant to 3 body ion-molecule collisions.

A series of experiments were carried out to see if cw laser oscillation could be achieved in a helium-iodine H.C.D., and to try to determine the energy transfer mechanism involved in the selective excitation of certain ionised iodine energy levels. These experiments are covered in 5.11.

(iii) Helium-neon and neon at low pressure.

This system is included as a separate treatment in 5.12, together with experimental work and results.

5.2 The neon-aluminium, metal vapour system

5.2.1 In order to achieve cw laser oscillation (1.3) shows that lifetimes of the upper and lower levels must be suitable, and that the rate of excitation to the upper level must be sufficient to enable the gain to be greater than the overall system losses.

The investigation of the neon-aluminium system consisted of two parts:-

(a) Calculation of the transition probabilities of the proposed Al II laser transitions.

(b) Experimental measurement of the absolute intensity of the proposed laser line, under optimum conditions, to determine the steady state population of the upper level and rate of excitation to the upper level.

5.2.2 Calculation of transition probabilities

The calculation of transition probabilities between levels of an atomic system entails the evaluation of transition integrals for the levels concerned. Bates and Damgaard (24) have shown that almost the whole contribution to the transition integrals involved arises from the region of the atom for which a Coulomb approximation for the potential is valid.

The integrals may thus be expressed, as in the case of the hydrogen atom, in terms of hypergeometric functions. The integral quantum numbers of hydrogen are replaced by the effective quantum numbers (n^*).

$$n^* = 1/\epsilon^{1/2} \qquad \ldots\ldots (5.3)$$

where ϵ is the energy in Rydbergs for exciting the neutral atom. Tables for evaluating the radial part of the transition integral have been given by Bates and Damgaard.

The spontaneous transition probability for radiation from state A to state B is given by Condon and Shortley (25) as

$$A(A,B) = (64\pi^4\nu^3/3h).S(A,B)/(2j_a+1) \qquad \ldots\ldots (5.6)$$

where S(A,B) is the line strength, j_a is the total angular momentum in state A, and ν is the wave number in cm^{-1}.

The line strength may be expressed in terms of the integral of the radial part of the wave function in the initial and final state R_i and R_f in the form

$$\sigma^2 = 1/(4l^2-1)\left[\int_0^\infty R_i R_f r\,dr\right]^2 \qquad \ldots\ldots (5.7)$$

where l is the larger of the two azimuthal quantum numbers. Values of σ^2 are obtained from the tables of Bates and Damgaard. With ν expressed in Rydbergs, the transition probability may be written as

$$A(A,B) = 2.662 \times 10^9\, k\nu^3\sigma^2 \quad sec^{-1} \qquad \ldots\ldots (5.8)$$

where k depends on the line of the multiplet considered (given in (25)).

Basically, in the Bates and Damgaard Central Field approximation, the charge is considered as lumped in a small radius, and that for r less than r_c the contribution to the potential is negligible. Bates and Damgaard take 1 per cent of coulomb departure as limit of $r_c \longrightarrow r_\infty$. The method results in the following agreement being obtained between calculated and experimental determinations for:

(i) <u>simple, light systems</u>, accurate on all transitions; agreement within 10 per cent for p - s transitions as far as atomic number 19, and p - d, d - f transitions further down the periodic table.

(ii) simple, heavy systems, not subject to interference farther down than atomic number 19, e.g. CuI or CsI, the agreement is to within about 50 per cent.

(iii) complex systems, e.g. the active electron is in a shell containing other electrons, fair agreement is shown; even TlI, (atomic number 81) is not expected to differ by a factor greater than 2.

Transition probabilities for Al II transitions

Aluminium has an atomic number of 13, and has neutral ground state electron configuration $1s^2\ 2s^2\ 2p^6\ 3s^2\ 3p$. Fig. 5.1 shows the proposed Al II laser transitions, which are:

$(3p^2\ ^1D_2 - 3s\ 3p\ ^1P_1)$ at 390.0nm, and

$(3s\ 3p\ ^1P_1 - 3s^2\ ^1S_o)$ at 167.1nm.

For these transitions, in a light complex system, fair agreement is expected between calculated and experimental transition probabilities. Using the method of Bates and Damgaard:

$$\sigma^2 \text{ for the transition Al II } (3p^2\ ^1D_2 - 3s\ 3p\ ^1P_1) = 0.64.$$

Carrying out a similar treatment for the lower transition

$$\sigma^2 \text{ for the transition Al II } (3s^2\ ^1S_o - 3s\ 3p\ ^1P_1) = 0.14.$$

From (5.6), and with the line strength S(A,B) calculated from Condon and Shortley (25), the ratio of the upper transition probability (A_{12}) to the lower (A_{23}) is equal to 1.28/1.79. Since A_{12}/A_{23} is less than 1, the transitions are just suitable for cw oscillation. The effect of the statistical weights factor (g_1/g_2) in (1.3) marginally reduces the cw suitability by a factor of 5/3.

Using (5.8), $A_{12} = 130 \times 10^6$ sec^{-1}, and $A_{23} = 162 \times 10^6$ sec.$^{-1}$

5.2.3 Measurement of the absolute intensity of the Al II 390.0nm line

The absolute intensity is defined as the radiant energy flowing per unit time in unit solid angle, through unit area perpendicular to the beam. This energy may be contained in a unit spectral range, or unit wave number i.e. I_λ or I_ν. If the energy is distributed over a spectrum line the integrated intensity is given by

$$I = \int I_\lambda d\lambda, \text{ or } \int I_\nu d\nu \qquad \ldots\ldots (5.9).$$

Generally $I_\nu = I_\nu(\theta, \phi)$ and the total radiant energy flow through an element of surface $d\sigma$ at a given place is

$$\mathcal{F}_\nu d\sigma = \int_0^{\pi/2}\int_0^{2\pi} I_\nu(\theta,\phi)\cos\theta \sin\theta d\theta d\phi d\sigma \qquad \ldots\ldots (5.10)$$

For energy over a small frequency range $d\nu$, within a small solid angle $d\Omega$,

$$\mathcal{F}_\nu d\nu d\sigma = d\Omega I_\nu d\nu d\sigma \qquad \ldots\ldots (5.11)$$

Absolute intensity measurements are made by comparing the fluxes through some optical dispersing system when the unknown is substituted by a standard source. The simplest method available possessing sufficient accuracy was the photographic method.

The Standard Source

Most desirable as a standard source is a cavity resonator at a uniform temperature T°K, so that the specific intensity

$I_\nu = B_\nu(T)$ is given by Planck's function

$$B_\nu(T) = 2h\nu^3/c^2\left[\exp.(h\nu/kT)-1\right] \qquad \ldots\ldots (5.12).$$

Using the Planck radiation law, the source energy $(\text{bandwidth})^{-1}$ $(\text{steradian})^{-1}$ $(\text{unit area})^{-1}$ can be calculated from

$$J_\lambda d\lambda = c_1 \lambda^{-5} / (e^{c_2/\lambda T} - 1) \quad \ldots\ldots (5.13)$$

where J_λ is the total radiant flux $(\text{unit area})^{-1}$ $(\text{solid angle } 2\pi)^{-1}$, T is in ^{o}K (colour temperature), and C_1 and C_2 are constants, (26).

For ease of computation, (5.13) is often reduced to the Wien Law approximation

$$J_\lambda = c_1 \lambda^{-5} e^{-c_2/\lambda T} \cdot \delta\lambda \quad \ldots\ldots (5.14)$$

where J_λ is in watt cm^{-2}, and λ, $\delta\lambda$ are in cm. This approximation at colour temperatures of $2500^{o}K$ and at $3000^{o}K$, results in inaccuracies of $< 0.5\%$, and $< 1.0\%$ respectively, (27).

$$\log_{10} J_\lambda = 4.57287 - 5 \log_{10} \lambda - 6245/\lambda T \quad \ldots\ldots (5.15)$$

was the form used in the computation here. The temperature applicable in (5.15) is the colour temperature. This is defined as the temperature at which a black body would have to be maintained to match the visible spectral distribution of the non-blackbody source. The colour temperature is usually higher than the actual temperature, as non-black body radiators have spectra shifted towards the blue.

Choice of Source

On the advice of the Light Division, NPL, a number of coiled filament car type bulbs were purchased and specifications given to G.E.C., (Wembley) for their calibration for Directional Intensity, at a specified standard colour temperature of $2854^{o}K$.

Standard lamp calibration

Since the calibration of the standard lamp is given in subjective visual Candela units, it is necessary to consider the eye sensitivity and variation of emissivity of the surface of the source with wavelength, in order to obtain the calibration in a form which enables the flux (steradian)$^{-1}$ (bandwidth)$^{-1}$ at the wavelength of interest to be calculated.

To be able to use calibration tables the effective area of the source in the calibration direction must be known. From Walsh (28)

$$\mathcal{F}_v = 10^6/1467 \int_0^\infty (V_\lambda \mathcal{F}_\lambda) d\lambda \text{ in lumens} \qquad \ldots\ldots (5.16)$$

where $\mathcal{F}_\lambda$ is the spectral flux in watts and V_λ is the eye visibility function.

At 380nm and 760nm the value of V_λ is about 0.01% of its maximum at 555nm (Daughters (29)), so that the visual response is determined by the interval $380 \leqslant \lambda \leqslant 760$nm. Thus (5.17) becomes

$$\mathcal{F}_v = 10^6/1467 \int_{400nm}^{760nm} (V_\lambda \mathcal{F}_\lambda) d\lambda \qquad \ldots\ldots (5.17)$$

which gives the radiant flux in erg (steradian)$^{-1}$ (cm)$^{-2}$ (sec)$^{-1}$ has emissivity taken into account and is given in the tungsten radiation tables of de Vos (30), against the true temperature.

From Fig. 5.4 a colour temperature of 2854°K is equal to a true temperature of 2800°K for a tungsten surface, (31).

Taking bandwidths of 20nm to give integration over the effective visible range, 400 - 760nm at 2800°K, and using 685 lumens = 1 watt at 555nm, the effective directional area of the coiled tungsten filament was determined as being 0.0076 cm^2.

This now enables use to be made of the de Vos tables, which give energy per unit area per steradian per micron per second.

Fig. 5.5 shows the calibration curve for tungsten at 390nm, where the temperature is in ^{o}K true. From this graph at $2854^{o}K$ (colour temp.) at 390.0nm the standard source gives 1.16×10^{7} (erg) $(cm)^{-2}$ (steradian)$^{-1}$ (micron)$^{-1}$ (sec)$^{-1}$.

5.2.4 Photographic plate calibration

Photographic Photometry

In determining the absolute intensity of a line it is necessary to relate the density of the image on the plate to the intensity of the source producing it. This is done by using a microphotometer and comparing the density produced by an exposure for a known time to the line whose intensity is required with the density produced by the standard source.

The response of an emulsion depends on at least seven factors:- the intensity of the light; its wavelength; the time of exposure; the nature of the emulsion and the time, type and temperature of the development that it undergoes. All of these are controllable.

Reciprocity failure

Intensity and time are interchangeable as far as a plate response is concerned, except for:

(i) low intensities —— long times

(ii) high intensities —— short times.

Letting D_o and D represent microphotometer galvanometer deflections through a clear portion of the plate close to a line and the deflection through the place at the point of interest, then $d = \log_{10} D_o/D$. The relationship between d and the intensity (I) of a source, acting for a time t, giving the characteristic curve is of the form:

$$d = g \log_{10} (It^p) - q \qquad \ldots\ldots (5.18)$$

q is small and is usually neglected, p is the Schwarzschild constant, g is usually called the gamma of the emulsion.

The Schwarzschild Constant

Schwarzschild enunciated the law that the product $It^{0.86}$, for a gelatine emulsion plate was constant for equal degrees of blackening, (Robertson, (32)).

Helmick, (33) got values of p ranging from 0.68 - 1.95; and Robertson obtained values of P=0.91 at 587.6nm and 0.74 at 447.1nm so that it can be concluded that p is not a constant and needs to be determined at each wavelength of interest.

The exposure ratios in these experiments were sufficiently different from unity to necessitate its evaluation, as exposures for emission spectra were up to 2 hr, and for the standard source were in the region 10 - 100 sec.

Eberhard effect.

If a region of high density is being developed on an emulsion, the developer in the centre becomes relatively exhausted compared with that on the outer parts of the region. To prevent errors being introduced due to this effect, it is essential to agitate the developer constantly close to the surface of the emulsion.

Elaborate wiper systems have been used in some experiments to do this necessary agitation. In this calibration, the sensitive balls of the 2nd and 3rd fingers were used to give constant agitation over the surface of the emulsion during the full period of development, in preference to designing and making a mechanical system.

Spectrograph illumination

Uniform spectrum lines are needed when measurements are being made to determine absolute, and even relative, intensities of lines.

To obtain uniform lines an image of the source must be focussed on the dispersing element used; with the Hilger large quartz/glass spectrograph used, this can be either the prism, or the collimator/camera lens.

To give maximum energy into the dispersing system, the whole of the prism must be illuminated. In all the experimental arrangements used in both the photographic plate calibration and the H.C.D. intensity determination uniform lines were obtained by focussing an image of the source on the collimator/camera lens by a suitable quartz condensing lens.

Slit width and parallelism

In the determination, comparisons are made between the integrated densities of spectrum lines. To allow such comparisons to be made from microphotometer readings taken across any cross-section of a spectrum line, parallel slits must be used. A knowledge of the slit width is also required. Both of these requirements were satisfied by separate experiments, and measurements were made on the detached slit assembly of the spectrograph, using a helium-neon laser that had been constructed in earlier work.

5.3 Experimental Apparatus, neon-aluminium

5.3.1 Vacuum/gas filling system

A conventional, mixed metal and glassware high vacuum system was constructed. It consists of an oil diffusion pump, and a P_2O_5 trapped rotary pump, connected via a greased cone and socket to the main pumping/filling glassware. The glassware used in this part of the project is shown in Plate 1 of Chapter 7. It is essentially a glass T-piece of 2" and 1" bore, with a cold trap built into the main pumping line above the base plate of the diffusion pump. It has facilities for pressure measurement, gas bleeding, and support and isolation of the discharge tubes. The ultimate pressure attainable with this system at the discharge tube is of the order of 10^{-5} torr. A background pressure of 10^{-5} torr represents an impurity content of 1 part in 100,000 in a gas at the pressure of 1 torr used in this experiment. With care in the processing of the H.C.D. tubes, clean, non-banded, spectra could be obtained with this system, over exposure periods of over 8 hours.

Low pressures are measured with Pirani/Penning gauges and the gas filling pressures by means of a differential oil manometer containing 702 diffusion pump oil, isolated from the main pumping line by a liquid nitrogen trap. The filling gases were obtained from B.O.C. Ltd. in 1l pyrex flasks, specified purity 5N5, with less than 1-2 p.p.m argon.

5.3.2 The hollow cathode discharge tube

As a workable H.C.D. laser would ideally be a small system removable from the pumping/filling system, a non-continuous flow tube was designed. No trouble was experienced from impurities, but gas clean-up was subsequently observed during the long exposures used. A diagram of the H.C.D. tube used

is shown in Fig. 5.6. It consists of a 1l pyrex chamber enclosing a hollow cylindrical cathode and a single probe anode. Connection is made to the vacuum system by means of a greased B14 cone and a 4mm greaseless stopcock.

The spectra excited in a H.C.D. depend to a considerable extent on the diameter of the cathode and to a small extent on the length, (Mitchell (34)). To maintain stable operation, the ratio of length to diameter must not be greater than 7, (A. von Engel, private communication).

The cathode is of 0.5" diameter, and 2" in length and is made of spectrally pure (5N) aluminium. It is supported by a mild steel rod at the lower end and by a 1" long stem of the same material as the cathode, at the upper end. The support, apart from the upper aluminium stem, is surrounded by pyrex tubing, which (a) prevents a discharge striking to the mild steel support and (b) acts as an additional support to the stem. Brazed to the bottom of the mild steel stem is a 1mm. diameter tungsten rod, which forms a connection through the glassware. The anode is a 1mm diameter tungsten rod, having 1" clear length in the tube, about 2.75" from the centre of the cathode.

The design of the tube results in striking voltages of approximately 600-800V and sustaining voltages of 300-400V at 50mA in neon, at a pressure of 1 torr. A resultant increase in sustaining voltage, due to gas clean-up, of about + 10V/hr when running at 50mA at an initial neon gas pressure of 1 torr, was observed when this tube was isolated from the rest of the system.

5.3.3 The spectrograph

The instrument used was a Hilger E578 Large Quartz/Glass, prism spectrograph of the Littrow type, having a range of 200 - 800nm and an inverse dispersion of 1.2nm/mm at 390nm.

5.4 Experimental procedure, neon-aluminium system

5.4.1 Calibration of plate

The standard lamp was set up in front of the spectrograph slit to satisfy the requirements stipulated in 5.2.4. To avoid contact troubles, leads were soldered directly on to the sole plates of the standard lamp.

To check the reproducibility of exposures, and the developing and fixing procedure a number of exposures were made under differing room conditions. Subsequent density measurements showed that reproducibility could not be obtained with the set-up used.

The simple replacement of a sliding type rheostat used to control the lamp voltage, by a clampable variable resistance made out of 20g tinned copper wire and an old ceramic coil former, having a value of $\sim$ 0.1 ohm completely eliminated the poor reproducibility experienced.

Exposure procedure.

The standard lamp was allowed to thermalise at its specified calibration voltage and current for a minimum period of 30 minutes before all calibration exposures. Exposures on Ilford Ordinary plates were made of 10,000 and 200 sec.

Development and fixing.

Development was carried out in full strength, fine grain ID 11 developer, and fixing in Hypo. Standard solutions were kept in dark, well

stoppered bottles, and used only for this experiment.

The typical temperature change that occurred in the developer during development was found to be about + 2°C, at an initial temperature of 22°C. To minimise this change, the developer was cooled to 21°C before commencing each development. To correct for exhaustion of the developer when a number of plates were developed, successive development times were increased by 10%. After a maximum of six plates, the developer was thrown away. After a quick rinse in water which contained a dash of fixer for stopping purposes, fixing was carried out for a standard period of 10 minutes. This standard period avoided any variable reduction in the density of the plate that could occur, due to the fixing process.

To prevent reticulation, developer, fixer and rinsing water were all kept within a 3°C range. After washing for ~ 30 minutes, plates were rinsed in a water-teepol wetting agent mixture and left to dry in the atmosphere.

5.4.2. Intensity of the Al II, 390.0nm line

The H.C.D. lamp was processed in a series of cycles of pumping, filling, running at high current, pumping, until band-free spectra were obtained. This could always be achieved in three cycles, unless a leak had developed in the system, usually in a metal/glass seal. Prior to processing, all glassware was flamed as far as the greased taps would allow, to remove surface water vapour.

Initial experiments indicated that gas clean up was occurring on running the discharge, when the tube was isolated from the system. To add

some additional volume to the tube, it was left connected to the vacuum system, giving an additional volume of about 2 litres.

Exposures of 2 hours were made on the central portions of Ilford Ordinary plates, over the neon pressure range of 0.7 - 3 torr. Immediately after completion of an exposure, the plate was developed and fixed.

5.4.3 Density measurement

Density measurements were made on a manual Hilger microphotometer modified to take an IP 21 photomultiplier. The microphotometer lamp was operated from a stabilised, variable voltage unit and run for a minimum period of 30 minutes to stabilise it before use. The output from the photomultiplier was taken through a 20,000 ohm resistor and a Cambridge precision microammeter with a f.s.d. of 100μAmp.

To obtain an accuracy of 0.05 in density at 0.7, deflections must be read to within $\pm$ 1 division for a D_o of 100 divisions. In scanning across a spectrum line, the microammeter was continually gently tapped to overcome the sticking friction of the meter movement. Without this, measurements were found to be irregular, and reproducibility could not be obtained.

All readings could be reproduced to within the accuracy of reading the meter ($\pm$ 0.2 division) on a complete re-traversal of a spectrum line, after an initial traversal requiring up to 10 minutes.

5.5. Results

5.5.1 The determination of the Schwarzschild constant (p).

Fig 5.7 shows the results of the 100,400 and 1000 sec exposures of the standard lamp plotted against the time of exposure for four positions around 390.0nm.

Assuming that the response of the emulsion will not vary appreciably over an interval of 5.0nm, by taking points of equal density, and knowing the light flux from the standard lamp at particular wavelengths (from the de Vos lamp calibration and using (5.18))

$$p = 0.4 \pm 0.05.$$

The variation of $\pm$ 0.05 is attributed to a variation of emulsion response over the wavelength interval used in the determination.

5.5.1 Standard lamp

Fig. 5.8 shows the plot of the density of three calibration plates of the standard lamp, against position (or wavelength) on the plate, for an exposure of 10 sec. At 390.0nm the density is 0.76 ± 0.03.

5.5.2 The intensity of the Al II, 390.0nm line

Fig. 5.9 shows the microphotometer density measurements for the 390.0nm line at three neon carrier gas pressures. Maximum density of about 0.63 is observed at a pressure of approximately 1 torr.

Whereas with a continuous source the luminance is directly proportional to the energy per unit bandwidth, the slit width and the inverse dispersion of the dispersing system, in intensity measurements of line spectra, where the dispersion is sufficient to avoid overlap of individual spectrum lines, the spectra are broadened without their luminance being affected. The area under the line profile represents the energy incident at the wavelength of the line considered, (Walsh (28), Sawyer (35) and Harrison, Lord and Loofbourow (36)).

Integrating under the curve of greatest density in Fig. 5.9 at 0.8 torr of neon, a mean density of 0.4 over the line profile is obtained.

(i) Using (5.16), the luminance of the standard lamp, and knowing the angle subtended by the slit image at the source, the exposure times which produced two known densities of blackening, and assuming no scatter losses in the spectrograph, the energy producing the blackening, of the Al II 390.0nm line,

$$W_{390.0nm} = 9.2 \times 10^{-13} \text{ watt.}$$

(ii) Taking equal densities produced by the standard source and the 390.0nm line and finding the time required by the standard source to give the mean density of 0.4 of the line,

$$W_{390.0nm} = 1.1 \times 10^{-12} \text{ watt.}$$

Taking $W_{390.0nm}$ as 1.0×10^{-12} watt, from a solid angle of 6×10^{-5} steradians of the H.C.D., the emission from the source at 390.0nm is approximately 2.1×10^{-6} watt.

Considering the source as a point source, the emission per cm^3 of discharge is of the order of 3×10^{-7} watt.

5.6 Gain and oscillation requirement

Since $I_{(absolute)} = N_2 A_{21} (h \nu_{21})$, the steady state population in the Al II, $3p^2\ {}^1D$ level is

$$\frac{3 \times 10^{-7}}{1.3 \times 10^{+8} \times 5.1 \times 10^{-19}} \text{ cm}^{-3}$$

$$\simeq 5 \times 10^{3} \text{ cm}^{-3}.$$

If $I = I_o e^{\alpha x}$ describes the intensity of a plane wave propagated through a medium with optical gain, the absorption coefficient of (1.1) resolves to:-

$$\alpha_{cm^{-1}} = 3.75 \times 10^{-10} \lambda^2_{(\mu m)} \cdot A_{21}/\Delta\nu_D \left[N_2 - N_1 g_2/g_1\right] \quad \cdots\cdots \quad (5.19).$$

Assuming that: for $(N_2 - N_1)$, $N_1 \ll N_2$ and $N_1 = 0$, $\Delta\nu_D = 2 \times 10^9$ sec^{-1}, and $A_{21} = 1.3 \times 10^8$ sec^{-1}, $\alpha_{390nm} = 2 \times 10^{-8}$ cm^{-1}.

The small signal gain constant (α cm^{-1}) at the line centre has been given by Bennett (37) on the following lines as:-

Helium-neon,	632.8nm	$= 2 \times 10^{-4}$
	1.153μm	$= 4.2 \times 10^{-4}$
	3.39μm	$= 1.7 \times 10^{-2}$
Helium-xenon,	2.02μm	$= 4.0 \times 10^{-3}$

The gain constant for the 390.0nm line, is therefore seen to be 10^{-4} down on the reasonable 632.8nm ($3s_2 - 2p_4$) neon oscillator gain constant.

Following Schawlow and Townes (38), and Heavens, Optical Masers, Ch. 4, the excess steady state population necessary to maintain oscillation in a practical system, in this aluminium system at 390.0nm can be shown to be of the order of 10^{10} cm^{-3}.

5.7 The sputtered population in the H.C.D.

In a H.C.D. under steady state conditions, the rate of production of sputtered cathode material will be equal to the rate of loss of sputtered material by diffusion to the walls of the cathode.

Tables have been given by Cobine (39) of the sputtering rate of hydrogen for metals with a cathode drop of 850V. If the momentum transfer model is

appropriate to the sputtering process, the rate of sputtering will be proportional to :

(a) the mass of the incident ions

(b) the current

(c) the cathode material. (Copper and silver are two of the most easily sputtered materials; aluminium, magnesium and molybdenum some of the hardest.)

Neon ions having a mass 6 - 20 times greater than H_3^+ or H^+ ions, will be 6 - 20 times more effective at sputtering than hydrogen. (The ions in hydrogen giving the figures quoted by Cobine could possibly include H_3^+ ions.) From Cobine, for a current of 10A that could be considered as a current for a H.C.D. laser system, the sputter rate of aluminium in neon is approximately 4×10^{19} atoms sec^{-1}.

Loss rate by diffusion

Consider a H.C.D. plasma in the form of a cylinder diameter d, and length L. The number of atoms (Q) which are lost by the column in unit time is given by

$$Q = S\beta\Delta N \qquad \ldots\ldots (5.20)$$

where S is the surface area of the cylinder, (neglecting the end areas),

$$\beta = \mu_o^2 D/d^2 \qquad \ldots\ldots (5.21)$$

where $\mu_o = 2.4$, is the 1st root of the Bessel function of zero order. D is the diffusion coefficient, ΔN is the difference between the concentration of atoms at the axis and at the surface of the column. D is

given by: $D = u\,\lambda_c/3$, where $u = (8kT/\pi m)^{\frac{1}{2}}$; m is the atomic mass of the impurity element (aluminium in this case) in the plasma, (Mandelstam and Nedler (40)).

$$\lambda_c = 1/\sqrt{2}\pi n^2 A^2 \qquad \ldots\ldots (5.22)$$

where n is the concentration of the main gas (neon) and A is the diameter of the gas atoms.

For a practical H.C.D. oscillator system,

L = 1 metre, d = 0.5 cm; from (5.21)

$$\beta = (2.4)^2\, D/0.25.$$

Assuming $m_{Al} \approx 4 \times 10^{-23}$ g, then at a pressure of 2 torr, $n = 10^{17}$ atom cm^{-3}. $A^2 \approx 10^{-15}$ cm^2, so that $D = 35$ cm^2 sec^{-1}, $\beta = 805$, and substituting in (5.20)

$$Q = \pi\,(0.5 \times 10^2)\; 805\; \Delta N \text{ sec.}^{-1} \qquad \ldots\ldots (5.23).$$

If the atomic concentration is assumed to decrease linearly towards the surface, $N/2 = N_o$, where N_o is the mean concentration of aluminium

$$Q \approx 3 \times 10^4\, N_o \text{ sec.}^{-1} \qquad \ldots\ldots (5.24)$$

Under steady state conditions the sputtering rate is equal to the diffusion rate. Equating 5.23 and 5.24, $N_o \approx 10^{15}$ atoms cm^{-3}.

The concentration of sputtered cathode material in a neutral or ionic form, realisable in a practical H.C.D. system is thus shown to be of the order of 10^{15} atoms cm^{-3}.

5.8 Intensity variation of the Al II 390.0nm line in various systems.

5.8.1 Neon-aluminium

The variation of the intensity of the Al II 390.0nm line, and the intensity of Al I, Ne I and Ne II lines with neon pressure in a H.C.D. is shown in Fig. 5.10. The curves merely show the way in which the intensity of each individual line varies with pressure and cannot be intercompared.

It is seen that maximum intensity of all the lines occurs in the range 1 - 2 torr of neon. The intensity curves for the Al II 390.0nm and Ne II 357.5nm lines have the same general shape, with a maximum intensity at approximately 1 torr. The ion lines appear to be more pressure-sensitive than the neutral lines of aluminium or neon.

The 390.0nm Al II line is particularly pressure-sensitive; at half peak amplitude its 'width' is $\sim$1 torr. At pressures greater than 3 torr of neon, excitation of both neutral and ion lines of aluminium is absent.

If resonance energy transfer was occurring between Ne 1s metastables and aluminium, it would be expected that the Al II 390.0nm line would show a similar pressure-dependence to the neutral neon lines. This is not the case. From this it could be concluded that the excitation of the Al II 390.0nm line is similar to that of the Ne II lines, that is by direct electron impact excitation, or that perhaps excitation of aluminium occurs through an asymmetric charge transfer reaction with neon ions.

5.8.2 Neon-aluminium rf discharge

The H.C.D. tube used in the previous experiments, was coupled via a matching unit to a 16 Mc/s rf oscillator.

At a neon pressure of 1 torr, the optimum for the dc excited H.C.D., a diffuse discharge was obtained inside the cathode, with a Cathode Dark Space 1/5 of the radius, as in the normal H.C.D.

An exposure of 7 hours showed that all the Al I resonance lines were present, together with both Ne I and Ne II lines, and the Al II 390.0nm line, which was relatively weak. Certain Ne I lines were stronger in this discharge than in the normal H.C.D. Differing electron energy distributions are probable in each of these discharges so that comparisons beyond the above are not considered meaningful.

5.8.3 Mercury-aluminium H.C.D.

Experiments were carried out with this system to determine whether mercury was an effective sputtering carrier gas, and to see if the 390.0nm Al II line was enhanced when a carrier gas other than neon was used. Selective excitation by resonant energy collisions is not expected in this system.

Strong resonance lines of Al I, and strong HgI lines were observed using an aluminium cathode and mercury as a carrier gas. The 390.0nm Al II line was not detected on any of the spectrum plates obtained, even though ion lines of mercury at 391.4 and 391.8nm were found to be particularly intense. These lines are from levels more than 24 eV above the neutral ground state, so that excitation of Al II lines would be expected also from inelastic electron impact collisions.

This would suggest that the Al II 390.0nm line is not excited in the neon-aluminium H.C.D. by electron impact, but more likely by the alternative method mentioned in 5.8.1 of asymmetric charge transfer.

The strong resonance lines of aluminium observed show that mercury is a very effective sputterer of aluminium.

5.9 Summary, neon-aluminium metal vapour system

(a) The steady state population of the $3p^2\ ^1D$ level in ionised aluminium in a H.C.D. at optimum excitation conditions, from a measurement of the absolute intensity of the Al II 390.0nm line, has been found to be approximately 6×10^3 cm^{-3}.

(b) The excess steady state population necessary to sustain oscillation is about 10^{10} cm^{-3}. It was evident at this stage, that although,

(i) the sputtering process provides a sufficient atomic population in which to sustain oscillation, and

(ii) the transition probabilities of the proposed transitions were suitable, that an increase in the steady state population by a factor of 10^6 would be unlikely to be realised.

5.10 Experimental apparatus.

5.10.1 The dc power supply

A circuit diagram of the power supply is shown in Fig. 5.11. It consists of a 3 phase, full wave rectifier, isolated from the mains by three step-up isolation transformers. To prevent breakdown of the semi-conductor diode rectifiers by transient pulses, to which these components are susceptible, two diodes in series are placed in each half-wave arm, giving a safety factor of 3 on the P.I.V of each. This unit gives voltages up to 1.2 KV at up to 5 Amp.

5.10.2 Hollow cathode discharge system

A number of systems of differing configurations were tried in this work, including prototypes of the multi-cathode tube shown in Fig. 5.12; the external type hollow cathode tubes shown in Figs. 5.13 and 5.14; and the negative glow test tube shown in Fig. 5.15.

In the work on helium-mercury mixtures a means was sought of obtaining H.C.D. of greater than 100 cm plasma length. Two systems were designed and constructed, which enabled a discharge to be maintained in a metallic cathode surround, with no apparent restriction on length.

The first system of the external type is similar to that shown in Fig. 5.14, which was used by Chebotayev (41) as a helium-neon laser system.

The second, enclosed in a glass vacuum system consisted of an aluminium tube 10" long, 0.5" I.D., in which a longitudinal slot was made, 1-2mm wide, along the full length of the tube. Facing the slot, at a distance of 0.75", a nickel wire which formed the anode ran the full length of the cathode.

The helium-iodine multi-cathode discharge tube used in the gain measurement experiments was made following preliminary experiments in which optimised cathode/anode geometries were determined for the enhanced ionised iodine lines. Fig. 5.12 shows this tube. It consists of a main body of 2 cm. bore pyrex tube, to the ends of which are sealed 7 mm. Brewster angled end tubes. Approximately mid-way along the tube is situated a cold finger into which iodine is condensed on bleeding it through from the reservoir in the main pumping/filling system. 10 cylindrical cathodes of molybdenum, 7.5 cm x 6mm diameter at a separation of 1.5 cm, are located by dimples made

in the pyrex of the body, and by the pointed ended 1 mm diameter rods which form the electrical connection from the cathodes through the side tubes on the body. The anodes are of 1 mm tungsten rod placed in side tubes so that anode glows are kept out of the line of sight through the Brewster angled end tubes and cathodes. Connection is made to the pumping/filling system through a 6 mm greaseless stop-cock and a greased cone and socket.

5.10.3 The gain measuring set-up

The experimental method chosen for the measurement of population inversion in a discharge was that of Resonant Cavity Spectroscopy of Zarowin et al. (42). In this method the single pass gain is obtained by comparison of the resonant intensity ($\overline{I_R}$) with the non-resonant intensity ($\overline{I_{NR}}$) from the end of a plane parallel Fabry-Perot cavity containing the fluorescent atoms. The non-resonant intensity is directly proportional to the spontaneous emission intensity in the medium.

Zarowin et al. show that:-

$$\Gamma = \left(\overline{I}_R - \overline{I}_{NR}\right)/\overline{I}_R = R e^{\alpha l} \qquad \ldots\ldots (5.25).$$

If α is small, R must be known to high accuracy to prevent masking of the difference; this is avoided by making two measurements of Γ with different discharge lengths l_1, and l_2, thus

$$\Gamma_1/\Gamma_2 = R e^{\alpha l_1}/R e^{\alpha l_2} = e^{\alpha(l_1 - l_2)} \qquad \ldots\ldots (5.26).$$

Thus four measurements suffice to give the gain or attenuation (α) over a distance ($l_1 - l_2$).

Fig. 5.16 shows the experimental layout used in the helium-iodine work.

The two choppers are phase locked by driving one of them with a small dc motor connected to a magslip transmitter/receiver and the other by an electrical link to another magslip transmitter/receiver. The reference signal from each chopper is provided by a small amplifier based on Mullard OCP 71 phototransistors. The chopper blades are mounted in a parallel light path position between bulb and photodetector. The resonant cavity of a mixed confocal type, incorporated a -2m mirror and one of -1m, at a separation of 175cm. Plate 5.1 shows the general arrangement of the apparatus, Plate 5.2 the 'resonant' chopper assembly.

5.11 Experimental procedure

5.11.1 Helium-mercury

After processing the discharges, by pumping, filling and overrunning, exposures were made over the range 300 - 800nm, using Ilford Long Range plates, and the spectrum lines identified. Apart from visual estimates with a hand spectroscope, and examination of spectrum plates, experiments of variation of intensity with current or pressure were not carried out.

5.11.2 Helium-iodine

Experiments were carried out on this system, in much the same way as the preliminary experiments in the helium-mercury system mentioned in 5.11.1. In these experiments spectrum line identification was carried out using a Hilger Large Quartz spectrograph.

Experiments were also carried out to determine the optimum cathode size, and cathode/anode geometry to give maximum spontaneous emission of the

ionised iodine lines 533.8 and 540.7nm and the strong yellow He I line, using a hand spectroscope, in cylindrical cathodes of 10cm x 1cm diameter, 5cm x 6mm diameter and 5cm x 3mm diameter, over the helium pressure range 0 - 20 torr, at a maximum current of 150mA per cathode.

The optimum cathode size from this, and other experiments, was found to be 7.5cm x 6mm diameter.

Processing procedure

Iodine flakes (4N8 purity), previously kept moisture free, in a dessicator containing anhydrous calcium chloride, were introduced into the reservoir with the pumping system at atmospheric pressure. After a rapid pump down to about 10^{-2} torr, a liquid nitrogen trap was placed around the reservoir to reduce the vapour pressure of the iodine. The H.C.D. tube and pumping/filling system was then pumped down to its ultimate pressure of better than 10^{-5} torr. The tube was then processed and outgassed by means of heating tapes, and by over-running the cathodes until they were red hot. When only helium line spectra could be observed, the cold trap was removed from the iodine reservoir and iodine vapour was allowed to diffuse through into the H.C.D. tube and into the cold finger. On running the discharges more iodine vapour had to be diffused through to replace that which was lost due to clean-up near the anodes.

It was, however, essential to maintain a low vapour pressure of iodine by using a liquid nitrogen trap round the cold finger. If the vapour pressure increased, the intensity of the ionised iodine lines decreased, the discharges became unstable and local overheating of the cathodes occurred.

Optimising conditions for oscillation

Using photoelectric, and phase sensitive detection techniques, intensity/current and intensity/pressure measurements were made of a number of ionised iodine and neutral helium lines in a helium-iodine mixture.

These experiments agreed with the results of Berezin and Yanovskaya (23) in that certain ionised iodine lines were enhanced (521.6, 533.8, 540.7 and 567.8nm) in a helium-iodine H.C.D. and that maximum intensity of these enhanced lines occurred at a high helium pressure of about 20 torr.

The intensity of the enhanced lines varied almost as the $(\text{current})^2$, so that some advantage would be indicated in using the largest currents permitted by the pyrex of the discharge tube. This maximum current was found to be 150mA per cathode.

The discharge tube was set up inside a mixed near confocal cavity of multilayer dielectric mirrors, having radii of curvature of -2m and -1m, at peaked relectivities of greater than 97 per cent at 550.0 and 632.8nm respectively, using the pinhole and cross alignment technique. Over the helium pressure range 5 - 20 torr and currents of 50 - 150mA per cathode, oscillation was not observed.

In order to optimise excitation conditions for population inversion, and to determine the gain or absorption in the system, experiments were carried out over the pressure and current ranges used above using the Resonant Cavity Spectroscopy (R.C.S.) method.

Initial measurements using a trial set-up of a movable chopper and phase sensitive detection showed that absorption was occurring on the single

line 540.7nm examined. Further measurements on the lines 540.7, 533.8 and 521.6 indicated that over the helium pressure range 8 - 16 torr, and current range 50 - 150mA per cathode absorption was occurring on these lines.

5.12 Helium-neon and neon at low pressure.

The H.C.D. was investigated as a means of obtaining oscillation in the visible at 632.8nm in a helium-neon mixture.

Various aspects of the operating conditions in helium-neon positive column and rf lasers, fully covered in Chapter 6, have led to the conclusion that a high electron temperature and a low electron concentration, is needed for 632.8nm optimisation, and that cw oscillation on this line might be obtainable in pure neon, (or in a neon-hydrogen mixture where resonant energy transfer does not give selective excitation to the Ne $3s_2$ level) by electron impact excitation in a H.C.D. To get high electron temperature and low electron concentration in a H.C.D. in neon requires operation at pressures below 1 torr.

Smith (43) has obtained oscillation in the infra-red, in helium-neon, and also in pure neon but not at 632.8nm in a similar hollow cathode structure to that used in the helium-iodine work described earlier. Since Smith's first report of oscillation, other workers have reported population inversion, and laser oscillation in a H.C.D. in the infra-red on a number of lines (Chebotayev (41), and Znamenskii et al. (44)).

Chebotayev, at the time this work commenced, also reported oscillation at 632.8nm in a 2:1 He-Ne mixture in a H.C.D., at a total pressure 0.3 torr.

Various hollow cathode structures included the two shown in Figs 5.13 and 5.14; some incorporating water cooling were constructed and tested for low pressure operation.

In none of these structures could a discharge be maintained at less than 0.8 torr neon.

The inability to operate hollow cathode discharges at low pressures, in structures which differed initially from those of Chebotayev, but which later were identical, and the considered uncertainties of the action of helium in lasers involving helium gas mixtures, led to an examination of the stated operating properties of (a) hollow cathode discharges and (b) positive column and rf helium-neon lasers, covered in Chapter 6.

5.12.1 Low pressure hollow cathode discharges.

The minimum pressure at which a H.C.D. can be maintained is determined by the diameter of the cathode, the carrier gas, and the cathode material. A general rule is that it is not possible to run a H.C.D. if the radius of the cathode is less than the width of the cathode dark space (C.D.S.). The C.D.S. is about ten times the electron mean free path.

As the C.D.S. varies inversely as the pressure, there is, for a given cathode radius a minimum pressure below which a discharge will not operate as a H.C.D. Below this minimum pressure the discharge goes over into a diffuse, 'suppressed mode' discharge, (Sturgess and Oskam (45)). Von Engel (46), and Parker (47) give values of cathode dark spaces, for various gases and cathode materials.

For neon, the radius of an iron cathode must not be less than 4 cm at 0.2 torr, in order that the C.D.S. does not overlap. Similarly in argon, which is an easily ionised gas, and hence has a small C.D.S., the radius must not be less than 1.5 cm at 0.2 torr.

Results, however, were given by Chebotayev (41) for laser operation down to 0.09 torr neon, in a H.C.D. of 2.5 cm diameter.

In spite of good theoretical reasons why a H.C.D. should not operate under the conditions claimed by Chebotayev, experiments were carried out on hollow cathode structures similar to those used in the Russian work. Altogether five structures were examined; in no case could low pressure operation be achieved, and the discharges went over into 'suppressed mode' discharges at pD values agreeing with the plane cathode results of Oskam and Sturgess, and with the general rule stated earlier.

To have any negative glow plasma, in a H.C.D. the length of the negative glow must be approximately less than the diameter of the cathode. Fig. 5.17 shows the extent of the negative glow, at cathode fall potentials of 300 - 340V, for varying neon pressure. Fig. 5.15 shows the construction of the simple discharge tube used to determine the results plotted in Fig. 5.17.

The conclusion arrived at in this work, was that Chebotayev must have some easily ionisable impurity (probably mercury) in his discharges, or was using a special thermionic hollow cathode which he had not mentioned, and so was able to sustain a H.C.D. at low pressures. This explanation need not now be invoked, as it appears likely that his hollow cathode discharges, are not cw discharges, but 'quasi-stationary' (200 - 300μ sec) pulsed discharges, (Chebotayev (48)).

5.13 Results and Discussion

5.13.1 Helium-mercury

The few experiments carried out, have shown that enhancement of certain mercury ion lines, on which oscillation has been observed under pulsed conditions, occurs in a H.C.D. in pure mercury, and a neon-mercury mixture, as well as in a helium-mercury mixture. The enhanced Hg II lines, 479.7, 567.7, 615.0 and 734.6nm were most intense in a 108 cm slotted cathode structure, at pressures around 10 μ , at the maximum currents used of 500mA. The intensity of these lines depended markedly on the pressure and current. From these observations, and the reported observations in 4.2.3, it is evident that the selective excitation of the upper levels of the enhanced lines can be due to direct electron impact excitation, in the case of pure mercury, and neon-mercury discharges, and in helium-mercury to the near resonant, charge-transfer collision:-

$$He^{+}(0) + Hg \longrightarrow \quad He(^{1}S_{o}) + Hg^{+'} + \Delta E$$

5.13.2 Helium-iodine

Enhancement of the ionised iodine lines 521.6, 540.7, 533.8, 567.8 and 576.0nm occurred when a helium-iodine mixture was excited in a H.C.D., compared with a H.C.D. in a neon-iodine mixture. In helium some of these lines were obtained with the same intensity as neutral helium lines under certain pressure conditions.

Figs. 5.18 and 5.19, show results obtained from hollow cathode discharges in cathodes 7.5cm long x 0.6cm diameter. Maximum intensity occurred at a high helium pressure of about 20 torr.

Fig. 5.19 shows that whereas the intensity of neutral helium lines varied linearly with current, the intensity of all the ionised iodine lines measured varied almost as the (current)^2.

In the studies of Berezin and Yanovskaya (23) the intensity of the ionised iodine line ($5d^5\ ^3D_1$ - $6p'\ ^3D_1$) at 448.854nm varied <u>linearly</u> with current. Following the pulsed iodine laser work described later in Chapter 7, it was important to determine why this line, which has an upper level ($6p'\ ^3D_1$) common to transitions on which laser oscillation can be obtained, did not vary in the same way as enhanced iodine lines on which oscillation is observed. Unless the enhancement was determined by effects on the lower levels (perturbations), the intensity should vary with current in a similar way to the enhanced ionised iodine lines. Over the pressure range 8 - 20 torr of helium, and current range 50 - 225mA per cathode, (which encompasses the ranges used by Berezin and Yanovskaya), the intensity was <u>not</u> observed to vary linearly with current, but almost as the (current)^2, similar to the intensity variation of the enhanced ionised iodine lines 533.8 and 540.7nm. Anomalous behaviour is therefore not exhibited by this line, contrary to the observations of Berezin and Yanovskaya.

The intensity vs (current)^2 dependence suggests that a two stage process is involved in the selective excitation. It is not due however, to first the production of an ion, and the excitation of the ion by electron impact, as the ($^4S^o$ core) p levels would be the first to be excited, (as in the inert gas ion lasers), and strong p-s transitions would be observed, - they are not in a helium-iodine H.C.D. There seems no other basis for suggesting that a metastable-metastable, or ion-excited species collision is involved.

Although considerable enhancement of certain ionised iodine lines in a helium-iodine H.C.D. was observed, laser oscillation could not be obtained. Moreover, measurements indicated that absorption was occurring over the helium pressure and current ranges investigated. In a pulsed helium-iodine positive column discharge (described in the next chapter) enhanced lines, on which oscillation was obtained, were observed 1) to have much higher intensities than in the multi-cathode, H.C.D. and 2) to be particularly sensitive to the applied voltage, current and vapour pressure of iodine. In view of these two observations and the determined intensity - vs - $(\text{current})^2$ dependence of the enhanced lines, it appears that this reported non-oscillation does not preclude oscillation being obtained in a H.C.D. structure which operates at a higher current density than that used in this work.

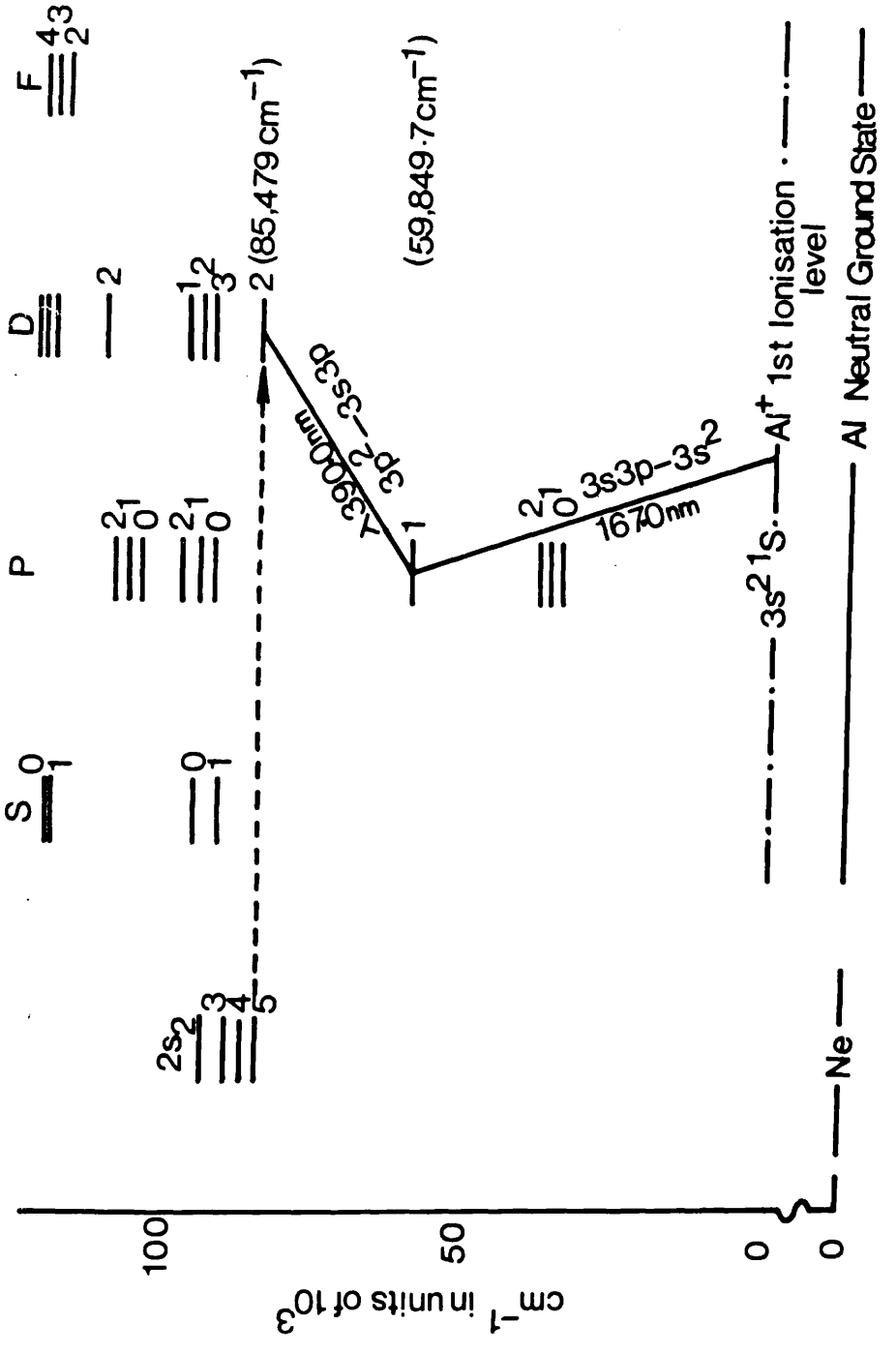

Fig. 5.1. Neon-aluminium partial energy level diagram showing proposed laser transition.

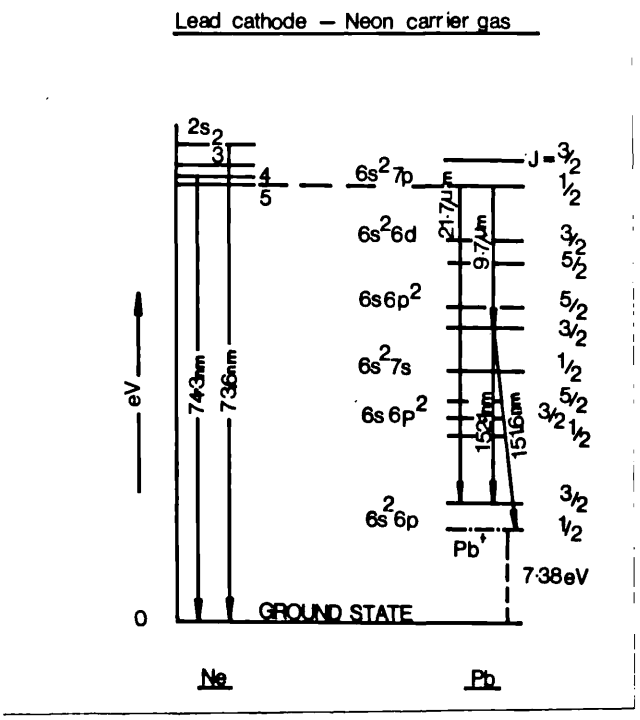

Fig. 5.2.

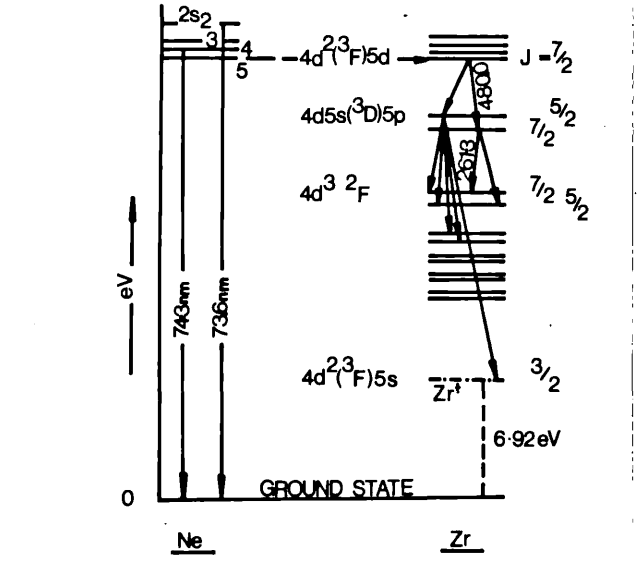

Fig. 5.3.

Energy level coincidences in lead and zirconium showing possible laser transitions.

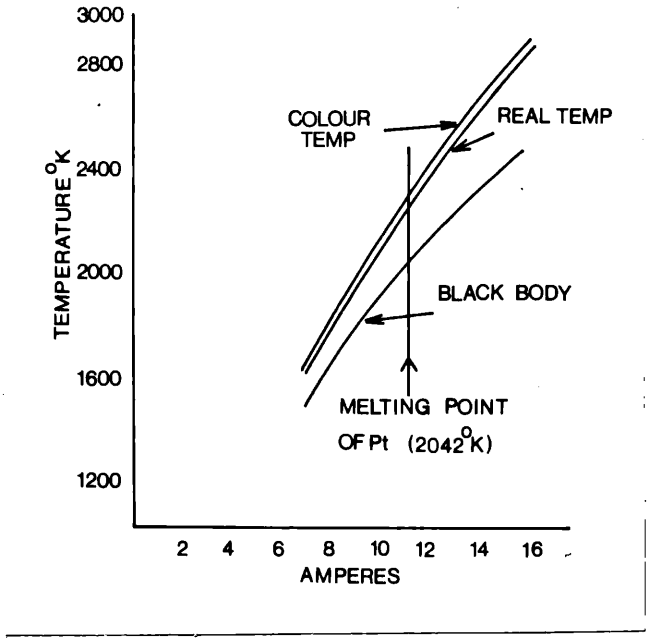

Fig. 5.4. Typical tungsten ribbon lamp calibration.

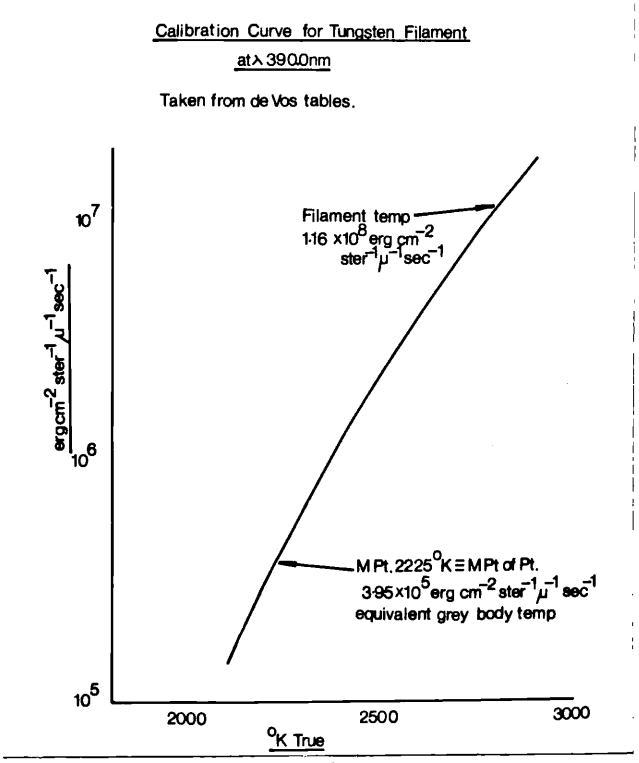

Fig. 5.5. Calibration curve for tungsten filament at 390.0nm.

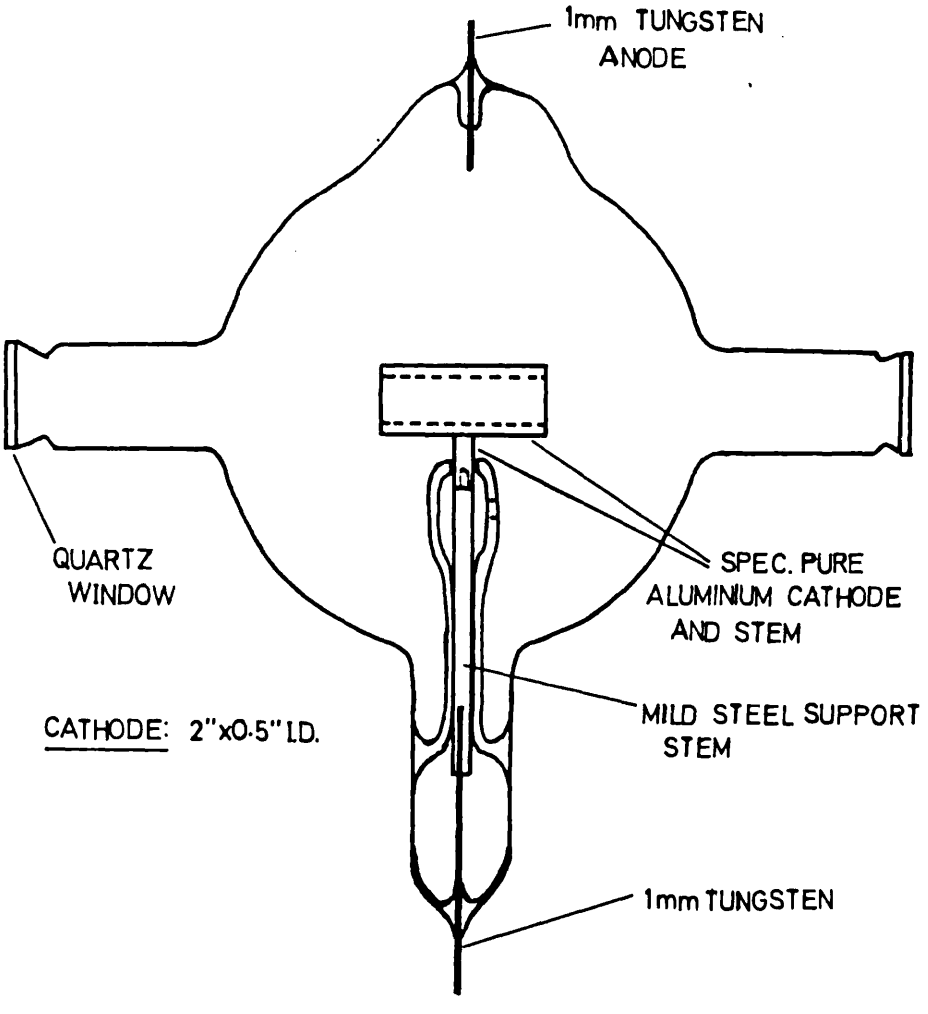

Ne-Al Hollow Cathode Discharge tube.

Fig. 5.6.

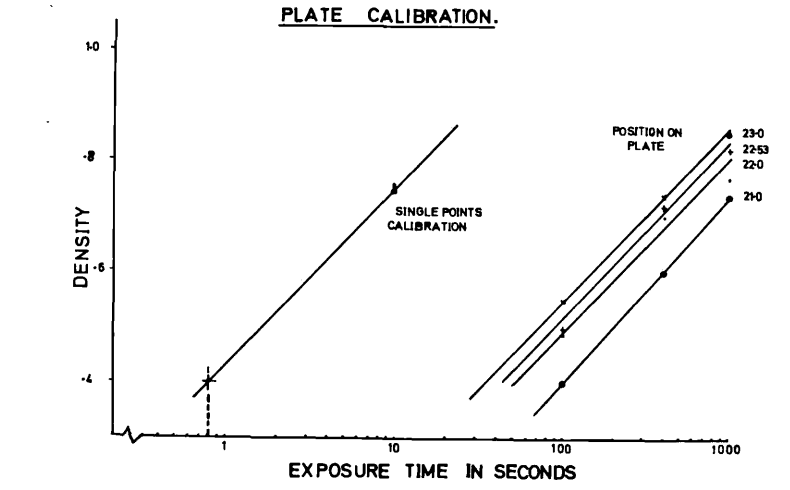

Fig. 5.7. Photographic plate calibration at 390.0nm.

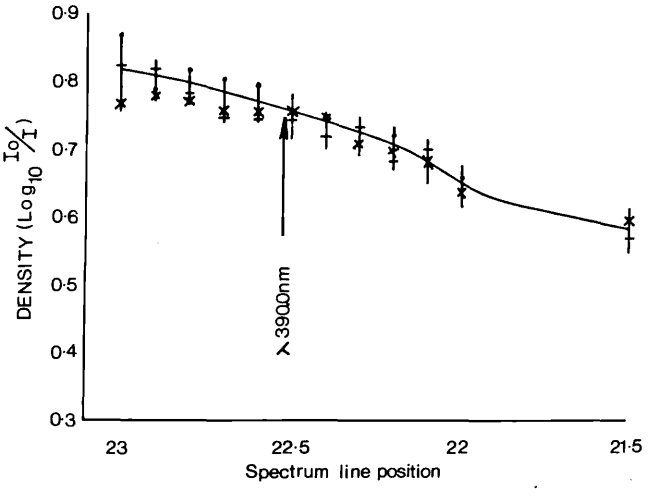

Fig. 5.8. Photographic plate calibration-continuous source.

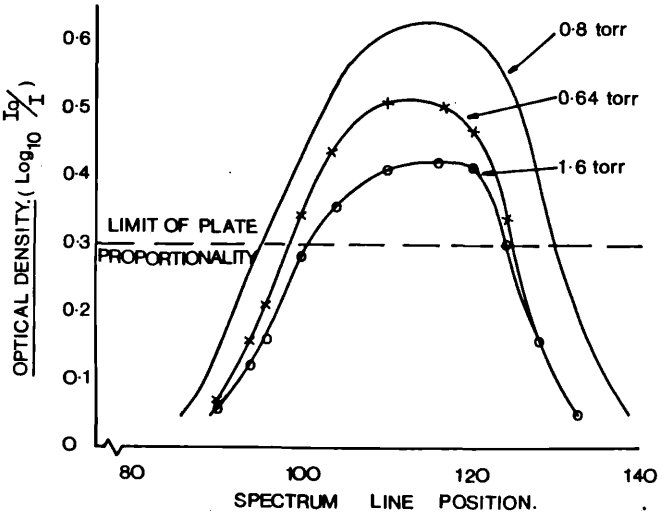

Fig. 5.9. Profile of ionised aluminium line at 390.0nm.

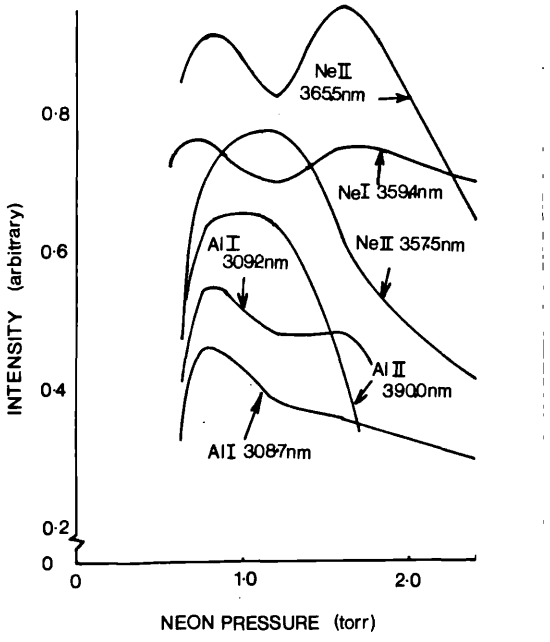

Fig. 5.10. Variation of intensity with pressure of neon.

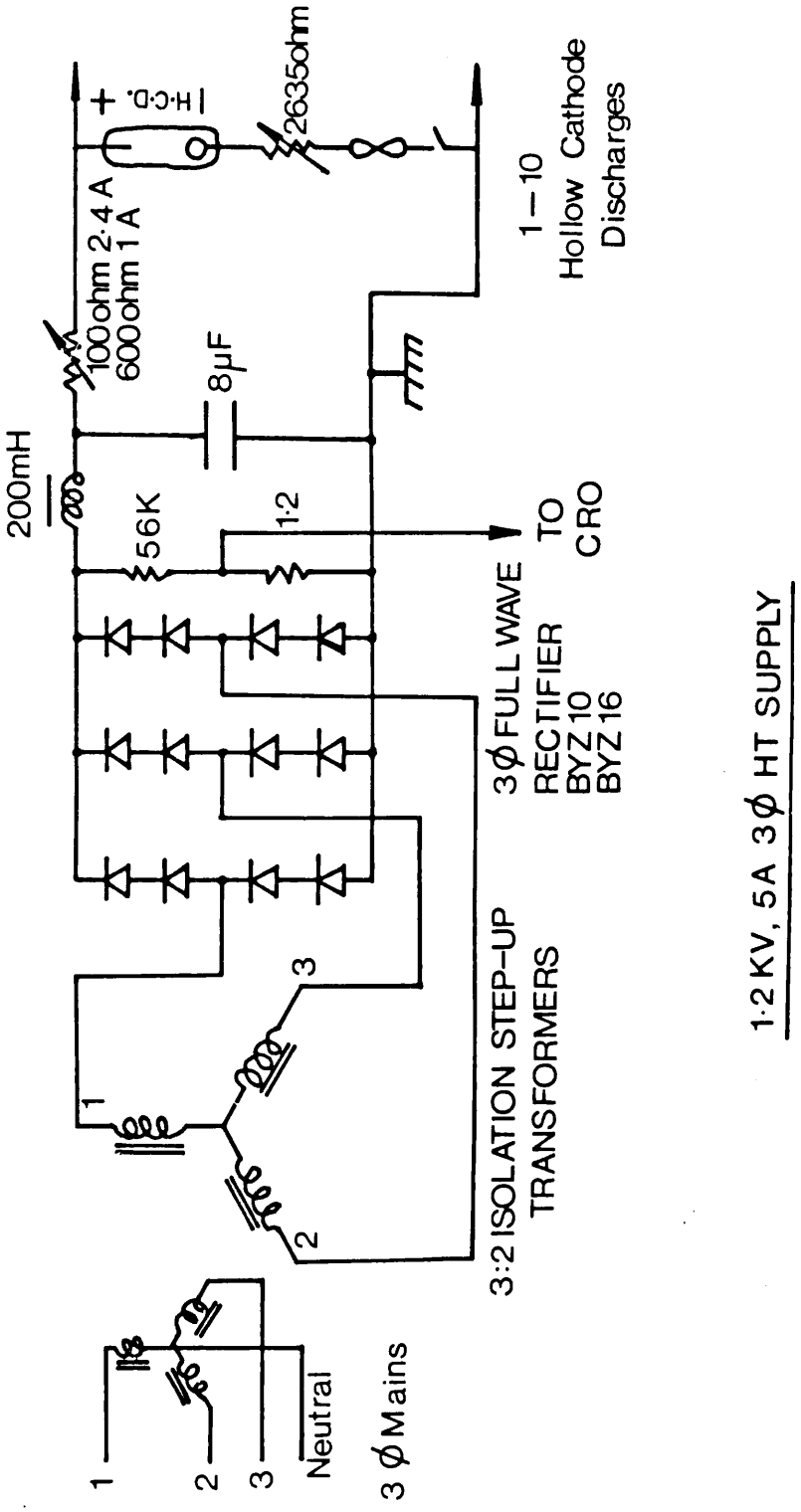

Fig. 5.11. Hollow cathode discharge power supply.

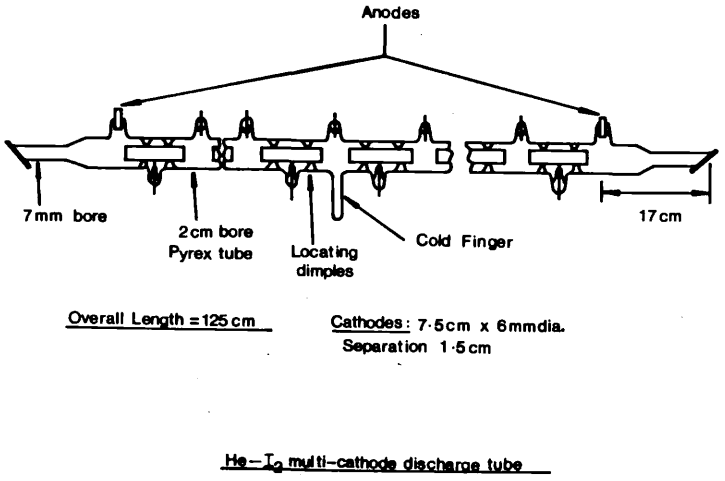

Fig. 5.12. Helium-neon multi-cathode discharge tube.

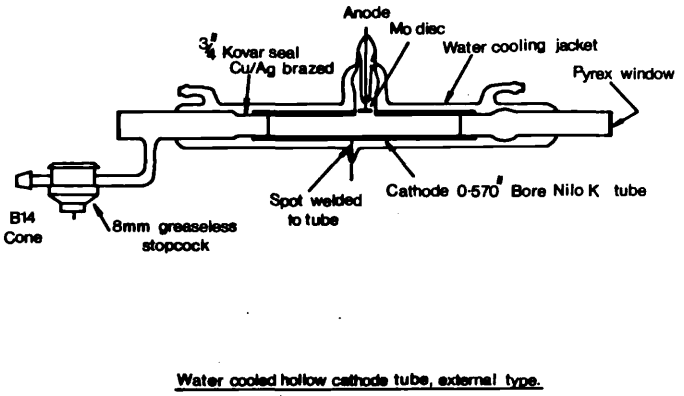

Fig. 5.13. Helium-neon and neon external H.C.D. tube.

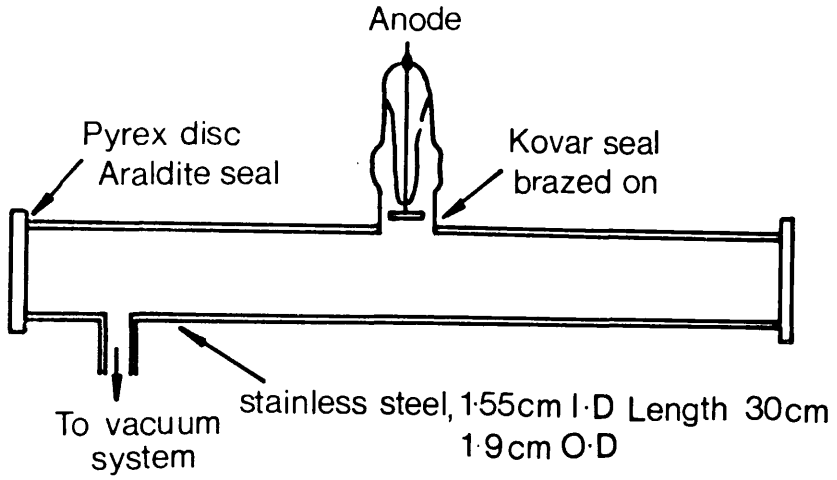

Fig. 5.14. Chebotayev tube without water cooling.

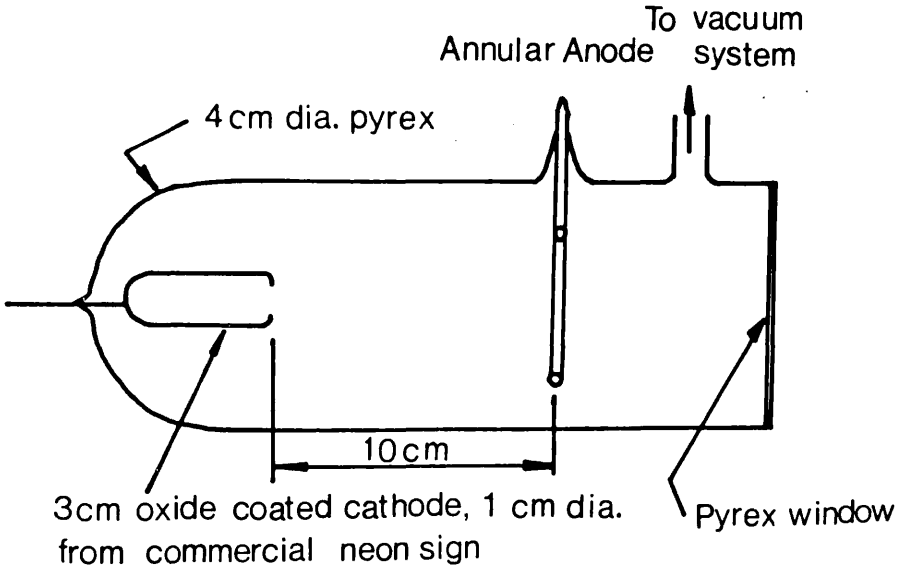

Fig. 5.15. Negative glow test tube.

Figs. 5.14 and 5.15. Experimental discharge tubes.

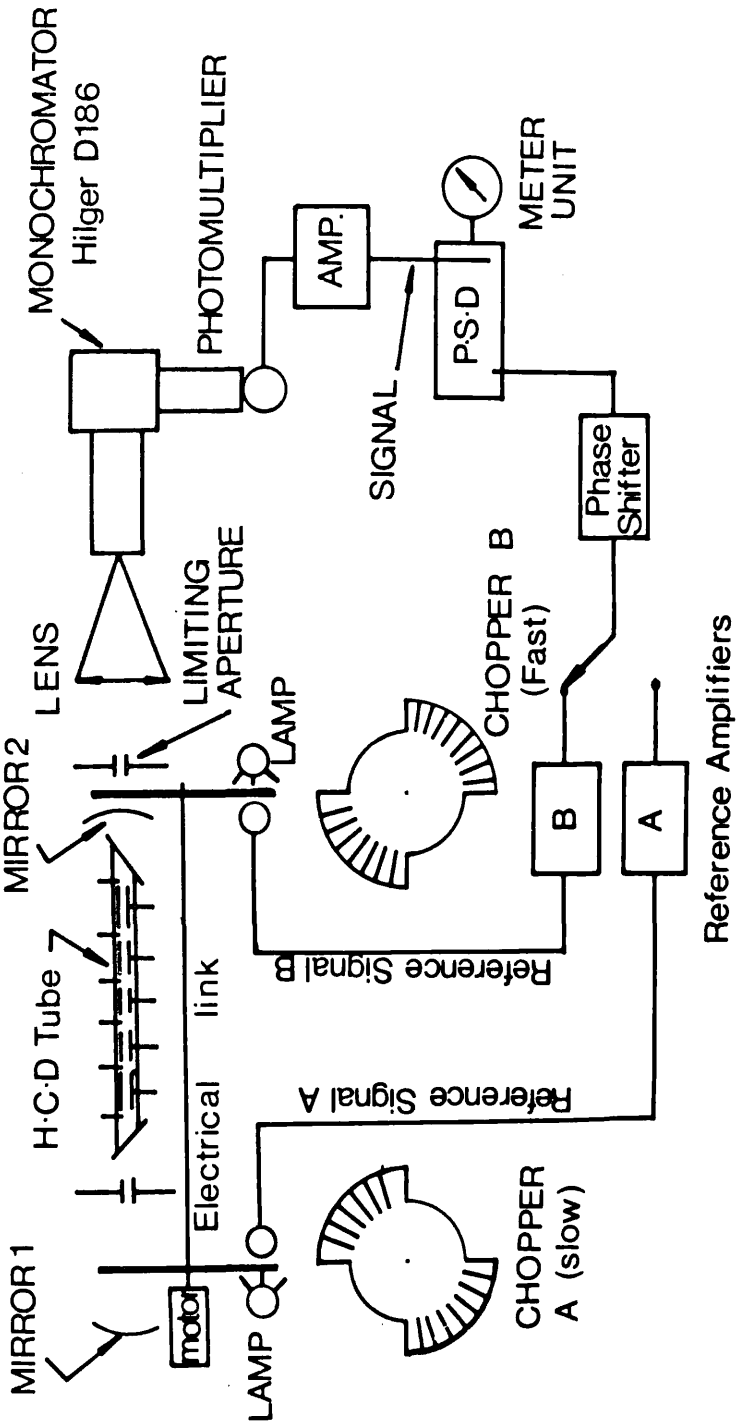

Fig. 5.16.

Experimental layout for gain measurements

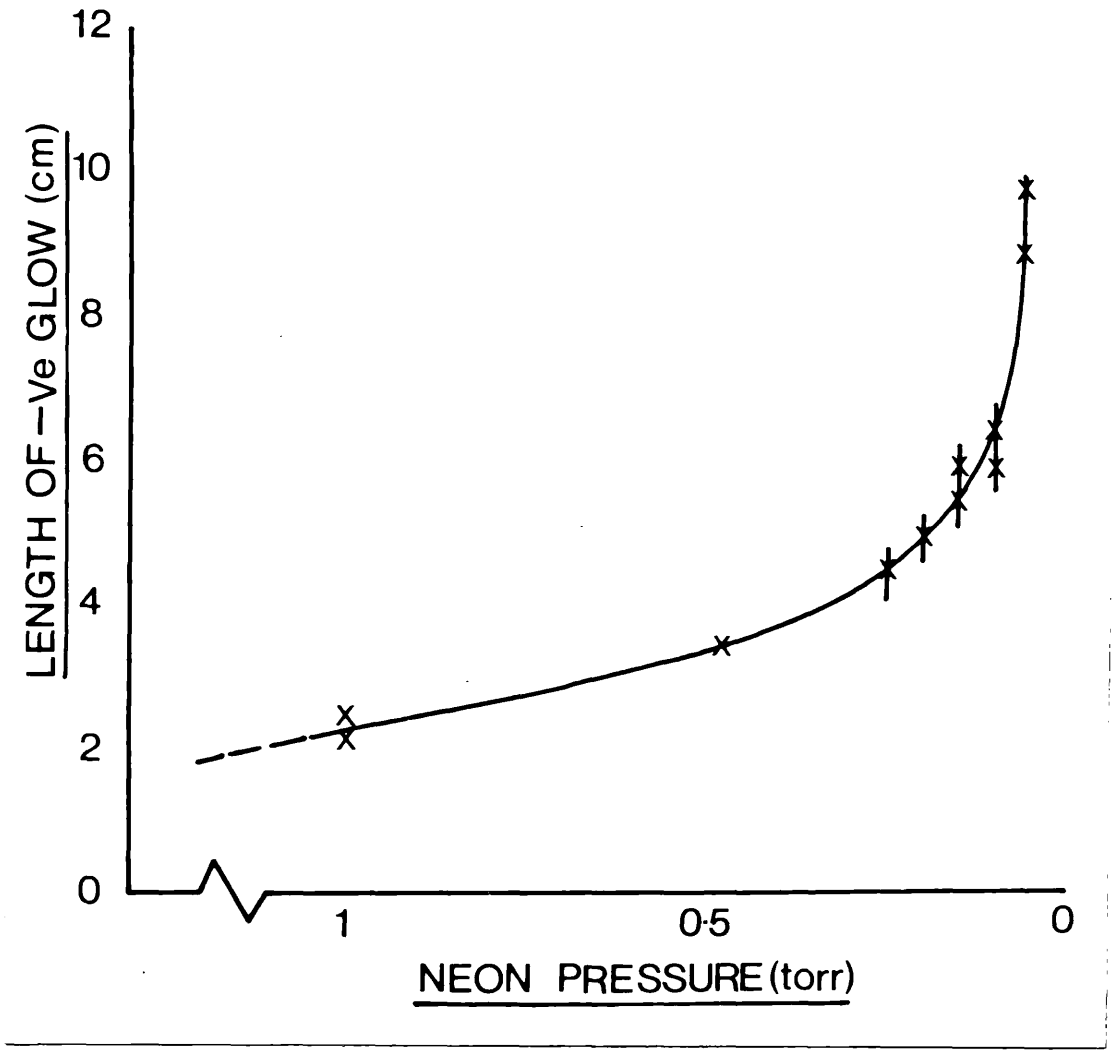

Fig. 5.17. Extent of negative glow-vs-pressure of neon.

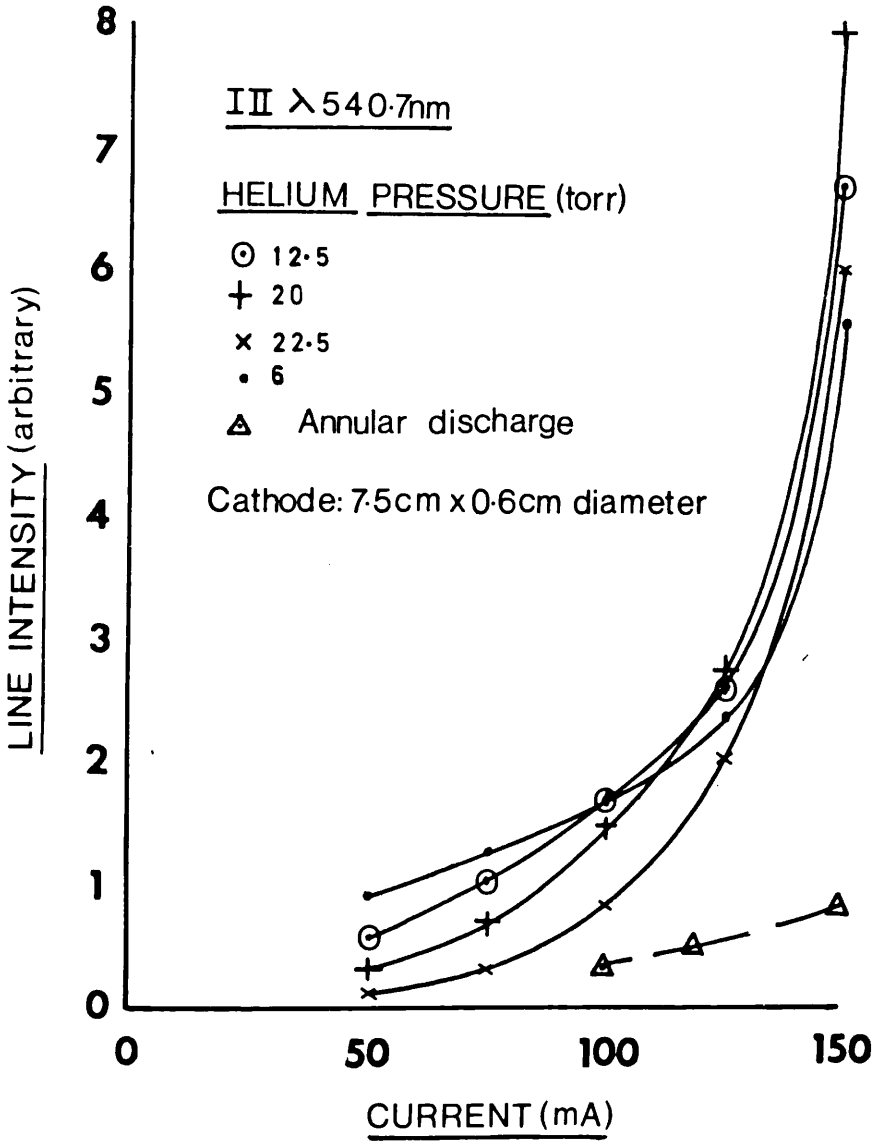

Fig. 5.18. Variation of line intensity with current.

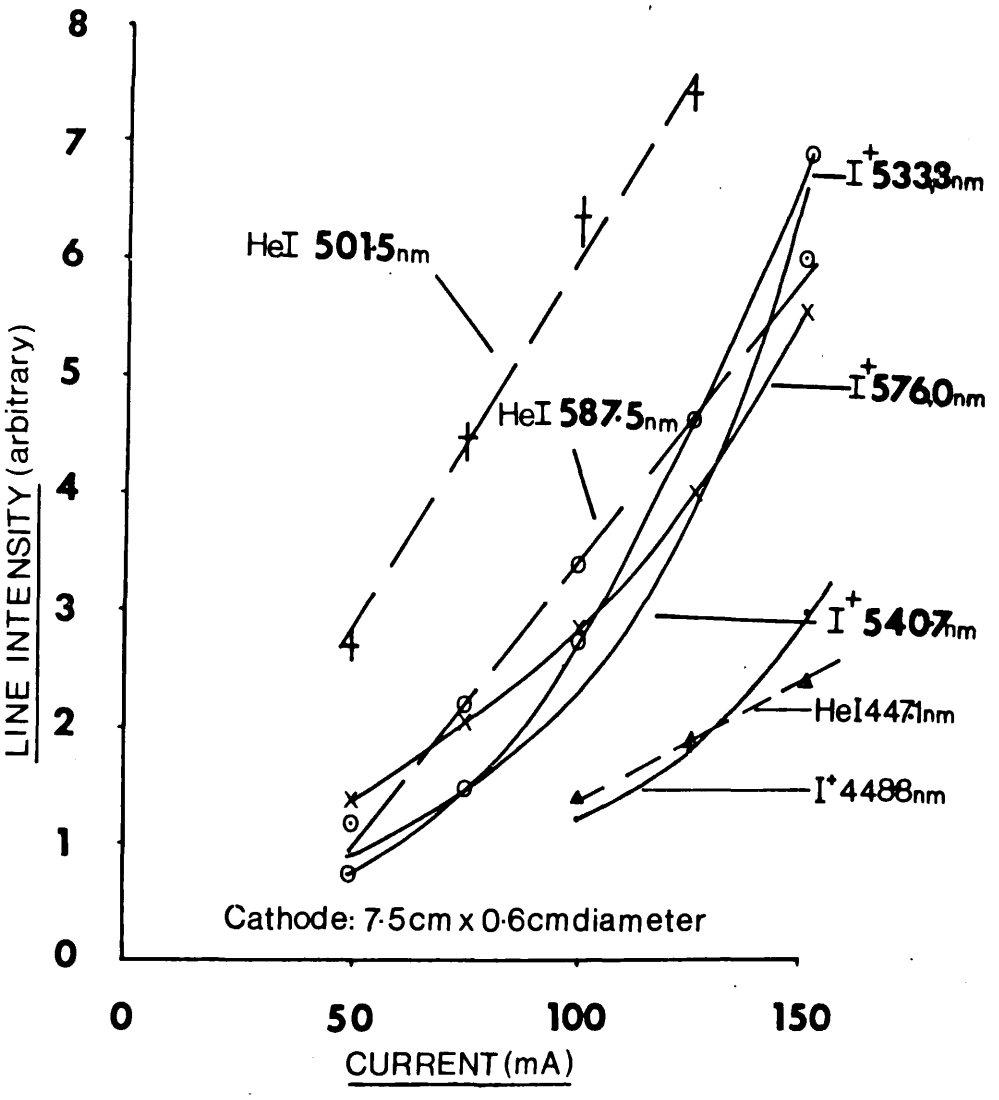

Fig. 5.19. Variation of intensity of ionised iodine and helium lines with current (15 torr of helium).

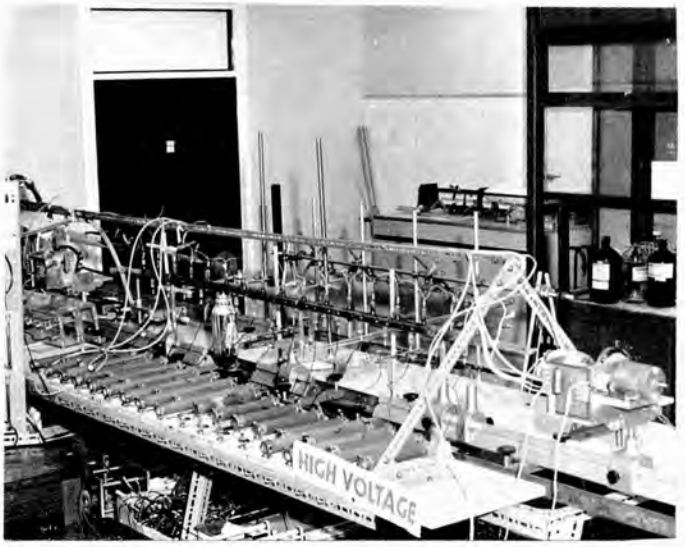

Plate 5.1. General arrangement of helium-iodine H.C.D. apparatus showing chopper systems.

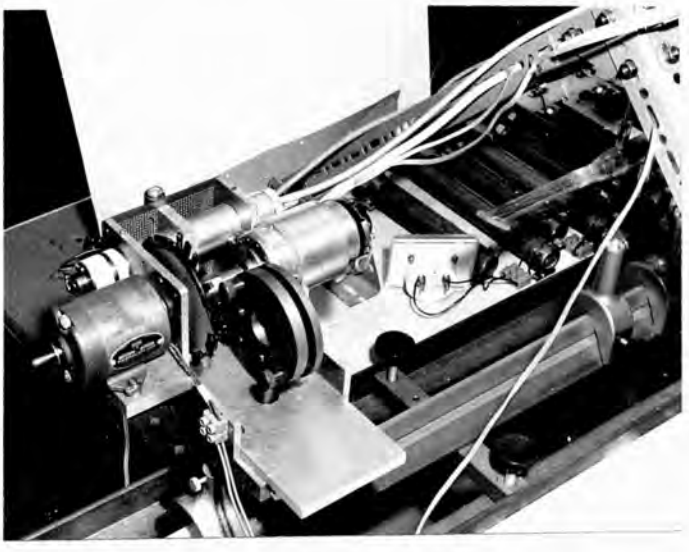

Plate 5.2. 'Resonant' chopper assembly.

CHAPTER 6

Population Inversion in positive column discharges

Introduction

This short chapter deals only with the helium-neon laser, and explains important aspects of the observed effects of the discharge tube diameter, the pressure, and the addition of helium, on this well documented laser system. It is not concerned with giving a detailed description of population inversion mechanisms in the positive column region of glow discharges, in a whole range of laser systems.

The first helium-neon laser reported by Javan, Bennett and Herriott (1) at 1.1523μm, used an electrodeless rf excited discharge. This type of discharge was used to avoid sputtering of the internal mirrors that were first used. It was later shown by White and Rigden (2), using an external mirror cavity, that oscillation could be obtained in the positive column of a glow discharge.

6.1 Population inversion problems.

A number of theoretical studies of population inversion in gaseous discharges have been made in which the assumption is made that a Maxwellian electron energy distribution is applicable,(Basov, (3), Javan (4)). The validity of this assumption is not obvious, and it has been questioned by Fabrikant (5), Ward (6) and Bennett (7).

In the first helium-neon systems operating in neon at 1.1523μm and at 632.8nm, the dominant mechanisms producing population inversion were considered to be those of resonant energy transfer collisions involving helium metastables and ground state neon atoms, as described in Chapter 4. Subsequently oscillation was obtained at 1.1523μm in an rf discharge in pure neon by electron impact excitation, and in the infra red in a number of pure noble gases by Bennett (8). However, the addition of helium was found to give increased gain, (notably in a helium-xenon discharge) in noble gases, where resonant energy transfer collisions do not occur, (Patel et al.(9)). At the same time as the above, Rigden and White (10) showed that the gain at 632.8nm in the helium-neon laser varied inversely as the discharge tube diameter. This inverse diameter dependence of the single pass gain has been attributed to the process of diffusion to the walls and de-excitation of the Ne 1s metastables, the presence of which results in electron excitation to the 2p levels, and also in radiation trapping of the 2p-1s emission.

Bennett (11), however, has analysed the helium-neon laser, and calculates that the only process that can result in a 1/r gain dependence is that of atom-atom collisional de-excitation of the lower laser levels, and that diffusion of metastables to the walls results in a $1/r^3$ gain dependence. This observed 1/r gain dependence led to the design of small bore lasers systems, and led to substantial gains being obtained. With tubes of diameter about 2mm it is difficult to couple in enough rf power and it is now customary to use dc discharges to provide the necessary excitation.

The observations above led to an examination of the discharge properties of the positive column (and rf) discharges, in an attempt to obtain a unifying qualitative explanation of helium-neon laser discharges, and the effect of helium in gaseous laser systems.

6.2 Discharge properties of positive column and rf laser discharges.

The elementary theory of the positive column and rf discharges, in which the ionisation rate and diffusion rate to the walls are equated, gives a good quantitative description of the relation between the axial and radial electric field, pressure, tube radius and the nature of the gas (von Engel (12)).

In the rf discharge, electrons gain energy from the oscillating field, and in the positive column, from the static electric field along the column. The only way that an electron can gain sufficient energy from an oscillating electric field to enable it to excite or ionise, is through elastic collisions. The average kinetic energy lost per collision $(2m/M)$, where m is the mass of the electron and M the mass of an atom or molecule, is more than made up by the gain in energy which can ensue by putting the electron out of phase with the oscillating field, and into accelerating phase with the next half cycle.

In the dc discharge, collisions, in the absence of plasma oscillations, can only result in a loss of kinetic energy by the electrons.

Two things immediately emerge, to produce high energy electrons capable of direct excitation in:-

(a) an rf discharge, the electron collision frequency must be as high as possible.

(b) a dc discharge, the ratio of electron drift velocity/random velocity must be large. This can only be achieved by making the gradient of the static electric field large.

1. Helium has the lowest ionisation efficiency of all the gases at all electron energies, (von Engel (13)) so that it will be the most efficient gas in producing elastic collisions whilst maintaining a high electron temperature (T_e). The action of helium in non-resonant laser systems, and rf laser discharges can thus be explained. This collisional interpretation and its importance in the 632.8nm helium-neon laser has been borne out by the observations of Toyoda and Yamanaka (14) who observed that in a 60 c.p.s. sinusoidally modulated helium-neon rf discharge, oscillation was observed only when the electron collision frequency was high. Whilst the collision frequency increased the electron density remained essentially constant.

2. A reduction in the bore of a discharge tube results in an increase in the electric field that is needed to balance the charge diffusion loss. As a result of the increase in the electric field, the average energy of the electrons increases, and more direct electron impact excitation occurs in the form of;

$$Ne + e \longrightarrow Ne(3s_2) + e \quad \ldots\ldots (6.1),$$

$$He(^1S_o) + e \longrightarrow He(2^1S) + e \quad \ldots\ldots (6.2),$$

or

$$He(^1S_o) + e \longrightarrow He(2^3S) + e \quad \ldots\ldots (6.3).$$

Wada and Heil (15) have recently shown that at a pressure x diameter of discharge (pD) of 0.6 torr - mm, in a helium-neon dc discharge, the average electron energy is 20eV. Direct excitation to the $3s_2$ level can therefore be appreciable.

A further examination of the properties of helium-neon laser discharges has resulted in the establishment of a relationship between such a discharge and 'transition discharges', and the fact that there is an optimum value for the average electron temperature for maximising population inversion on the ($3s_2$ - $2p_4$) 632.8nm neon transition in a helium-neon discharge.

6.3 The relationship between the 632.8nm helium-neon laser discharge and transition discharges.

Using the elementary theory of the positive column in a single gas (von Engel and Steenbeck (16)), and extensions to the theory by Dorgelo, Alting and Boers (17) for binary gas mixtures, Young (19) has shown that the average electron energy in the positive column of a helium-neon discharge is a function only of the pressure-diameter product (pD) and the mixture ratio of the two gases. Fig. 6.1 (after Young (18)) shows the variation of the average electron temperature with pD and the mixture ratio. The full line is the calculated temperature, the dashed line is a straight line approximation to the calculated temperature. Good agreement is shown between the calculated and experimentally determined electron temperature estimates of Labuda and Gordon (19).

Shown plotted in Fig. 6.1 are results derived from graphs given by Korolev, Odintsov and Mitsai (20) and results given by Mielenz and Nefflen (21) for optimum 632.8nm laser output, for dc and rf discharges respectively. The pD products against the ratio of neon pressure/total pressure are plotted giving the relevant electron temperature in 10^4 ^oK for each discharge. The range of electron temperature over which optimum population inversion on the $3s_2$ ..... $2p_4$ levels occurs is about 8,000^oK for each type of excitation in each experimental determination.

At helium:neon ratios greater than 5:1, or P_{Ne}/P_{total} of 0.166, the reported optimum for 632.8nm laser gain, (Gordon and White (22)) energy transfer from $He(2^1S)$ metastables, or the production of high energy electrons via superelastic collisions with helium metastables, can explain the movement of $p_{optimum}$ D to lower electron temperatures.

The effect of reducing the diameter of a plasma tube, or reducing the pressure is to increase the electron temperature in agreement with the results of Bochkova et al. (23), (24). This increase is extremely rapid below 5mm bore, and partly explains the increase in gain experienced with small bore laser tubes (10).

In Fig. 6.1 assuming that the average electron temperature 6.0 x 10^4 ^oK is an optimum for 632.8nm oscillation in a typical rf helium-neon discharge, and remains constant at P_{Ne}/P greater than 0.3, the pD required to maintain this electron temperature in pure neon is approximately 2.9 - 3.2 torr-mm; with D = 12mm, p = 0.26 torr. This pressure corresponds closely to the pressure of 0.24 torr in a tube of 12mm bore, in an rf discharge, at which a transition from a 'weak' to a 'strong' discharge in neon occurs, see

Table 6.1, (after Bochkova and Razumovskaya (25)) and Figs. 6.2 - 6.3 (26, 23) for variation of excited atom concentrations with electron concentration in these transition discharges, and the pressure dependence of the brightness of some helium spectral lines in tubes of different diameters respectively.

To maintain an electron temperature of 6.0×10^4 °K in a pure helium rf discharge, requires a pD of approximately 7 torr-mm. For a 12mm diameter tube, p = 0.58 torr. This is again in reasonable agreement with a p = 0.4 torr, D = 12mm, transition point in pure helium (25). It has been reported by Bochkova and Razumovskaya (25) that population inversions occur in similar transition discharges in helium. Under these transition discharge conditions, the electron mean free path is of the same magnitude as the diameter of the discharge tube, and appears to be similar to that in a 'constricted' glow discharge (von Engel (12)). Bochkova and Razumovskaya (23) attribute these population changes to dissociation of ion-molecular complexes, since the influence of the walls of the discharge tube when $\lambda_e \simeq D$, is to produce a Maxwellian distribution of electron velocities.

Constant electron temperature

Korolev et al. (20) have shown that as long as the neon pressure - diameter product is high enough to give complete radiation trapping of the 60.004nm vacuum UV transition, $3s_2$ - the neon ground state, the 632.8nm helium-neon laser output depends only to a small extent on the helium pressure.

Results shown in Table 6.2 derived from reference (20), show that the pressure-current product is constant for optimum 632.8nm laser output, when radiation trapping is complete. This is consistent with the maintenance of constant electron temperature (von Engel, priv. communication). It is, however, contrary to the observations of Labuda and Gordon (19) who have shown, using a microwave noise measurement technique, for a given pressure-radius product, that the electron energy is <u>not</u> dependent on the discharge current over a wide range of pressures in a typical 632.8nm helium-neon discharge.

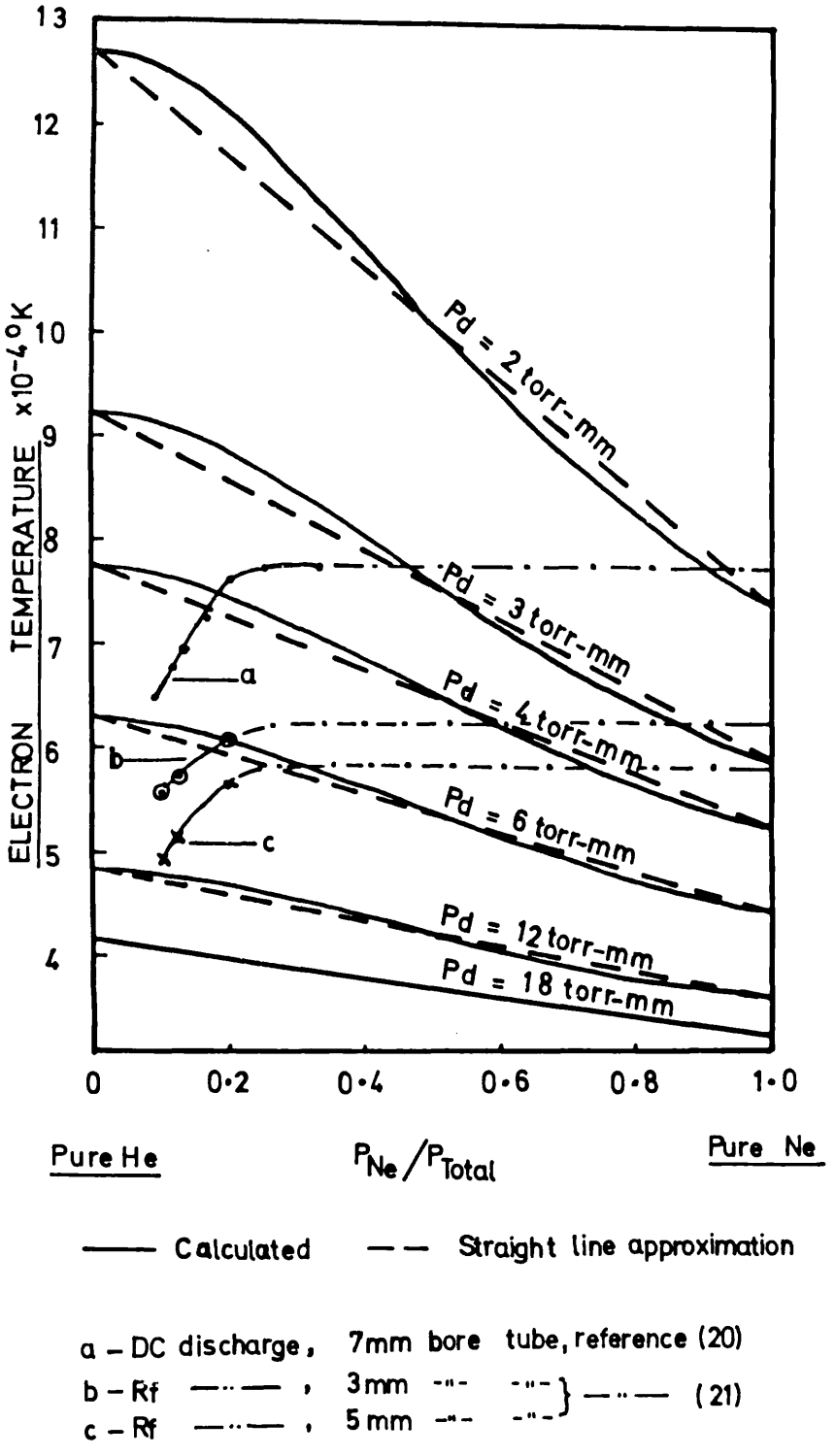

Fig. 6.1. Variation of electron temperature with helium-neon mixture ratio showing 632.8nm Pd optima.

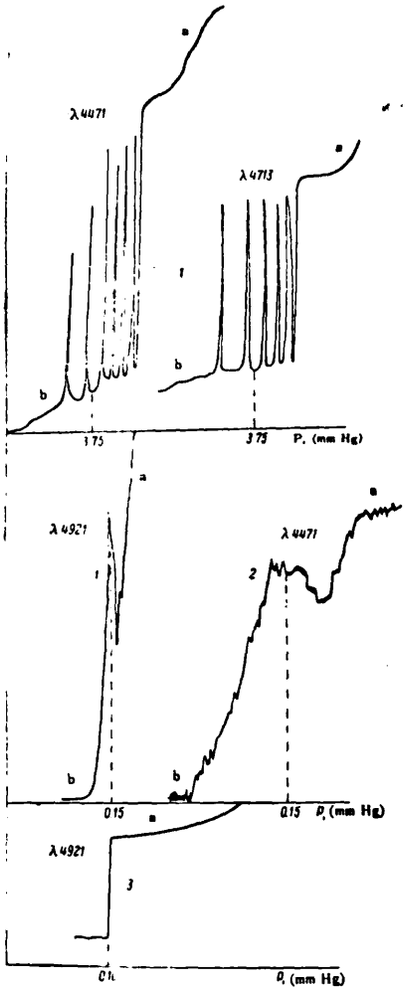

Pressure dependence of the brightness of some helium spectral lines in tubes of different diameters. 1—3, 2—35, 3—60 mm.

Fig. 6.2

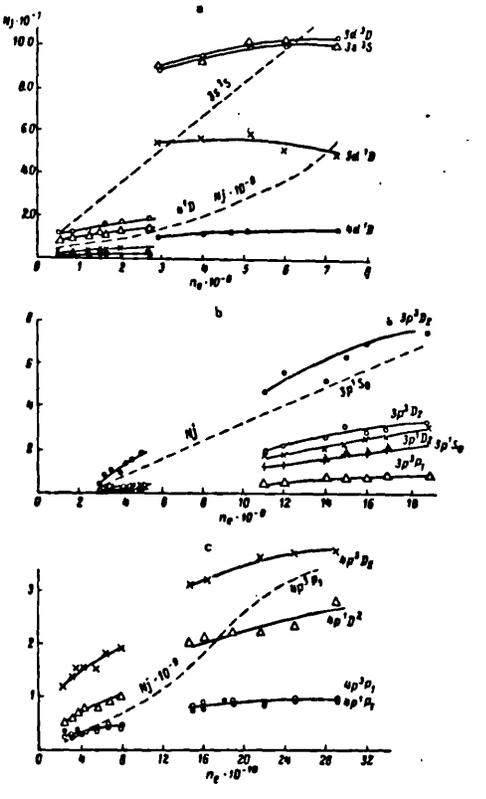

Variation of the concentration of excited atoms in the higher energy levels of (a) helium, (b) neon, and (c) argon with the electron concentration in "weak" and "strong" discharges. The dashed line gives the calculated curve for one of the levels of Ne, He, and Ar. The prints on the left refer to the "weak" discharge (small n_e), and on the right to the "strong" discharge (large n_e).

Fig. 6.3

GAS	Tube diameter(mm)			
	3·0	12·0	35·0	60·0
Helium —	3·8-20	0·4	0·15	0·10
Neon —	—	0·24	0·10	—
Argon —	—	0·06	—	—

Table6·1 Transition pressures (torr)

He: Ne ratio	Total Pressure (torr)	Optimum Current (mA)	Pressure X Current (torr–mA)
= 7:1	1·4	25	35
	1·2	30	36
DC discharge	1·0	32	30
	0·8	42	33·6
7 mm bore tube	0·6	52	31·2
	0·5	82	41

Table6·2 Pressure/optimum current relationship for maximum output at λ 632·8nm

CHAPTER 7

Population Inversion in pulsed discharges - the Helium - Iodine system

Introduction

As stated in 5.1.2, laser oscillation in ionised iodine was first observed by Jenson and Fowles (1) in the afterglow of a pulsed helium - iodine mixture. Oscillation on twelve lines was subsequently reported by them (2) using a few torr of helium and 0.1 torr vapour pressure of iodine, in a cold cathode discharge of 5mm bore and length 1.2m.

Oscillation was also observed at 562.5 and 690.4nm in a neon-iodine discharge, and at 690.4nm in a krypton-iodine discharge.

As all the upper levels, except for the 562.5nm line, are within 0.51 eV of the helium ion ground state $He^+(0)$, Fowles and Jenson (2) suggested that the selective excitation, in the case of the helium-iodine system, was by the following process,

$$He^+ (^2S_{1/2}) + I(^2P_{3/2}) \longrightarrow He(^1S_o) + I^+(X) \qquad \ldots\ldots (7.1)$$

If the excited level of ionised iodine (X) in this asymmetric charge exchange reaction is a triplet, spin is conserved, but not if it is a singlet. Figure 7.1 shows that laser oscillation is only observed from triplet levels.

Both helium and neon metastable states have sufficient energy to excite an iodine ion by a process analogous to that reported by Dana and Laures (3) for the Kr and Xe afterglow lasers,

$$He(2^3S) + I^+(0) \longrightarrow He(^1S_o) + I^+(6p') + \Delta E \qquad \ldots\ldots (7.2)$$

$$Ne(1s) + I^+(0) \longrightarrow Ne\ (^1S_o) + I^+(6p') + \Delta E, \qquad \ldots\ldots (7.3)$$

the iodine ion being formed either by prior collision with another helium or neon metastable, or by photodissociation in the discharge. Using the notation of Martin and Corliss (4):

(i) There are three singlet levels ($6p'\ ^1F_3$; $6p'\ ^1P_1$; $5d'\ ^1D_2$) which are closer to the helium ion ground state than the upper laser levels, but these do not undergo population inversion, implying that spin conservation is important in the populating process.

(ii) There is a transition from the singlet level $6p'\ ^1F_3$ giving a strong ionised iodine line at 607.5nm, analogous to a very strong laser transition ($5s'\ ^1D_3 - 5p'\ ^1F_3$) observed in pure bromine by Keefe and Graham (5), and isoelectronic with a laser transition in doubly ionised xenon (463.7nm) (6), so that laser oscillation is to be expected on this transition if the singlet levels were being populated at a rate equal to that of the triplet levels, and also if the selective excitation was by electron impact.

(iii) There is also a very strong transition ($6s'\ ^3D_2 - 6p'\ ^3F_3$) at 533.8nm, from a triplet level closer to the helium ion ground state than any of the upper laser levels, which does not oscillate. This line is equal in intensity to the 540.7nm laser line, which is enhanced 1) when used with helium under pulsed conditions; 2) in the H.C.D. work reported in Chapter 5; and 3) in the work of Berezin and Yanovskaya (7). This line corresponds to a laser transition in Cl II at 490.5nm (8), and by comparison with Xe III, is expected to have a large relative line strength. (Fig. 7.17). Furthermore the line ($5d\ ^3D_2 - 6p'\ ^3F_3$) at 456.06nm from

the $6p'\ ^3F_3$ triplet level, analogous to a weak laser transition at 505.4nm in Br II, does not oscillate under the conditions used.

Absence of laser oscillation on these lines would appear to indicate that the $6p'\ ^3F_3$ level is not being selectively excited at the same rate as the other triplet levels or that transition probabilities are not suitable for oscillation.

Table 7.1 gives a list of transitions in the range 480.0 - 830.0nm, in ionised iodine which have upper levels within approximately 0.5 eV of the ion limit of $He^+(0)$. Indicated are those lines which are enhanced in helium, (E), and those on which laser oscillation has now been observed (L).

The following sections describe the apparatus constructed, and the experiments carried out, in the helium-iodine system, to determine the excitation mechanism responsible for the population inversion, and subsequent laser oscillation.

7.1 Experimental Apparatus

7.1.1 The pumping/filling vacuum system

The pumping/filling system used was that described in Chapter 5, which was used for the H.C.D. investigations. Plate 7.1 shows the general arrangement of the apparatus.

7.1.2 The Pulse Modulator.

The pulse modulator constructed was designed to give high voltage pulses at up to 40KV at up to 25A, at a variable repetition

rate of 500 - 1,500 c/s., with the length of the current pulse determined by the delay line and the power capabilities of the high voltage dc power supply constructed.

Fig. 7.2 shows the basic circuit of the modulator, which was based on a modified government surplus radar pulse modulator, kindly given by R.R.E., Malvern, for this work.

The discharge capacitor or delay line is charged from a dc power supply having a maximum output voltage of 10KV, resonant charging of the line occurs through a 10H charging choke, and H.V. diodes are included in the charging circuit to disconnect the line or capacitor from the supply when the voltage reaches a maximum and is beginning to fall (9). The discharge is triggered by a heavy duty thyratron. To isolate the discharge and to help match the non-linear discharge to the delay line and to step up the discharge voltage a 4:1 bifilar-wound pulse transformer is incorporated in the circuit.

The discharge current was monitored by means of a 1:1 current transformer on the earth return from the discharge tube. Provision was made for monitoring waveforms of the charging current, thyratron anode and output to the pulse transformer.

7.1.3 The Laser tube

A number of discharge tubes with diameters from 7 to 20mm and from 1m to 2.5m in length were constructed throughout the work to be described.

A typical discharge/laser tube consists of a fused silica tube to which are sealed 7mm bore fused silica Brewster angled end tubes, with windows flat to $\lambda/10$, and parallel to 30 secs of arc. Fused silica was always used for the discharge tube, as this enables end tubes to be sealed directly to it without graded seals, resulting in greater mechanical strength. Moreover, fused silica is believed to give under discharge conditions (10) a lower contamination rate than pyrex.

Internal electrodes from discarded flash tubes are mounted in side arms, with a pumping/filling arm attached close to the large electrode (cathode), where a higher concentration of impurities is expected than elsewhere.

The laser tube could be isolated from the vacuum system by means of a large bore, Viton A, greaseless stopcock.

7.1.4 The laser cavity

Near Confocal arrangement

This consists of two multilayer concave mirrors, dielectric-coated, high reflectivity, (greater than 98 per cent over the range 600 - 680nm) used in a near confocal configuration. This configuration, although having the disadvantage of not using the whole volume of the active medium, is comparatively easy to set up and enables mixed radii of curvature mirrors to be used.

The orthogonal movement mirror mounts shown in Fig. 7.3 provide a means of holding the cavity mirrors without damaging the dielectric coatings, and of adjusting the mirror alignment. The 40 TPI micrometer

screws provided all the coarse and fine adjustment that was necessary, with 45 minutes of arc per turn, and a minimum setting variation of about 3 minutes.

Prism wavelength selection

In later work in the helium-iodine system it was desired to select single laser transitions from amongst a number competing for upper level populations. A modified version of the prism wavelength technique suggested by White (11) was used, as shown in Fig. 7.4. Plate 7.2 shows the prism/mirror arrangement.

The Brewster angled prism of fused silica, n = 1.4601 at λ 546nm, giving a prism angle of $68^{\circ}\ 50'$, with a total cavity loss approaching 0.5 - 1 per cent, is mounted on a rotatable table so that it can be positioned for minimum deviation. A cross slide enables one of the resonator mirrors to be positioned and adjusted in an off-axis position to complete the cavity. With the cavity shown in Fig. 7.4A, single wavelength oscillation could be obtained, when the wavelengths differed by more than about 6nm. With smaller separation, simultaneous oscillation at two wavelengths on different parts of the cavity mirrors occurred.

7.2 Experimental details and procedure.

7.2.1 Cleaning of laser tubes

The condition of the Brewster angled end tube windows is critical in most laser oscillators. For this reason, care was taken to avoid

condensation occurring on the end tube windows during glass blowing by using a drying tube and by flaming with a hot, blue, torch flame. After assembly laser tubes were washed out with warm Decon 75 and thoroughly rinsed out with distilled water. Finally, to remove any remaining distilled water, the tubes were washed out repeatedly with methyl alcohol and pumped out on a two stage gas ballasted rotary vacuum pump. Prior to connection to the vacuum system, tubes were pumped out and closed off to prevent ingress of dust from the room.

7.2.2 Outgassing

Accidental impurities can have a deleterious effect on collisional processes occurring in a laser discharge. (In the helium-neon laser, an oxygen contamination in neon of 1 part in 10^4 gives a reduction in gain of 1 per cent, and 1 in 10^3 gives 100 per cent reduction, (Taylor (12)).

To outgas the laser tubes, electrothermal heating tapes were wound around the tube and electrode assemblies and gradually run up to above 250°C with the diffusion pump on. At the same time any exposed glassware of the pumping/filling system was flamed in a direction towards the pumps.

After a minimum of two hours the heating tapes were removed, helium added to a pressure of approximately 10 torr and a pulsed discharge run. As impurities were removed from the electrodes and walls of the tube, the line spectra of helium changed to band spectra. The tube was then evacuated as quickly as possible. When this procedure had been carried out for three or more times, the discharge would maintain emission of line spectra.

Although the system used was not bakeable at the usual temperature of 400 - 500°C, the outgassing procedure used proved satisfactory, and laser oscillation could be obtained in a tube after it had been left isolated for periods of at least one week.

After filling with helium to the desired pressure, iodine was allowed to diffuse through from the iodine reservoir. To maintain laser oscillation it was found necessary periodically to bleed in iodine vapour to replace that which became absorbed on the walls of the tube close to the electrodes.

7.2.3 Resonator alignment

Cavity mirror alignment was achieved by means of the simple pinhole and illuminated cross method. Alignment was indicated by the appearance of a bright 'moon' when looking through the pinhole along the axis of the discharge tube. Once this bright 'moon' was seen, it was centralised by minor adjustments to both mirrors. This adjustment was carried out before conditions were optimised for laser oscillation.

Observation of oscillation

Cavity mirrors peaked at 632.8nm were used when oscillation was first obtained. Oscillation was initially indicated by a regular diffuse yellow pattern which could be seen when the laser tube was viewed axially through a small 15,000 LPI transmission diffraction grating. This faint pattern developed as the pulse voltage was increased and disappeared on further increase of voltage. Optimum output was then achieved by careful adjustment of the helium pressure, the vapour pressure of iodine

and the pulse voltage. It was later found that greater output and stability was obtained if the 2μsec delay line was replaced by a 0.0066μF H,V. capacitor, and a simple capacitor discharge used instead of one having a fixed interval, determined by the delay line.

Oscillation on seven lines 703.3, 658.5, 612.7, 576.0, 567.8, 540.7 and 498.7nm, previously reported by Fowles and Jenson, was observed subsequently with a number of cavity mirrors with reflectivity greater than 98 per cent over the wavelength range 500 - 700nm, using a laser tube of 7mm bore.

The 'mildness' of the excitation necessary to give laser oscillation, the sensitivity of each transition to modulator input voltage, and the observation that a short current pulse gave maximum output, suggested that the means by which population inversion occurred in this system was different from that occurring in the inert gas ion laser systems. It was decided, therefore, to use a larger bore laser tube, where collisional recombination processes would be increased and wall effects diminished, where cataphoresis would be reduced, and in which the variation of radial gain due to the electric field would also be reduced, (Ahmed and Faith (13)).

The use of a 126cm long laser tube, having a plasma length of 100cm and bore of 2cm, subsequently enabled higher gains of up to 10 per cent per metre, and a new intercombination laser transition at 651.6nm to be obtained (14). Further, by maintaining a high vapour pressure of iodine, oscillation on the hyperfine components of a number of lines was

obtained for the first time (15), contrary to the observations of Fowles and Jenson, (16).

Plates 7.3 and 7.4, showing dispersed laser lines crossed with Fabry-Perot fringes, indicate by the double and triple fringe systems that simultaneous oscillation is occurring on hyperfine components of individual laser lines.

During attempts to obtain laser oscillation on the 533.8nm line and certain other lines, using prism wavelength selection, oscillation was obtained on further new lines: 682.5nm ($6s'\ ^3D_3 - 6p'\ ^3F_2$); and 713.9nm ($5d'\ ^3D_3 - 6p'\ ^3D_2$), and on a number of hyperfine components, (17), analysed in 7.3.

7.2.4 Wavelength measurement and hyperfine components determination.

(a) Wavelength measurement

Measurements made on spectrum plates, obtained on a Hilger and Watts D186 Constant Deviation spectrograph having a linear dispersion of approximately 7.0nm/mm at 650.0nm, were not sufficiently accurate to enable identification to be made to less than $\pm$ 1.0nm of the line observed at about 652.0nm. There are two possible transitions in this wavelength region,

(i) ($5p^5\ ^1P_1 - 6p'\ ^3F_2$) at 651.618nm, and

(ii) (tentative classification, $5d'\ ^3D_2 - 6p'\ ^3F_3$), at 651.891nm.

(Martin and Corliss (4) do not classify this 651.9nm line; and the classification above was arrived at by assuming that the laser line would be likely to have an analogous laser transition in

isoelectronic doubly ionised xenon, and that it might be from the $6p'\ ^3F_3$ level in ionised iodine from which oscillation had not been observed. The XeIII laser line at 487.0nm ($5d'\ ^3D_2 - 6p'\ ^3F_3$) (6), gives the correct wave number interval for the 651.891nm I II line.)

A Beck Reversion Spectroscope, No. 3505, was used to determine the wavelength of this line and other lines to within an accuracy of $\pm$ 0.1nm in the following way.

A series of thirteen readings was taken of the closest laser line at 658.5nm and on the unknown line alternately in pairs. From the measurements on the 658.5nm line the instrument error at this wavelength was determined as being 0.63nm. Assuming the instrument error and setting errors at the unknown wavelength would be the same as at 658.5nm, the unknown wavelength is (652.18 - 0.63)nm = 651.65 $\pm$ 0.1nm (σ = 0.05nm on sets of 13 measurements). The line is thus the ($5p^5\ ^1P_1 - 6'\ ^3F_2$) transition, at 651.618nm.

Although this is a doubly forbidden transition involving a change of spin, and being a p - f transition, it recommends itself because the line behaves in a similar way to other laser lines from the $6p'\ ^3F_2$ level. It is later shown in 7.4 to be a line having a lower level that is very strongly perturbed.

Another line at approximately 607.0nm obtained only by using prism wavelength selection, was identified in the same way, using the close 612.7nm laser line as a reference, giving 606.9 $\pm$ 0.1nm (σ = 0.04nm, on sets of 11 measurements).

This ionised iodine line at 606.893nm ($6s'\ ^3D_1 - 6p'\ ^3F_2$) is a line on which laser action might be expected since it has both upper and lower levels common to other laser lines, and it would only oscillate when the very strong laser line ($6s'\ ^3D_1 - 6p'\ ^3D_2$) at 576.0nm was suppressed.

(b) Hyperfine component identification

A Fabry Perot etalon was crossed with the D 186 Constant Deviation spectrometer, with the etalon placed in the parallel light position between the collimator lens and dispersing prism, (Tolansky (18)).

Typical ranges of the hyperfine components in the ionised iodine spectrum are 0 - 0.6cm $^{-1}$. To avoid overlapping of the components of one order with those of another, the separation between orders of the etalon, ($1/2t$ cm $^{-1}$), where t is the separation of the etalon plates, must be greater than the spread of components. Having established the relationships of the components, an etalon with a larger spacer can be used for more accurate hyperfine separation measurements.

In the work described here, an etalon having a fused silica spacer of 10.12mm, with order separation of 0.494cm^{-1} was used, as well as one having ruby ball bearing spacers of 0.125 in, (accurate to 0.0001 in), giving approximately 1.5 cm^{-1} between orders.

The finesse of the 10.12mm etalon, which had aluminised flats and a specified reflectivity of 90 per cent, was calculated as being 360. The instrumental half-width for this finesse, given by $B^2 = 1/(1 + F \sin^2 \delta/2)$, is equal to 1/30 of an order (19), where B^2 is the transmitted intensity, and F is the finesse.

This was checked using a 632.8nm helium-neon laser, in single mode operation, in which the line width is less than the instrumental width. Under these conditions the measured half-width gives directly the instrumental half-width. It was found to be less than 1/10 of an order, so that sufficient resolution was obtainable to enable separation of hyperfine components of greater than 0.05 cm^{-1}, and Doppler line widths of this order, to be determined.

No optics were used between the slit of the spectrometer/spectrograph and the laser, and the laser beam shone directly on the slit. Typical exposure times were 10 - 120 sec, (using Ilford R40 plates), with Fabry-Perot fringes in on-axis and off-axis positions.

Scans were made of the Fabry-Perot fringes shown in Plates 7.3 and 7.4, on a Joyce - Loebl microdensitometer, and measurements made to within $\pm$ 0.02mm using a micrometer eye-piece.

The hyperfine components separation was calculated using:

(a) linear interpolation on the off-axis fringes

(b) the D^2 array method of Meissner (20), on on-axis fringes, (see Appendix 7.1).

A typical calculation is given in the Appendix 7.2, for the three component identification on the 658.5nm line.

By comparison with transition diagrams given by Murakawa (21) - (23) and Tolansky (24, 25), and calculated transition diagrams to give agreement with Tolansky experimental results, the hyperfine components were identified.

7.2.5 Line width determination of lasing components.

Measurements were made on the microdensitometer scans of the Fabry - Perot fringes to yield the line width of the individual lasing components.

7.3 Treatment of Results and Conclusions.

7.3.1 Laser Oscillation

Laser oscillation in ionised iodine was found to occur during the excitation pulse but mainly in the afterglow period, having a duration of up to approximately 250μsec. The duration depends on the vapour pressure of iodine and on the pressure of helium, with oscillation occurring over the helium pressure range of 3 - 60 torr. Maximum laser output occurs at $\sim$ 6 torr of helium, at $\sim$ 0.2 torr vapour pressure of iodine.

Fig. 7.5 shows the time relationship of the 576.0nm laser output (upper trace) and the current pulse (lower trace), at a repetition frequency of 1 Kc/s. (The apparent structure on the waveforms is due to use of 'Chop' on the Tektronix oscilloscope used.) A similar time behaviour is exhibited by the 658.5, 612.7, 540.7 and 521.6nm lines examined. Fig 7.6 shows that maximum spontaneous emission occurs on the 576.0nm line, when the current pulse is practically zero, at about 3μsec after the commencement of the pulse. A similar time dependence is shown by the non-laser ionised iodine 533.8nm line, neutral iodine and helium lines, - Figs. 7.7 - 7.9.

As the vapour pressure of iodine decreases on running the discharge, a reduction in laser output occurs, and finally oscillation ceases. Prior to cessation of oscillation, and after, the spontaneous emission of laser lines has a different time behaviour from that when lasing strongly.

There is an initial rapid increase in intensity on commencement of the current pulse, then a less rapid increase to a maximum at about 20μsec, and finally a slow decay, (Fig. 7.10).

Ionised iodine lines on which oscillation was not observed, neutral helium and iodine lines exhibit the same intensity behaviour, Figs. 7.11 and 7.12.

7.3.2 Laser transitions

The higher terms of I^+ are of three types according to whether the parent term in I^{++} is $5p^3$ - $^4S^o$, $^2D^o$, or $^2P^o$

i.e. $5s^2\ 5p^3$ ($^4S^o$)

" ($^2D^o$)

" ($^2P^o$), indicated by

nx, nx' and nx'' respectively (4).

All the laser transitions (except one) observed by Jenson and Fowles, and the 713.9, 682.5, 651.6 and 606.9nm lines are transitions from three triplet 6p' levels close to and within the range 0.23 - 0.51 eV below the helium ion ground state.

All the laser transitions have UV terminal transitions to the triplet iodine ion ground state, or the triplet $5p^4\ ^3P_1$ level close to the ion ground state. The intercombination laser transition 651.6nm ($5p^5\ ^1P_1$ - $6p'\ ^3F_2$) has an intercombination UV terminal transition to this level. Fig. 7.1, a partial energy level diagram for ionised iodine, shows the laser transitions observed, and the non-laser transition ($6s'\ ^3D_2$ - $6p'\ ^3F_3$) at 533.8nm.

7.3.3 Comparison of ionised iodine and ionised bromine laser transitions.

Grotian diagrams Figs. 7.13 and 7.14, show that laser transitions in ionised iodine differ significantly from those observed in pure bromine by Keefe and Graham (5), where the selective excitation is by electron impact excitation from the ion ground state. All the transitions in ionised iodine except the usual p - s (6p - 6s) ion laser transition at 562.5nm in the $^4S^o$ core and the 521.6nm np' - (n-1)d transition differ.

No laser transitions from singlet levels have been observed, even though similar energy levels in iodine are at a lower energy above the ion ground state than in bromine, from which oscillation occurs.

Fig. 7.15 and Fig. 7.13 show that iodine provides the majority of the np' - ns' laser transitions in the ionised halogens.

7.3.4 Comparison of laser transitions in ionised iodine, and doubly ionised Argon, Krypton and Xenon.

Fig. 7.16 shows that laser transitions in ionised iodine obey the selection rules;

$\Delta s = 0$, $\Delta L = \Delta J$, just as those of doubly ionised argon, krypton and xenon, except that more laser transitions occur in iodine for

$$\Delta J = 0 \quad \text{and} \quad \Delta L = +1 \; ; \quad \text{and}$$

$$\Delta J = -1 \quad \text{and} \quad \Delta L = +1 \; .$$

Fig. 7.17 gives the calculated line strengths of transitions in doubly ionised noble gas atoms and with Fig. 7.13 shows that oscillation on the ($^2D^o$) core transitions in ionised iodine does not occur on those transitions analogous to those with large relative line strength in the doubly ionised noble gases, or on those in Xe III on which oscillation has been observed.

7.3.5 Laser oscillation on hyperfine components

Iodine is particularly advantageous for a study of oscillation on hyperfine components because it is monoisotopic with a nuclear spin of 5/2, and has wide hyperfine structure to its spectrum lines, (25). It has strongly perturbed energy levels, the exact cause of which has yet to be determined, ((21) - (25), (27)).

Simultaneous laser oscillation on hyperfine components has been observed for the first time on the following ionised iodine lines; in nm 703.3; 658.5; 612.7; 606.9; 576.0 and 567.8, as shown in Plates 7.3 and 7.4.

Previously, laser oscillation had been reported by Fowles and Jenson (16) as only occurring on a single hyperfine component of a given line, even though adequate gain for oscillation to occur on other components was realised in their experiments.

Oscillation in this work was observed, wavelengths in nm, at:-

(1) 703.3 on two components $165 \pm 30 \times 10^{-3}$ cm^{-1} apart

(2) 658.5 on three components, with separation from the strongest of

(i) $130 \pm 30 \times 10^{-3}$ cm^{-1}

(ii) $210 \pm 38 \times 10^{-3}$ cm^{-1}

(3) 612.7 on two components, $190 \pm 30 \times 10^{-3}$ cm^{-1} apart

(4) 606.9 on two components, $180 \pm 35 \times 10^{-3}$ cm^{-1} apart

(5) 576.0 on two components, $104 \pm 20 \times 10^{-3}$ cm^{-1} apart, and at

(6) 567.8 on two components, $324 \pm 15 \times 10^{-3}$ cm^{-1} separation.

As a result of the nucleus possessing a mechanical moment I, coupling is experienced between the total mechanical moment J of the extranuclear electrons, giving a resultant moment of the nucleus F. The hyperfine splittings of hyperfine structure due to nuclear spin are small compared with multiplet splittings on which LS coupling is based, so that the interaction of I is much smaller than that between L and S, or any other interactions that are involved, (Kuhn (28) and White (29)).

In the case of iodine, the rules applicable to multiplet analysis will apply to hyperfine determination, L, S and J being replaced by J, I and F respectively, where F has the values:

$$F = J + I,\ J + I - 1 \ldots\ldots\ldots |J - 1|$$

(a) The intervals between two components F and F + 1 will be given by the Landé Interval Rule

$$\Gamma = A(F + 1) \qquad \ldots\ldots (7.4)$$

where A is an interval factor depending on the levels concerned. Irregularities in intervals, and deviations from the Interval Rule occur due to perturbations.

(b) The relative intensities of hyperfine components will be given by the F - sum Rule of Dorgelo (30), Ornstein and Burger (31), in which the ratio of the sums of the intensities of all transitions from two quantum levels F and F' are in the ratio of their statistical weights $(2F + 1) / (2F' + 1)$.

All the lasing components have been identified and are shown in Figs. 7.18 - 7.23.

In transitions from the $6s'\ ^3D_2$ and $6p'\ ^3D_1$ levels, oscillation is observed in order of the calculated relative intensities, calculated using the F - sum Rule.

In transitions from the $6p'\ ^3F_2$ level (567.8 and 606.9nm), oscillation occurs on the strongest calculated component, from the F $9/_2$ level, and then from the F $5/_2$ level, even though there are stronger calculated components from the F $7/_2$ level, (see Further work).

Using the observed laser components in nm for the lines 658.5 ($6s'\ ^3D_1$ - $6p'\ ^3D_1$), 606.9 ($6s'\ ^3D_1$ - $6p'\ ^3F_2$) and 576.07 ($6s'\ ^3D_1$ - $6p'\ ^3D_2$), the intervals for the $6s'\ ^3D_1$ and $6p'\ ^3D_1$ levels have been established so that agreement of observed and calculated components is now obtained. With the 567.8nm line ($6s'\ ^3D_2$ - $6p'\ ^3F_2$) agreement of laser components has been shown with the components observed by Murakawa (22) which disagreed with those reported by Tolansky (23).

It has been established from the measurements made, and the identification of the lasing components on the 658.5, 612.7, 606.9 and 576.0nm lines, that the upper laser level $6p'\ ^3D_1$, and the lower laser level $6s'\ ^3D_1$ are very strongly perturbed.

The hyperfine intervals for these two levels do not obey the interval rule, since they are not proportional to the statistical weights of the hyperfine levels. Since the interval rule is not obeyed, this perturbation could be attributed to a Schuler - Jones (32) perturbation, due to the close approach of two terms.

From measurements of the two lasing components of the ($5d'\ ^3D_2$ - $6p'\ ^3F_2$), 703.3nm line the two lasing components have been identified as the two strongest calculated hyperfine components, if the interval factor is taken as 69 for the $5d'\ ^3D_2$ term. Tolansky (24) gives the interval factor as being either 69 or - 89 for this term. This value of A is much larger than is expected for this $5s\ 5p^3\ 5d$ term and indicates that this term is also strongly perturbed, supposedly by a Shenstone - Russell perturbation (32) due to term(s) as much as a few thousand cm^{-1} away. In this type of perturbation the interval rule is obeyed, but the interval factor is large.

The intercombination laser transition at 651.6nm ($5p^5\ ^1P_1$ - $6p'\ ^3F_2$) may occur as a result of perturbation, since the interval factor for the $5p^5\ ^1P_1$ term is the largest (80 - 90) for any term of J = 1, and also (according to Murakawa (27)) does not obey the interval rule.

The terms responsible for the assumed Schuler - Jones perturbation have not been determined. No classified energy levels are close to either the $6p'\ ^3D_1$ or the $6s'\ ^3D_1$ levels so such term(s) can only be hypothetical.

The ratio of the quadrupole coupling constant, B/A, can be obtained from the formula of Casimir (28), where the interval, ($\Delta\nu_{ab}$), between two hyperfine levels, in the absence of term interaction, is given by:-

$$\Delta\nu_{ab} = 1/2A(C_a - C_b) + 3/8B\left[C_a(C_a + 1) - C_b(C_b + 1)\right] / I(2I - 1)\ J\ (2J - 1) \quad \ldots\ldots\ (7.5)$$

where $C = F(F + 1) - I(I + 1) - J(J + 1)$.

Assuming that the perturbation of the $6p'\ ^3D_1$ and $6s'\ ^3D_1$ terms is not due to term interaction, but is due to an electric quadrupole moment,

B/A is -3.2, and -3.12 for each term respectively.

These values are larger than that of B/A of + 1.385 for I^{127} from the $^2P_{3/2}$ level given by Kuhn, and are of a different sign.

As the ratio for both terms is negative the perturbation cannot be due to a common term, (the terms also do not obey the interval rule,) and further it seems unlikely that perturbation due to two terms would give the same values for B/A.

If the wave functions of the $(^2D)\ 6p\ ^3D_1$ and $(^2D)\ 6s\ ^3D_1$ terms can be calculated, with the value of B, a value for the quadrupole moment ($Q\ (I^{127})$) should be calculable and be equal to approximately - 0.6 barn (27). Failing agreement, some other perturbation is evident.

7.3.6 Non equilibrium population of hyperfine sublevels of the $6s'\ ^3D_1$ of ionised iodine during laser oscillation.

If two terms have nearly the same energy and differ only in values of J or F, their population in a gas discharge corresponds very closely to statistical equilibrium. The ratio of intensities of transitions from these terms, in the absence of self absorption, is equal to the ratio of the statistical weights times the transition probabilities. This forms the basis of the intensity sum rules.

Previous studies by Turkin in 1959 (34) of thallium show that non-equilibrium population conditions are obtained in hyperfine sub-levels of this element in a high current hollow cathode discharge. Similar studies by Schrammen (35) and Schuler (36) of cadmium showed that the relative intensities of hyperfine components depended on the excitation conditions. Turkin (37) reported that the anomalous intensity changes reported previously in cadmium depended on the current density or the pressure of the cadmium vapour.

The expected ratio of the theoretical intensities was observed only at low current densities in both hollow cathode and positive column discharges. In all the lines studied the intensity of the long wavelength component increased with increase in current density whilst the intensity of the short wavelength component decreased.

Similar anomalous intensity changes, resulting in a change of oscillating components of the ionised iodine line 658.5nm ($6s'\ ^3D_1$ - $6s'\ ^3D_1$) are reported in this thesis.

Oscillation on the 658.5nm line has been obtained on three hyperfine components simultaneously with two components of the 576.0nm line, as shown in Fig. 7.24. With a high vapour pressure of iodine, oscillation occurred on the F 7/2 - 5/2 transition of the 658.5nm line alone. This component has a lower theoretical relative intensity than that of the F 7/2 - 7/2 hyperfine transition at a slightly longer wavelength.

As the vapour pressure of iodine decreased due to clean up in the discharge, the intensity of the oscillating component decreased, but

oscillation commenced on the longer wavelength F 7/2 - 7/2 transition. Further reduction in the vapour pressure of iodine resulted in oscillation alone on this longer wavelength component.

Since the two oscillating components have a common upper hyperfine level (F 7/2), the change of the oscillating components cannot be attributed to changes in population of the sub-levels of the upper laser level $6p'\ ^3D_1$, and can only be attributed to non-equilibrium in the populations of the sub-levels of the lower $6s'\ ^3D_1$ level.

Hyperfine transitions of the 576.0nm line into the F 7/2 or 5/2 levels populating these levels, cannot account for the variation in population inversion, as the final intense oscillating components at low pressure are long wavelength components having a common F 7/2 sub-level of the lower $6s'\ ^3D_1$ level.

Similar anomalous behaviour in the oscillating components is observed when the 658.5nm line is oscillating only.

In all the other lines on which oscillation on hyperfine components was observed, no anomalous intensity changes occurred, and the intensity of the lasing components followed the observed and theoretical intensities.

From these changes in oscillating components it is evident that there is a non-equilibrium population of the $6s'\ ^3D_1$ level, as the ratio of the populations of the sub-levels 5/2 and 7/2 must be lower in a discharge at higher vapour pressure of iodine than at a lower pressure. Such changes could also be due to current changes determined by changes in the vapour pressure of iodine.

7.3.7 Line width of oscillating components

658.5nm The linewidth of the strongest oscillating component was found to be approximately 0.07 cm^{-1}.

567.8nm The linewidth of the strongest component was 0.11 cm^{-1}. This linewidth of approximately 4,000 Mc/s is similar to that observed in the noble gas ion lasers (Byer et al. (38)), and is approximately 3 to 4 times the Doppler width for iodine at room temperature.

7.3.8 Selective excitation mechanism

Strong np - ns transitions are observed in the doubly ionised noble gases, and in singly ionised fluorine, chlorine and bromine in pulsed discharges. These transitions occur in ionised iodine only when an rf discharge is coupled with a pulsed discharge, suggesting that the principal selective excitation of the other 6p' upper laser levels in iodine is by an atomic/ionic collisional mechanism and not by electron impact excitation from either the neutral or ion ground states.

In ionised iodine the np levels of the $^4S^o$ core are of lower energy than the np $^2D^o$ core levels, and these would be expected to be excited if, as in the noble gas lasers, the excitation was purely electronic. Further, the high helium pressure (up to 60 torr) used in this work would, according to Bridges and Chester (39), suppress normal electron impact excited ion laser lines.

All excitation mechanisms 7.1 - 7.3 are possible. Argon and the heavier inert gases do not have sufficiently energetic metastables to be able to excite iodine ground state ions in a single collision so that oscillation in a krypton - iodine mixture (1) cannot be explained by mechanisms similar to 7.2 and 7.3 involving helium and neon metastables.

In helium - iodine mixtures the selective excitation appears to be most likely that of asymmetric charge transfer (10/01') between a helium atomic ion and a ground state iodine atom, with the energy discrepancy of 0.2 - 0.6 eV accounted for by the polarisation energy involved in the collision. In this reaction Wigner spin selection applies, as in the ion-atom, resonant energy transfer excited helium-krypton, neon-xenon ion lasers of Dana and Laures (3).

A further possible reaction, in view of 1) the oscillation at high (60 torr) helium pressures, 2) the enhancement of certain ionised iodine lines in the high pressure, recombination-dominated plasma of a hollow cathode discharge, could involve a He_2^+ molecular ion as follows

$$He_2^+ + I(^2P_{3/2}) \longrightarrow \quad 2He\ (^1S_o) + I^{+'}(6p').$$

Note:- Professor Murakawa has confirmed the analysis of the hyperfine components of the line at 658.5nm with recent high accuracy measurements made on this line. See Fig. 7.25 for unpublished results kindly sent by Professor Murakawa.

Table 7.1

Partial list of transitions having upper levels within approximately 0.5 eV of ion limit of $He^+(0)$.

Wavelength - (nm)	Lower level	Upper level	ΔE eV	Enhanced in helium (E)	Laser Action (L)
480.64	$5d\ ^3D_2$	$6p'\ ^3F_2$	0.34	(E)	-
488.48	$6s'\ ^3D_2$	$6p'\ ^1F_3$	-0.01	-	-
498.69	$5d\ ^3D_1$	$6p'\ ^3D_2$	0.23	(E)	(L)
504.64	$6s'\ ^3D_1$	$6p'\ ^3P_o$	- 0.01	-	-
521.63	$5d\ ^3D_1$	$6p'\ ^3F_2$	0.34	(E)	(L)
526.52	$6s'\ ^3D_1$	$6p'\ ^1P_1$	0.02	-	-
533.82	$6s'\ ^3D_2$	$6p'\ ^3F_3$	0.2	-	-
540.74	$6s'\ ^3D_2$	$6p'\ ^3D_2$	0.23	(E)	(L)
559.31	$5d\ ^3D_1$	$6p'\ ^3D_1$	0.51	(E)	-
559.82	$5p^5\ ^1P_1$	$6p'\ ^1P_1$	0.02	-	-
567.81	$6s'\ ^3D_2$	$6p'\ ^3F_2$	0.34		(L)
571.05	$6s'\ ^3D_3$	$6p'\ ^1F_3$	-0.01		-
576.07	$6s'\ ^3D_1$	$6p'\ ^3D_2$	0.23		(L)
585.53	$5d'\ ^3D_2$	$6p'\ ^1F_3$	0.01		-
606.89	$6s'\ ^3D_1$	$6p'\ ^3F_2$	0.34		(L)
607.50	$6s'\ ^1D_2$	$6p'\ ^1F_3$	-0.01		-
612.75	$6s'\ ^3D_2$	$6p'\ ^3D_1$	0.51		(L)
616.22	$5p^5\ ^1P_1$	$6p'\ ^3D_2$	0.23		-
620.49	$6s'\ ^1D_2$	$6p'\ ^1P_1$	0.02		-

Wavelength - (nm)	Lower level	Upper level	ΔE eV	Laser Action (L)
625.55	$5d'\ ^3D_2$	$6p'\ ^1F_3$	-0.01	-
634.00	$6s'\ ^3D_3$	$6p'\ ^3F_3$	0.2	-
651.62	$5p^5\ ^1P_1$	$6p'\ ^3F_2$	0.34	(L)
651.89	$(5d'\ ^3D_2$	$6p'\ ^3F_3)$	0.2	-
658.52	$6s'\ ^3D_1$	$6p'\ ^3D_1$	0.51	(L)
662.24	$5d'\ ^3D_2$	$6p'\ ^3D_2$	0.23	-
676.42	$5d'\ ^3F_4$	$6p'\ ^1F_3$	-0.01	-
682.52	$6s'\ ^3D_3$	$6p'\ ^3F_2$	0.34	(L)
690.48	$6s'\ ^1D_2$	$6p'\ ^3D_2$	0.23	(L)
701.89	$5d'\ ^3D_3$	$6p'\ ^3F_3$	0.20	-
703.30	$5d'\ ^3D_2$	$6p'\ ^3F_2$	0.34	(L)
711.51	$5p^5\ ^1P_1$	$6p'\ ^3D_1$	0.51	-
713.90	$5d'\ ^3D_3$	$6p'\ ^3D_2$	0.23	(L)
761.85	$5d'\ ^3D_3$	$6p'\ ^3F_2$	0.34	-
773.58	$5d'\ ^3D_2$	$6p'\ ^3D_1$	0.51	-
817.01	$5d'\ ^3F_3$	$6p'\ ^3D_2$	0.23	-
825.38	$5d'\ ^3P_o$	$6p'\ ^3D_1$	0.51	(L)

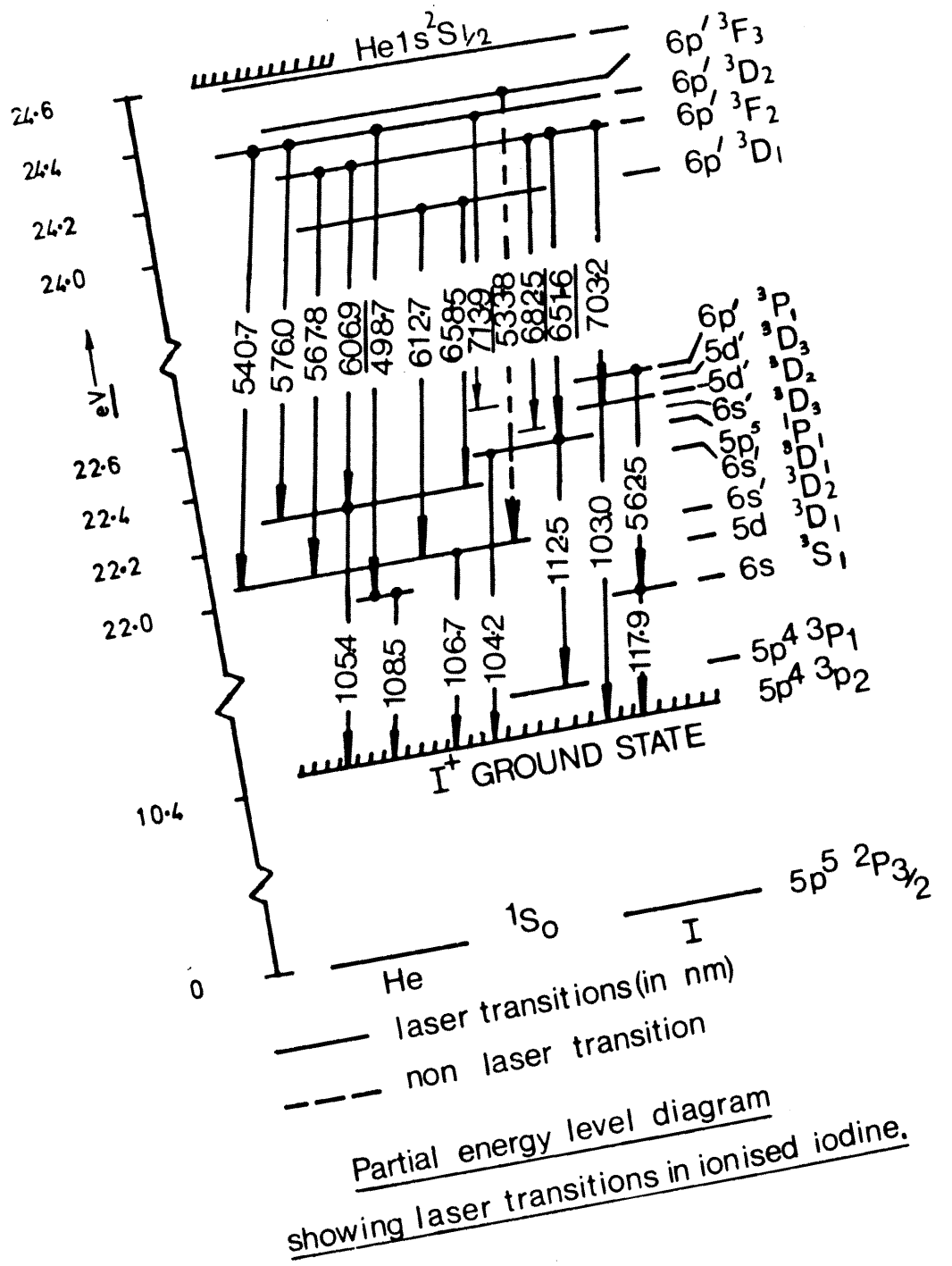

Partial energy level diagram showing laser transitions in ionised iodine.

Fig. 7.1.

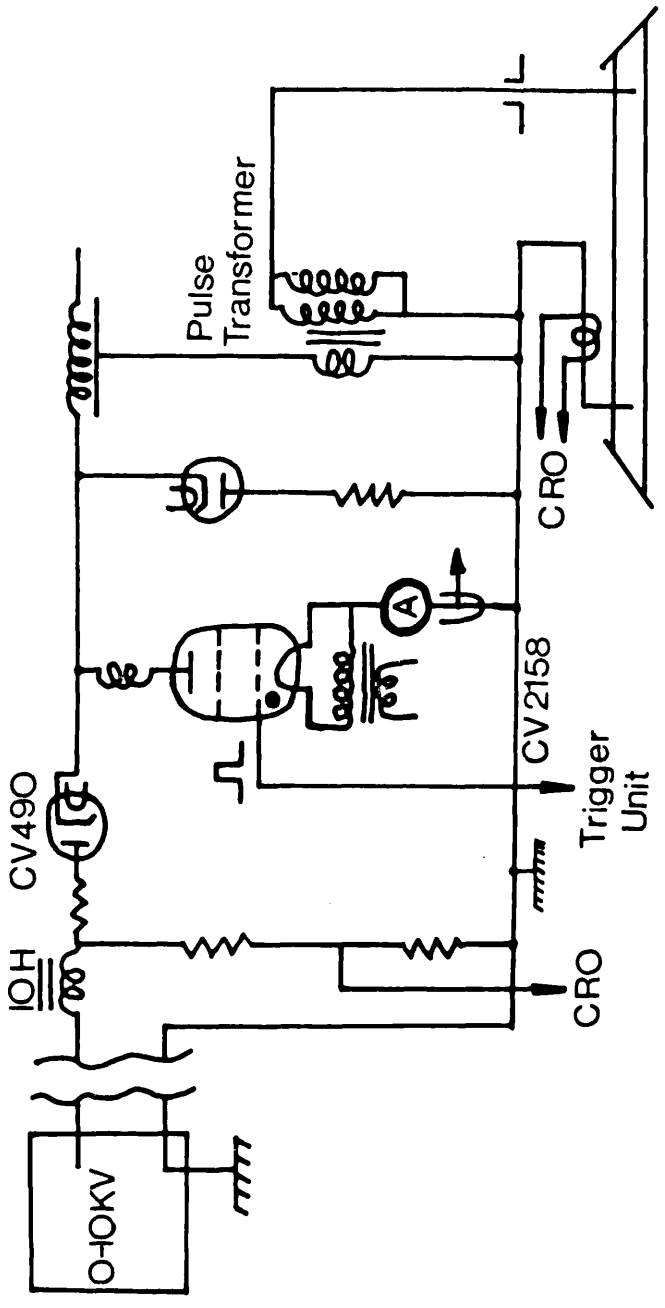

BASIC CIRCUIT OF PULSE MODULATOR.

Fig. 7.2.

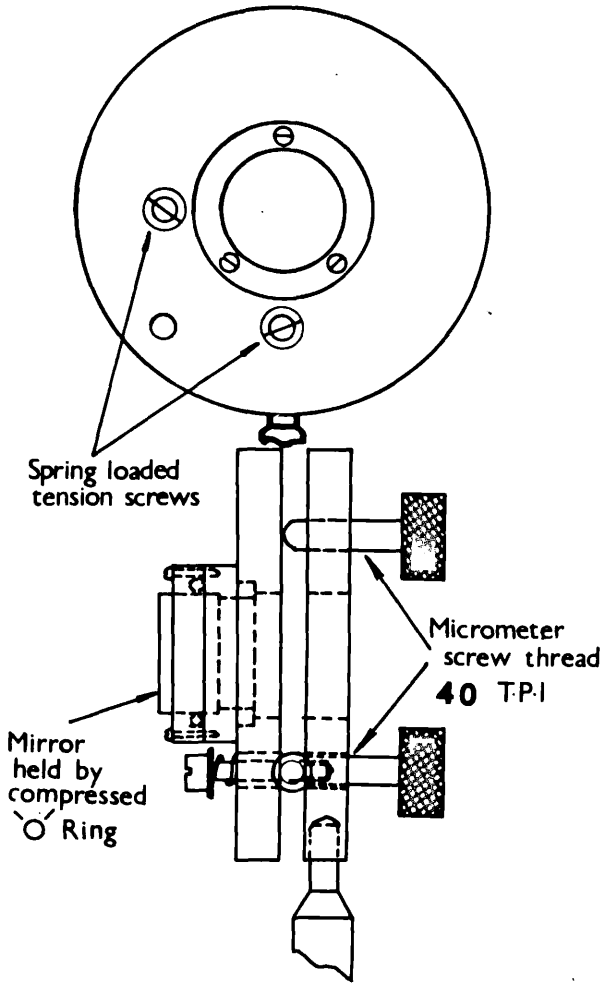

Fig. 7.3. Laser mirror mounts.

A.

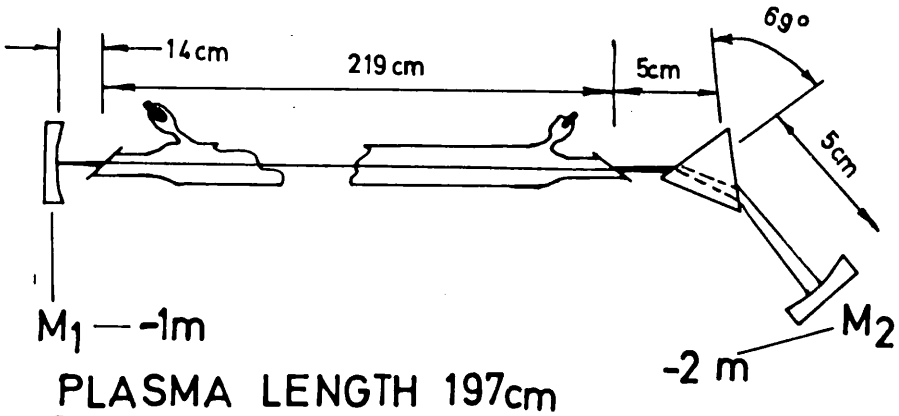

PLASMA LENGTH 197cm

B.

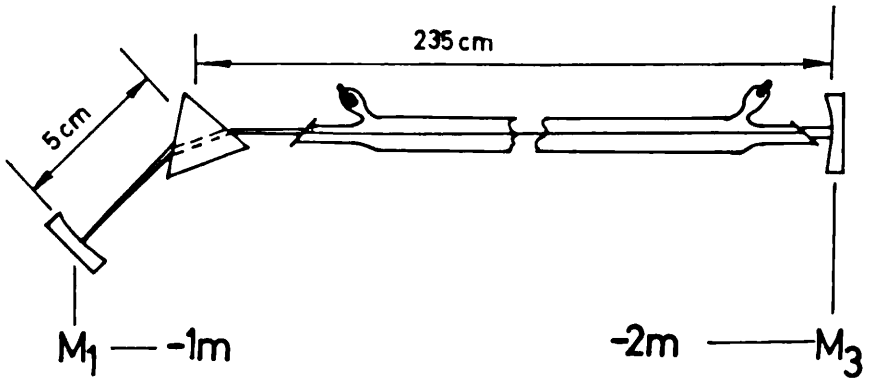

Mirrors: Peaked reflectivity $M_{1,2}$ 6328 nm
M_3 5500 nm

ARRANGEMENT FOR PRISM WAVELENGTH SELECTION.

Fig. 7.4.

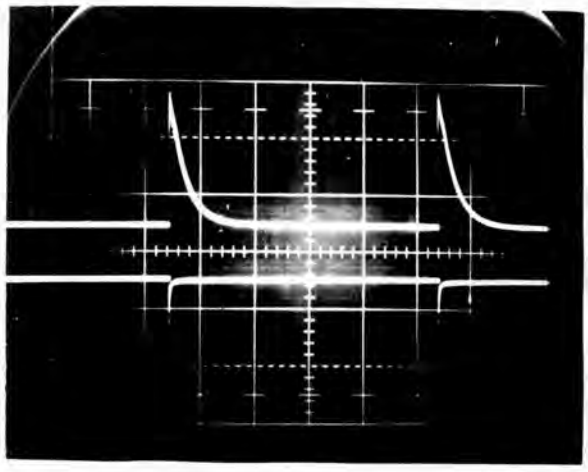

Fig. 7.5

Relationship of the 576.0nm laser output (upper trace) and the current pulse (lower trace), at a repitition rate of 1 kc/s.

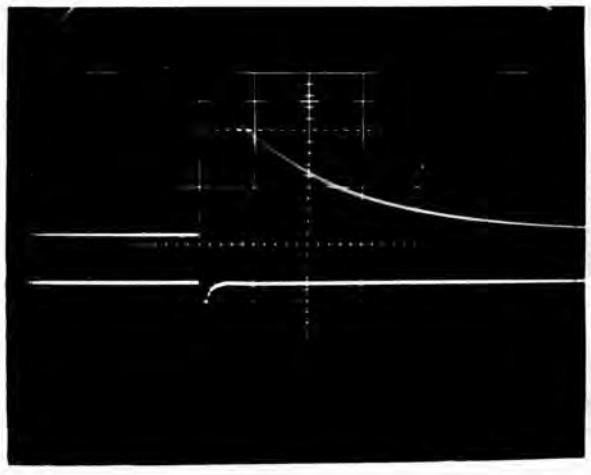

Fig. 7.6

Relationship of the 576.0nm spontaneous emission (upper trace) and the current pulse under lasing conditions. Scan: 20μsec/cm.

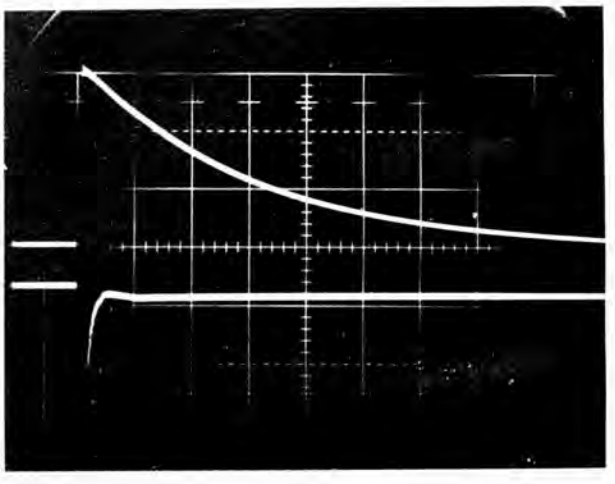

Fig. 7.7

Relationship of the intensity of the non-laser ionised iodine line at 533.8nm (upper trace) and the current pulse under lasing conditions. Scan: 20 μsec/cm.

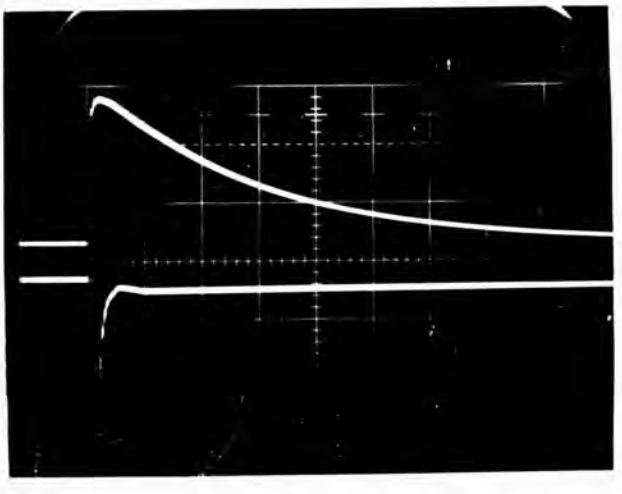

Fig. 7.8

Relationship of the intensity of the neutral iodine line at 589.4nm (upper trace) and the current pulse under lasing conditions. Scan: 20 μsec/cm.

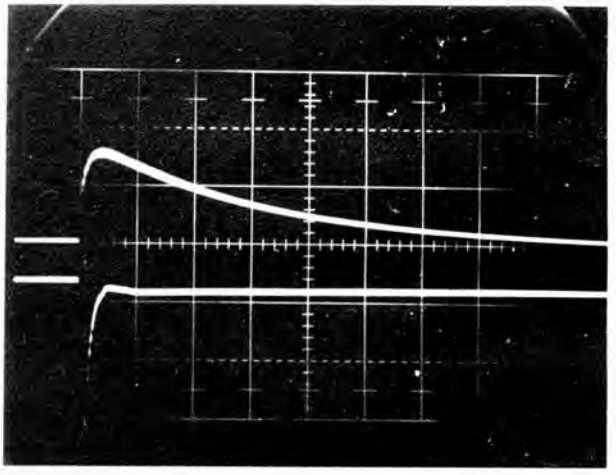

Fig. 7.9

Relationship of the intensity of the neutral helium line at 388.9nm (upper trace) and the current pulse. Vapour pressure of iodine lower than optimum for laser oscillation. Scan 20 μsec/cm.

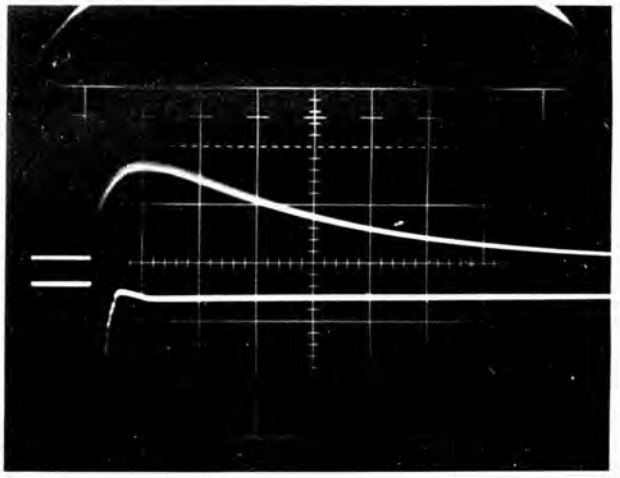

Fig. 7.10

Relationship of the spontaneous emission of the 576.0nm laser line (non lasing) at a low vapour pressure of iodine(upper trace) and the current pulse. Scan: 20 μsec/cm.

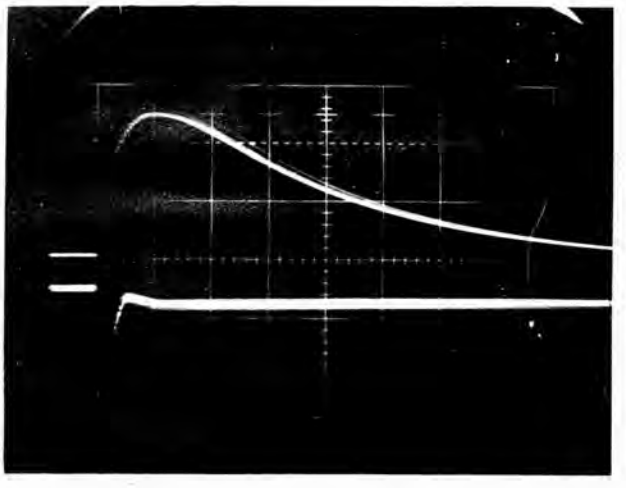

Fig. 7.11

Relationship of the intensity of the non-laser ionised iodine line at 533.8nm (upper trace), and the current pulse at a low vapour pressure of iodine. Scan: 20 μsec/cm.

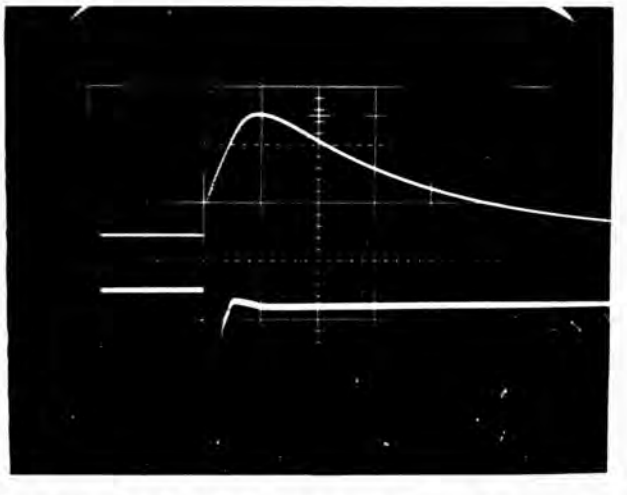

Fig. 7.12

Relationship of the intensity of the neutral helium line at 388.9nm (upper trace) and the current pulse at a low vapour pressure of iodine. Scan: 20 μsec/cm.

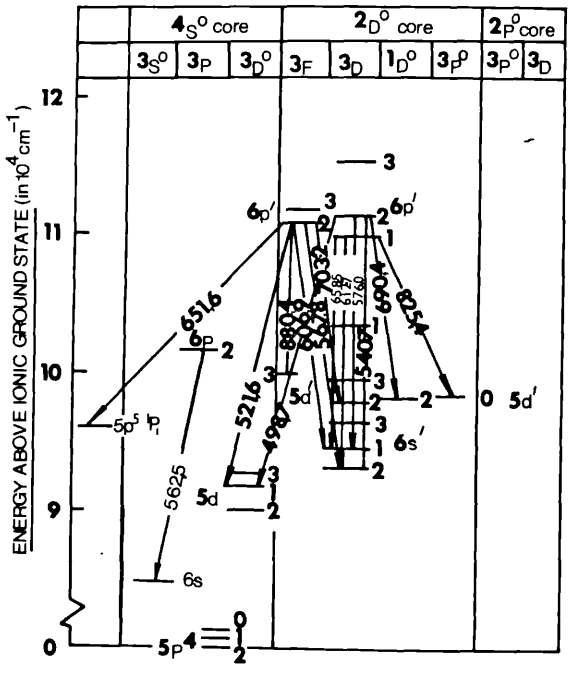

IONIC GROUND STATE

Grotian diagram of singly ionised iodine indicating observed laser transitions (λ in nm)

Fig. 7.13.

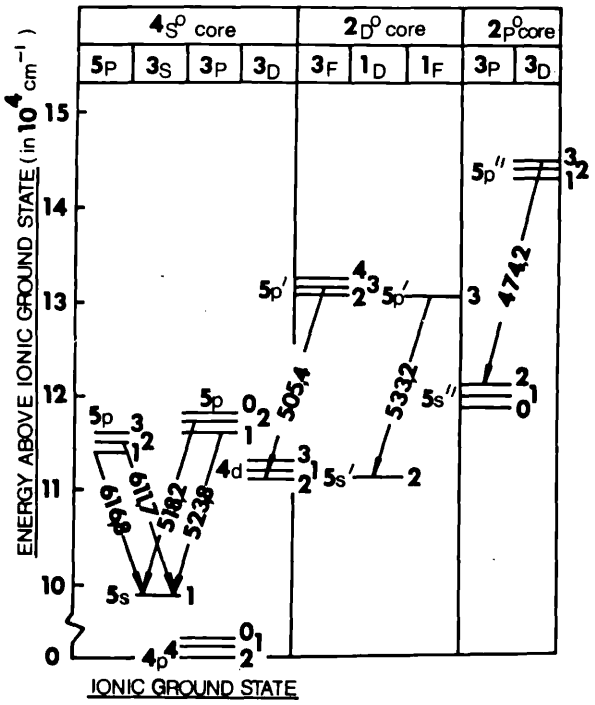

IONIC GROUND STATE

Grotian diagram of singly ionised Bromine indicating observed laser transitions (λ in nm)

Fig. 7.14.

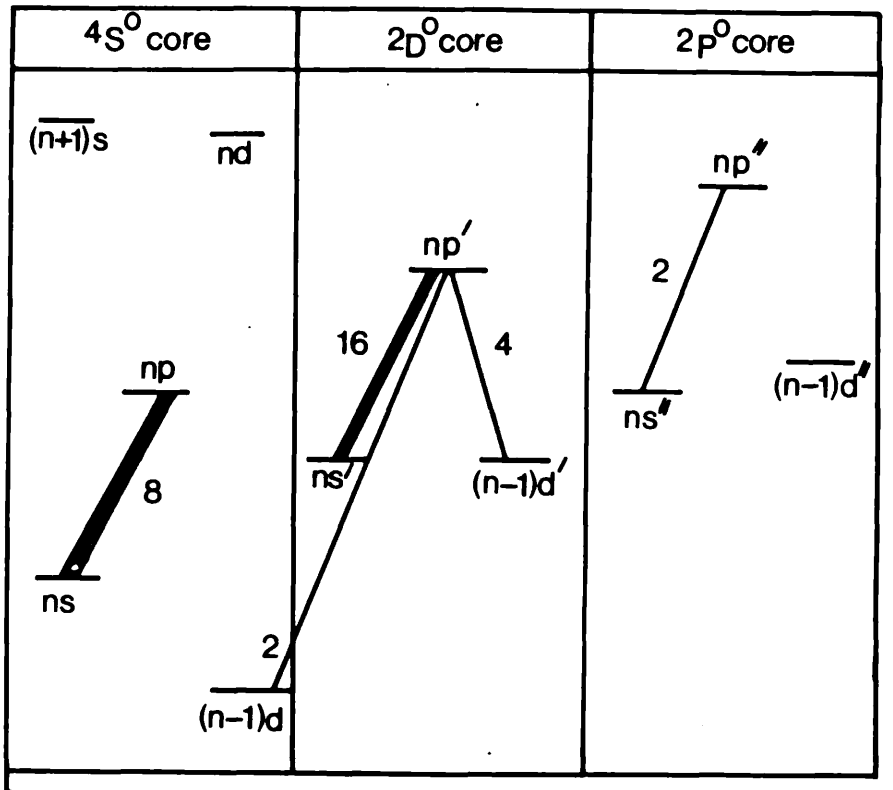

ELEMENT	F	Cl	Br	I
n	3	4	5	6

Generalised energy level diagram for singly ionised halogen atoms. The number shown beside each transition is the number of laser transitions so far observed.

Fig. 7.15.

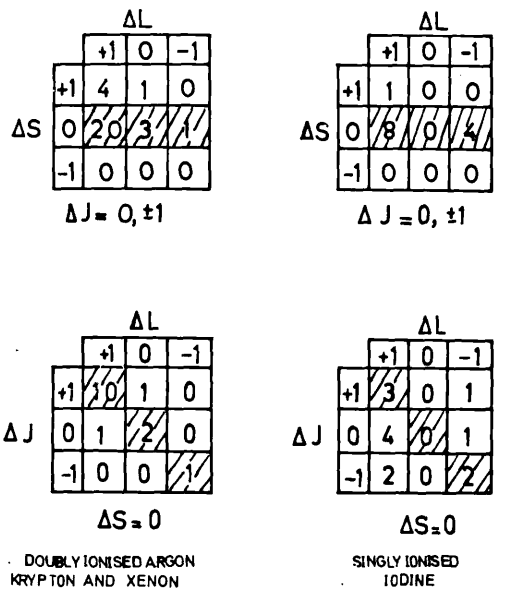

Fig. 7.16.

$$\Delta L = L_{UPPER} - L_{LOWER}$$

The selection rules $\Delta S = 0$, $\Delta L = \Delta J$ are shown shaded.

COMPARISON OF LASER TRANSITIONS IN IONISED IODINE, AND DOUBLY IONISED ARGON, KRYPTON, AND XENON.

		$ns^3 3^0$
		1
$np\ ^3P$	0	1.0
	1	3.8
	2	5.0

		$ns'\ ^3D^0$			$(n-1)d'\ ^3D^0$		
		3	2	1	3	2	1
$np'\ ^3P$	0	0	0	1.33	0	0	3.5
	1	0	.75	.25	0	7.9	2.6
	2	1.4	.25	.02	14.7	2.6	.2
$np'\ ^3D$	1	0	.75	2.3	0	2.6	7.9
	2	.8	3.5	.8	2.7	12.2	2.6
	3	6.2	.8	0	21.8	2.7	0
$np'\ ^3F$	2	.02	.8	4.2	.01	.22	1.2
	3	.8	6.2	0	.22	1.8	0
	4	9.0	0	0	2.6	0	00

Element	n
Neon	3
Argon	4
Krypton	5
Xenon	6

Xenon III laser oscillations shown by underlining.

Calculated relative line strengths of transitions in doubly ionised noble gas atoms.

Fig. 7.17.

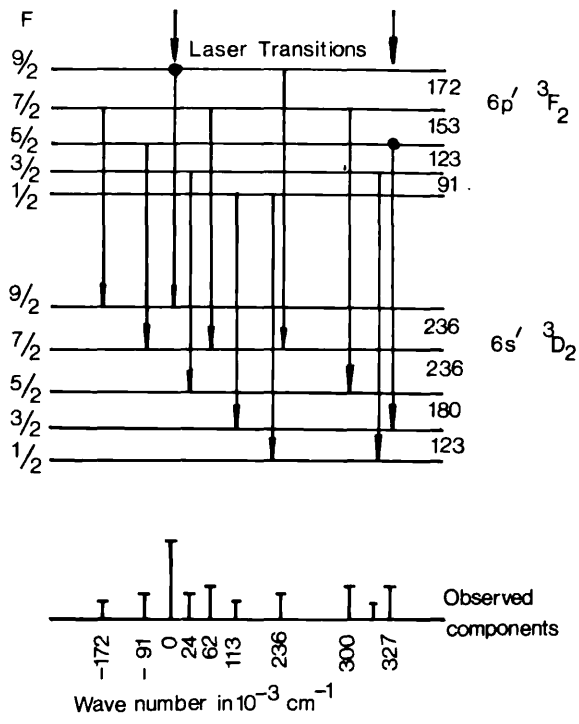

Fig. 7.18.

Transition diagram for the ionised iodine line at 567·8nm

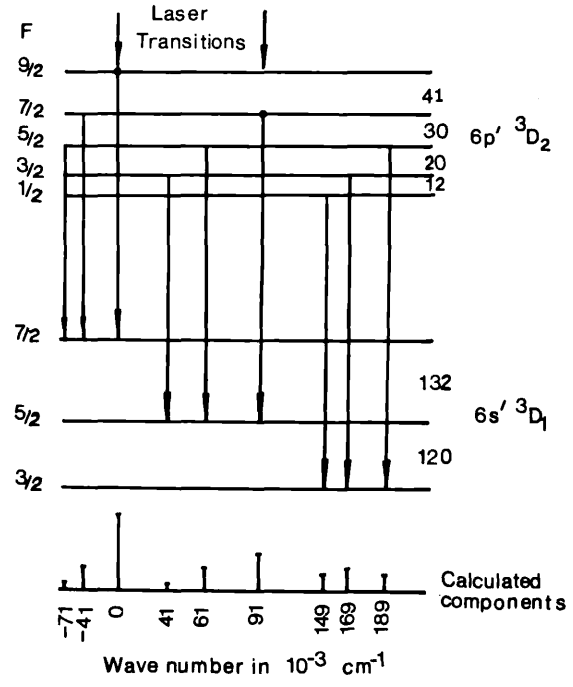

Fig. 7.19.

Transition diagram for the ionised iodine line at 576·0nm

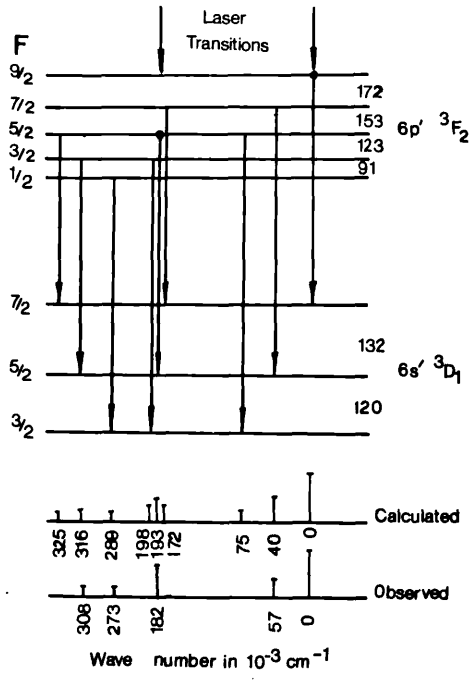

Fig. 7.20.

Transition diagram for the ionised iodine line at 606·9nm

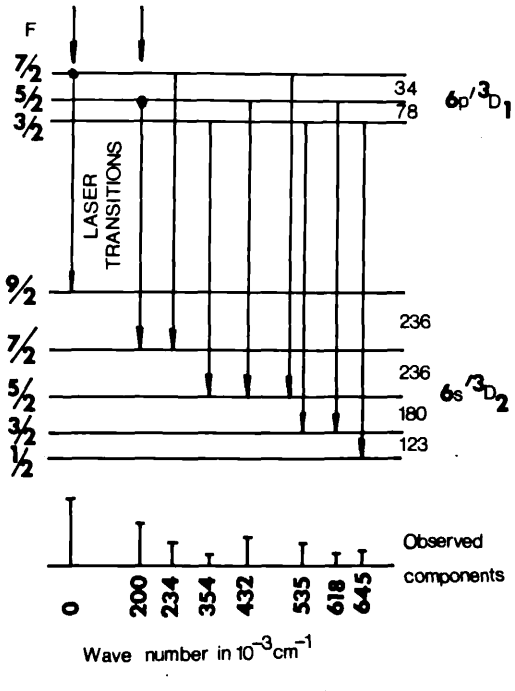

Fig. 7.21.

Transition diagram for the ionised iodine line at 612·7nm

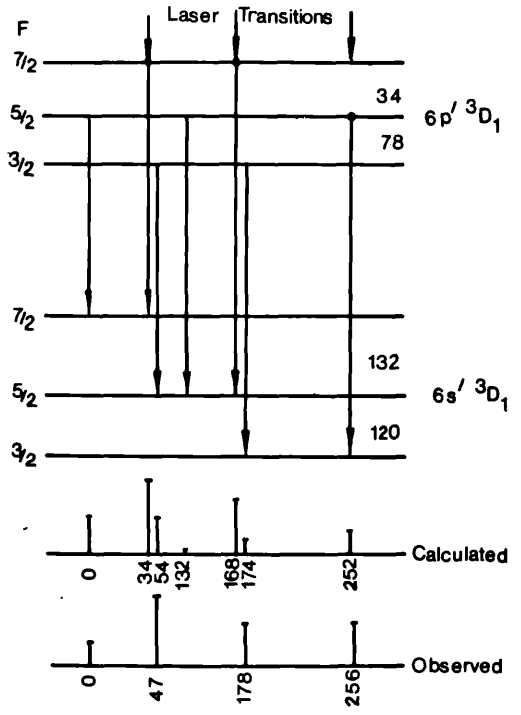

Transition diagram for the ionised iodine line at 658·5nm

Fig. 7.22.

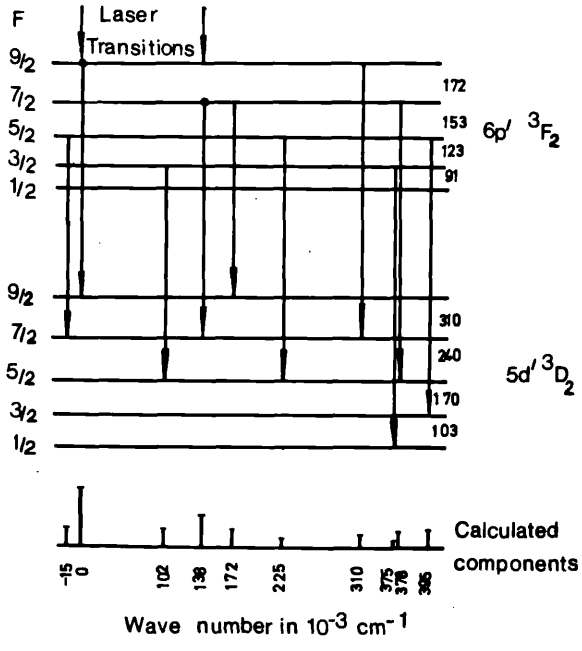

Transition diagram for the ionised iodine line at 703·3nm

Fig. 7.23.

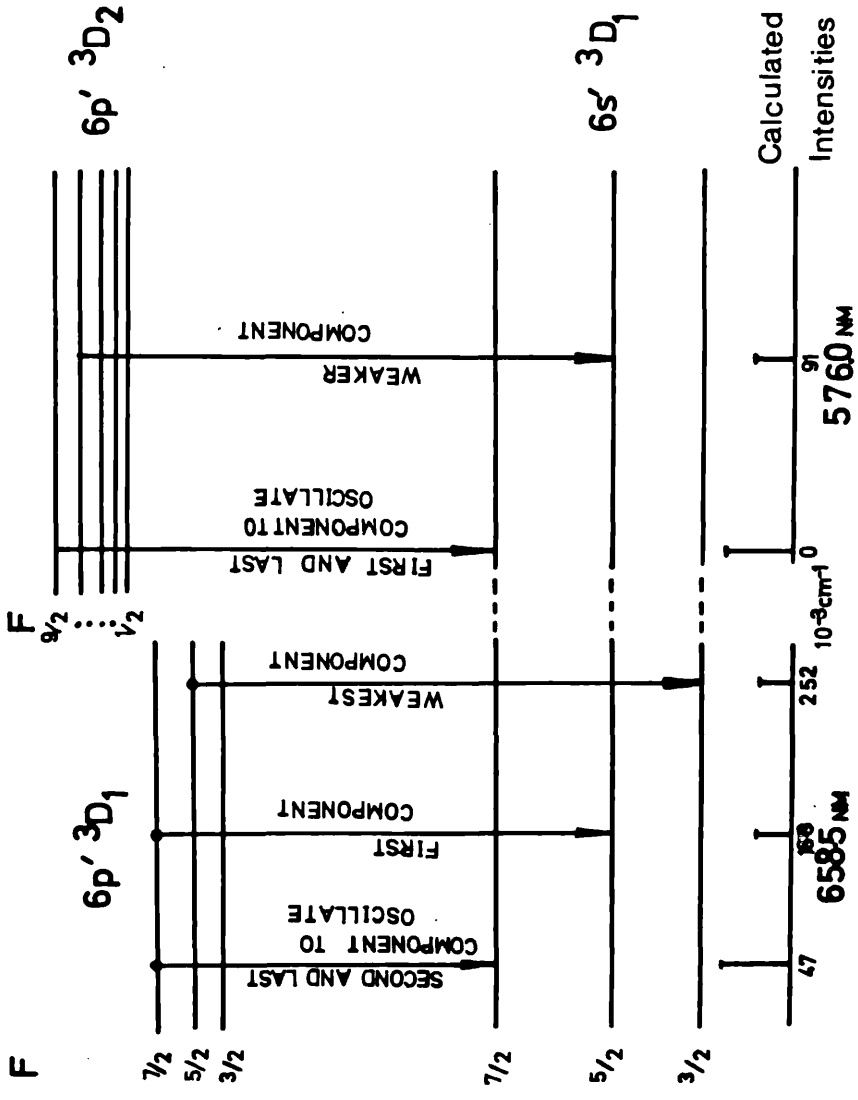

Diagram of oscillating hyperfine components showing anomalous variation in oscillation into the $6s'\,^3D_1$ level.

Fig. 7.24.

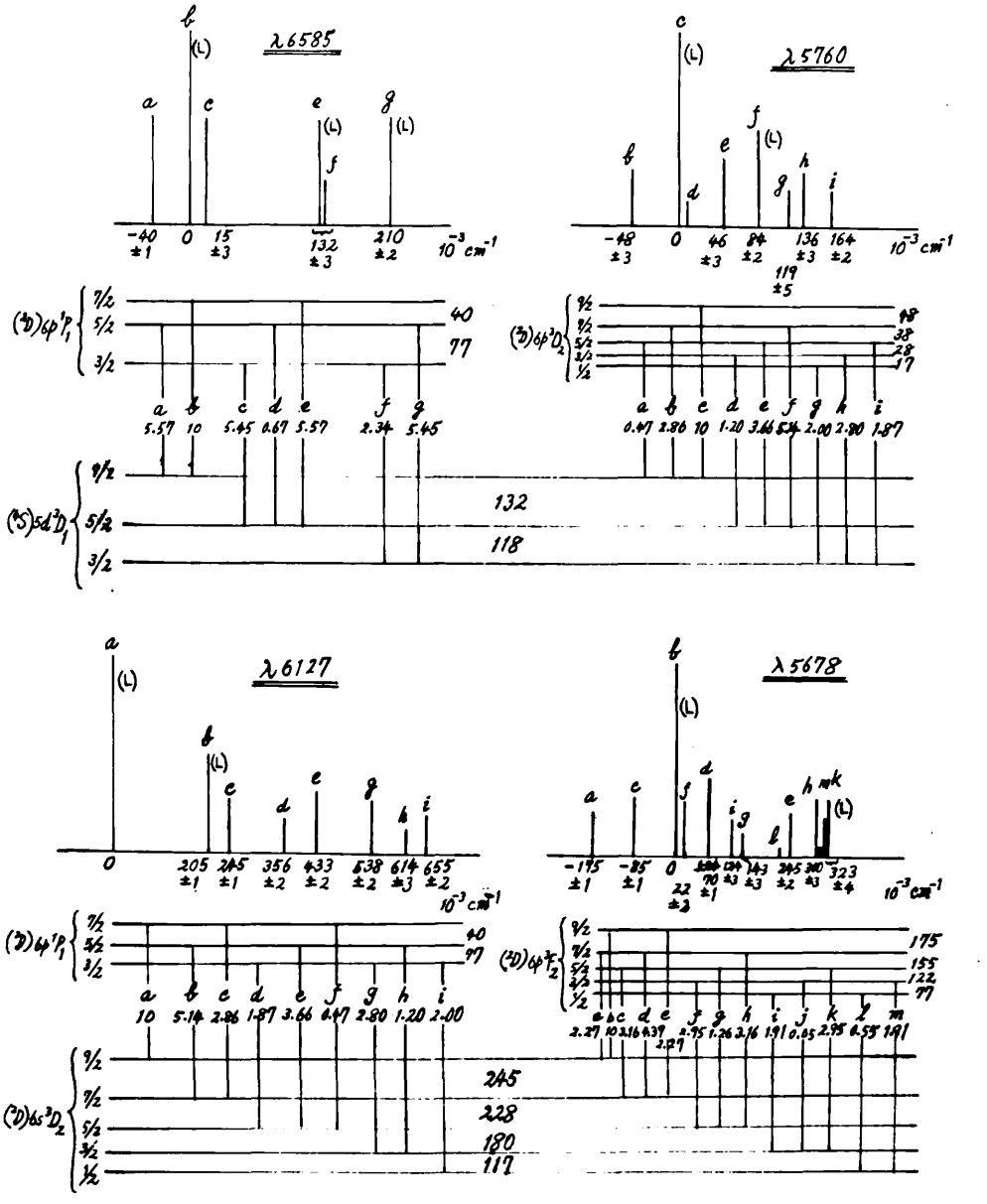

Fig. 7.25. Ionised iodine hyperfine structure (after Murakawa).

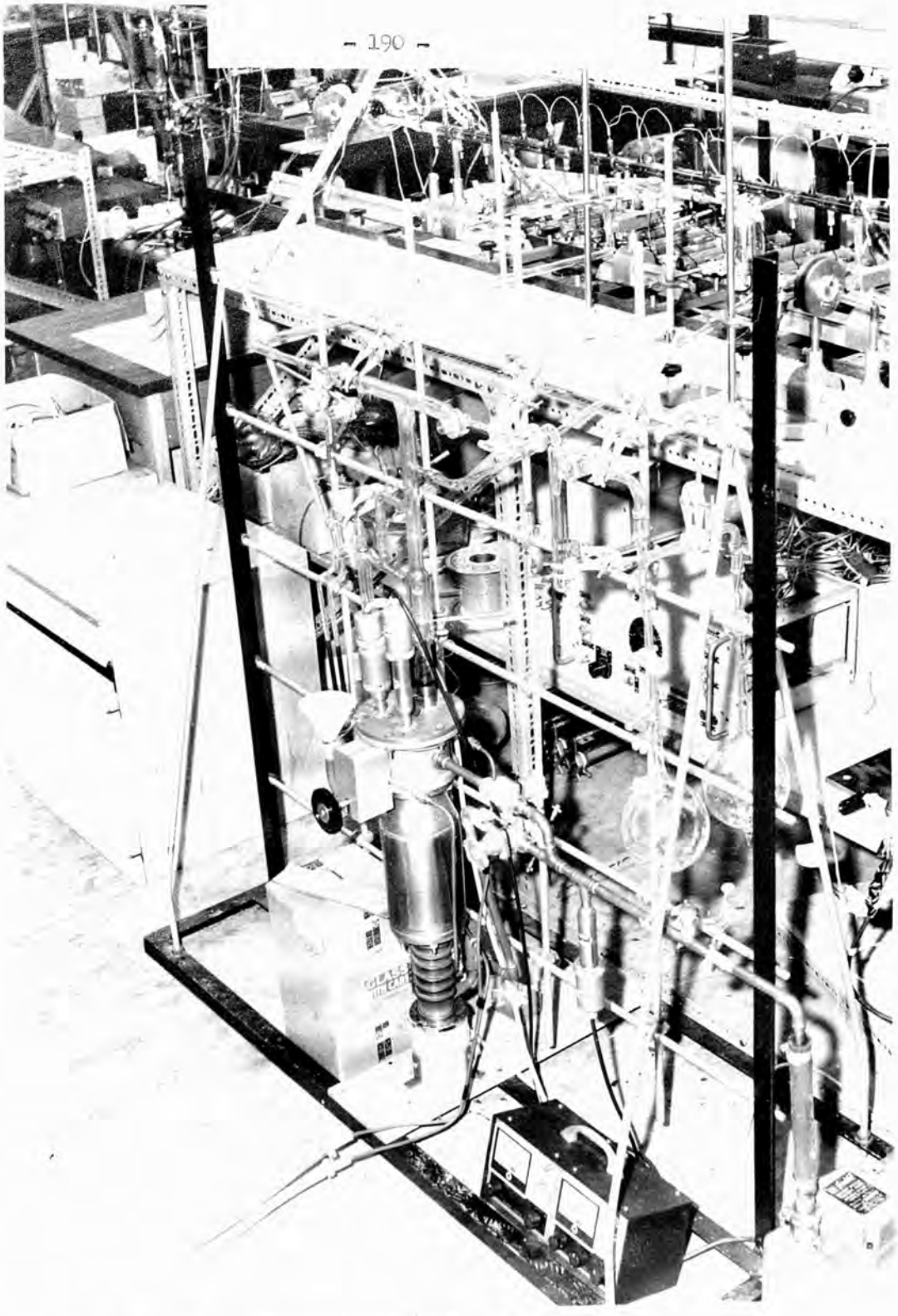

Plate 7.1. General arrangement of vacuum system.

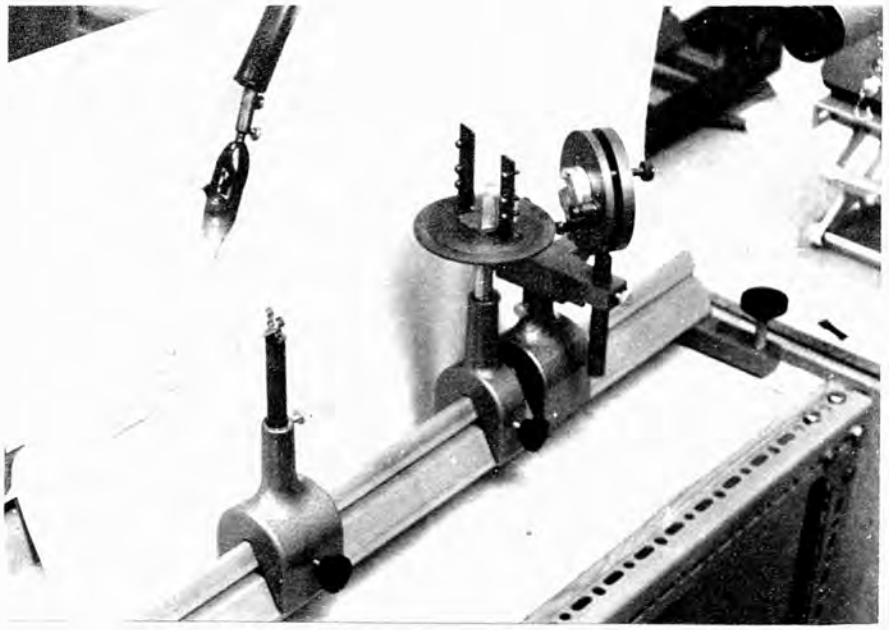

Plate 7.2. Wavelength selection arrangement showing Brewster-angled prism and laser cavity mirror.

Plate 7.3. Dispersed ionised iodine lines showing simultaneous hyperfine laser oscillations.

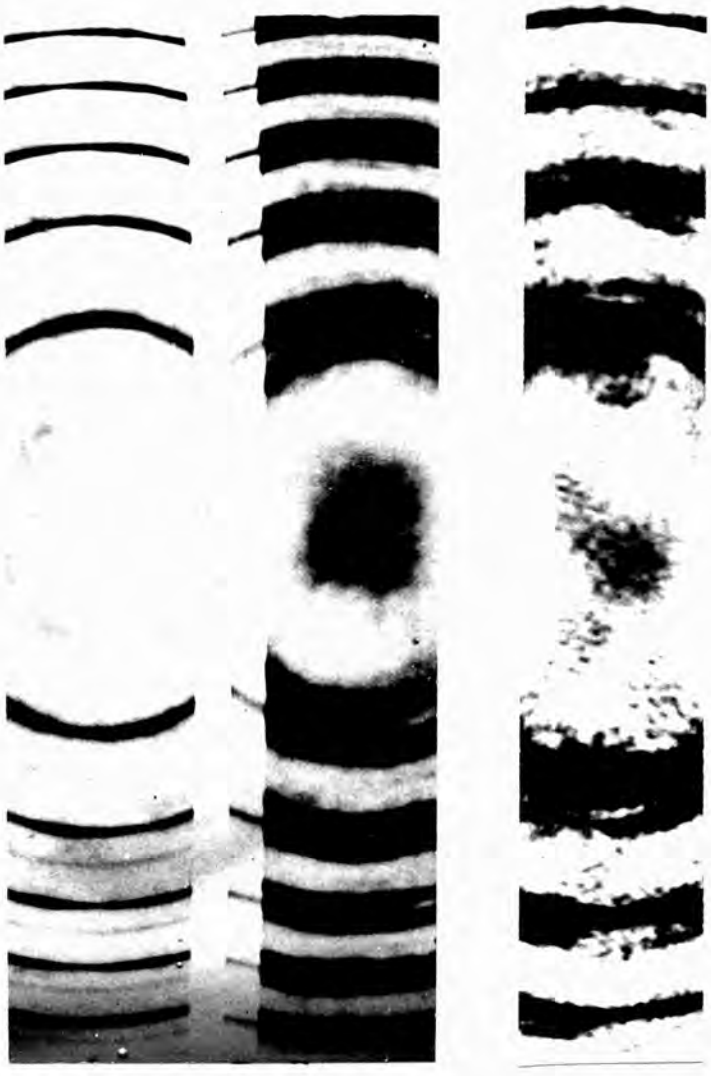

Plate 7.3. Dispersed ionised iodine lines showing simultaneous hyperfine laser oscillations.

Summary

The work described in this thesis is concerned with the ways in which population inversion is achieved in a number of gas discharges used as optical maser media.

After a brief introductory chapter, Chapters 2 to 4 cover in detail selective excitation, excitation processes in gas discharges and specific laser systems respectively. In these chapters attention has been given to analysing the extensive literature that has become available on gaseous optical maser systems throughout the period covered by this work, and to relating it to the area of atomic collision physics. In these chapters, the part played by helium in gas discharge processes has been emphasised, as throughout the project period, its behaviour as (i) a buffer gas, and (ii) a means of transference of energy has not been entirely predictable.

A short study of the 632.8nm helium-neon laser discharge is made in Chapter 6, in which aspects of the discharge are discussed which are not covered in the literature. On the evidence presented in this chapter as to the relationship of the helium-neon 632.8nm laser discharge and the transition 'weak to strong' discharges, there are aspects of this discharge of sufficient importance to warrant detailed experimental investigations.

Lastly, in Chapter 7 results are reported of experiments on a pulsed helium-iodine laser. These results provide information about laser oscillation on hyperfine components, and support the proposal that asymmetric charge transfer, between the atomic ground state helium ion and a ground state iodine atom, is the selective excitation process.

Future work.

The following is a list of investigations that appear worthwhile undertaking to clarify aspects of laser discharges and discharges in general, that have become apparent during this work:

1. Electron energy distributions, in helium-neon, and neon, rf and dc discharges.

   (a) It is not known with any certainty what contribution direct electron impact excitation makes in excitation of the $Ne(3s_2)$ level, in the helium-neon laser.

   (b) The addition of helium to a neon discharge results in increased excitation of the $Ne(3s_2)$ level. It is not clear whether the presence of helium results in resonance energy transfer between helium and neon, or if it puts the discharge into the 'weak to strong' transition discharge region, noted in rf discharges by Bochkova and Razumovskaya, (Chapter 6).

   (c) In 'weak to strong' transition discharges the electron concentration has been observed to increase abruptly, without an appreciable change in electron temperature. It is of considerable interest to see 1) if the same effect is observed in dc discharges, and 2) if there is any change in the electron temperature or electron concentration at this transition point.

Electron energy distribution, coupled with electron and atom concentration measurements should enable one to elucidate (a), (b) and (c).

2. Flowing afterglow technique

The exact selective excitation process in the case of the helium-mercury and helium-iodine lasers has yet to be determined. The use of the flowing afterglow technique would show to what extent the excitation is due to the $10/01'$, or $0^m0^m/01'e$ processes. It should also show if a molecular helium ion is responsible for the selective excitation.

3. Induced electric dipole radiation

(a) Bell and Bloom (1), have obtained laser oscillation in singly ionised bromine. The observed wavelengths for the Br^+ transitions at 518.2 and 533.2nm, are outside their range of probable error. These two lines are lines which Assagoe (2) observed to be broadened and shifted in high pressure, high current discharges. Similar shifts and broadening were also observed on lines of chlorine, and in iodine on which laser oscillation has been obtained in this work. It is possible that the 'error' ($\pm$ 0.2nm) in the Bell and Bloom results could be accounted for by the effect noted by Assagoe. If this is the case, such large shifts would surely indicate that appreciable changes in transition probability were occurring. It is important to determine the magnitude and mechanism of such changes.

4. Microwave studies of transitions among individual hyperfine levels in ionised iodine.

In obtaining laser oscillation on hyperfine components of certain ionised iodine transitions, the possibility that induced forbidden

transitions of $\Delta F = 2$ could account for laser oscillation occurring on one hyperfine component and not on another, was apparent. Changes in oscillating components were observed in another transition when discharge conditions varied. Microwave studies at a wavelength of about 10cm, should show if changes in hyperfine transitions can account for this behaviour, and might give further information on the selective excitation mechanism involved in the helium-iodine laser.

5. Preferential enhancement

There are now numerous examples in the literature where selective excitation of ion levels appears to be through $10/01'/01\emptyset$ or $0^m0^m/01'e$ near resonant processes. To the writer's knowledge there is no theory to account for the preference that appears to be shown for selective excitation of ^3D levels, as against ^3F levels in enhancements attributed to the $10/01'/01\emptyset$ process. At higher atomic helium ion energies, in the range 100-500eV, Dworetsky et al. [4], Deheer et al. [5] have found that maximum cross sections for charge transfer in inert gases occurs with excitation into D levels at lower ion energies than the P or S levels.

Further work is needed to determine if there is indeed any tendency for certain triplet levels to be excited in collisions with low energy ions, in which spin is conserved, and if so, to determine if the effect is similar to the high energy effect reported above.

6. Measurement of the velocity of light using lasers.

Bennett and Knutsen (3) suggested using the two cw infra-red laser lines at 1.15228 and 1.15250 microns in the helium-neon laser, in the manner of the microwave interferometer used by Froome (6) in a determination of 'c' by measuring the wavelength and the difference frequency of the two lines. The inability to obtain comparable intensity in these lines has prevented such an experiment being carried out.

There is now very good ground for suggesting that a mixture of iodine and chlorine, in an inductively pumped plasma, would provide two visible cw laser lines, with a suitable small wavelength separation. These lines are Cl^+ 521.776nm and I^+ 521.627nm, giving difference fringes of 0.9mm, (suitable for long path interferometry.) at a frequency of approximately 166Kmc/s. Doubtless unforeseen complications could be involved, but it would appear that such an experiment is not too formidable to undertake.

Acknowledgments

The writer wishes to make grateful acknowledgment of the help received from, and the forebearance shown by Professor O. S. Heavens, throughout the period in which the work described here was carried out at the Royal Holloway College and the University of York.

It is a pleasure to acknowledge the communications the writer has had with Dr. D. W. O. Heddle, University of York; Dr. A. von Engel, The Clarendon Laboratory; Dr. R. T. Young, Harry Diamond Laboratories, Washington, and the stimulating discussions with Dr. L. Brown, Australian National University, Canberra, and Dr. V. Smiley, N.E.L., San Diego, both Visiting Fellows at the University of York.

Appreciation is expressed to Professor K. Murakawa, University of Tokyo, for recent prepublication information on hyperfine structure in ionised iodine; Dr. A. Bloom, Spectra-Physics, Inc., and Dr. Walter, T.R.G. Inc., for prepublication information on pulsed hollow cathode discharges and transient lasers respectively.

Thanks is also due to R.R.E., Malvern, and English Electric, Chelmsford, for gifts of surplus equipment and technical guidance which enabled the Pulse Modulator, used in the latter part of this project, to be constructed; and to the B.N.F.M.A., London for the loan of photoelectric recording equipment used whilst at Royal Holloway College.

Throughout the whole period of this work, the cheerful, skilled personal assistance of Mr. J. Clarke has been appreciated.

A maintenance grant from the United Kingdom Atomic Energy Authority during the period 1965-1967, and a College Postgraduate Studentship in 1964-1965, awarded by the Council of Royal Holloway College, which made this work possible, are acknowledged with gratitude.

APPENDIX 4.1

Equivalent laser transitions in Zinc, Cadmium and Mercury

Oscillation conditions: Fowles and Silfvast (1); Silfvast et al. (2); and Bloom et al. (3). As yet unlased lines are shown underlined.

Element	Wavelength in nm	Upper laser level	Process in helium △E in eV		Comments
			$0^m0^m/01'e$	$10/01'$	
Zn	610.2	$5d\ ^2D_{5/2}$	- 0.1	0.56	V. Strong, He only
Cd	<u>673.0</u>	6d "	1.	2.0	-
Hg	734.6	7d "	0.1	- 1.5	$He^*(^1S)$ V. Strong
Zn	747.9	$4s^2\ ^2D_{5/2}$	> 6.	> 7.	He only
Cd	441.6	$5s^2$ "	Cascade	lasing	Strong, He only
Zn	775.8	$6s\ ^2S_{1/2}$	0.25	1.0	He only
Cd	<u>840.0</u>	7s "	1.5	2.3	-
Hg	1058.3	8s "	0.6	1.0	$He^*(^1S)$
Zn	758.8	$5p\ ^2P_{7/2}$	2	2.5	He only
Cd	<u>750.0</u>	6p "	3	4.	-
Hg	615.0	7p "	0.17	0.15	V.V. Strong
Zn	492.4	$4f\ ^2F_{7/2}$	- 0.02	0.63	V. Strong He only
Cd	537.8	$4f\ ^2F_{7/2}$	1.2	3.5	He and Ne
Hg	567.7	5f "	± 0.5	1.5	$He^*(^1S)$ V.Strong

APPENDIX 4.2

Partial list of energy levels for Zinc, Z = 30

1st I.P. 75,767 cm^{-1}, or 9.391 V

	Level Configuration	Design.	J	Level (in cm^{-1})
ZnI	$3d^{10}$ (^1S) $4s^2$	^1S	0	0
	4s 4p	$4p\ ^3P^o$	0	32,300
			1	32,501
			2	32,890
ZnII	$3d^{10}$ (^1S) 4s	4s ^2S	1/2	0
		$4p\ ^2P^o$	1/2	48,480
	(^1S)		3/2	49,354
	$3d^9\ 4s^2$	$4s^2\ ^2D$	5/2	62,722
			3/2	65,441
	$3d^{10}$ (^1S) 5s	^2S	1/2	88,437
	" 4d	^2D	3/2	96,909
			5/2	96,960
	" 5p	$^2P^o$	1/2	101,365
			3/2	101,611
	" 6s	^2S	1/2	114,499
	" 4f	$4f\ ^2F^o$	7/2	117,263
			5/2	117,263
	" 5d	^2D	3/2	117,969
			5/2	117,993

APPENDIX 4.3

Partial list of energy levels for Cadmium, Z = 48

1st I.P. 72,539 cm^{-1}, or 8.991 V

	Level Configuration	Design.	J	Level (in cm^{-1})
CdI	$4d^{10}\ (^2S)\ 5s^2$	^1S	0	0
	5s 5p	$^3P^o$	0	30,114
			1	30,656
			2	31,827
CdII	$4d^{10}\ (^2S)$ 5s	^2S	1/2	0
	5p	$^2P^o$	1/2	44,136
			3/2	46,619
	$4d^9\ 5s^2$	^2D	5/2	69,259
			3/2	74,894
	$4d^{10}\ (^1S)$ 6s	^2S	1/2	82,991
	" 5d	^2D	3/2	89,689
			5/2	89,844
	" 6p	$^2P^o$	1/2	94,710
			3/2	95,383
	" 7s	^2S	1/2	107,301
	" 4f	$^2F^o$	5/2	108,419
			7/2	108,432
	" 6d	^2D	3/2	110,174
			5/2	110,248

APPENDIX 4.4

Partial list of energy levels for Mercury Z = 80

1st I.P. 84,184 cm^{-1}, or 10.43 V

	Level Configuration	Design	J	Level (in cm^{-1})
HgI	$5d^{10}$ (^1S) $6s^2$	^1S	0	0
	6s (^2S) 6p	$^3P^o$	0	37,645
			1	39,412
			2	44,043
HgII	$5d^{10}$ (^1S) 6s	^2S	1/2	0
	$5d^9$ $6s^2$	^2D	5/2	35,514
			3/2	50,552
	$5d^{10}$ (^1S) 6p	$^2P^o$	1/2	51,485
			3/2	60,608
	" 7s	^2S	1/2	95,714
	" 6d	^2D	3/2	104,983
			5/2	105,543
	" 7p	$^2P^o$	1/2	108,298
			3/2	111,970
	" 8s	^2S	1/2	121,416
	" 5f	$^2F^o$	7/2	123,152
			5/2	123,409
	" 7d	^2D	3/2	125,324
			5/2	125,578

APPENDIX 4.5

Partial list of energy levels for Helium, Z = 2

1st I.P = 198,305 cm^{-1}, or 24.58 V

Confign.	Design	J	Level
$1s^2$	^1S	0	0 ± 15
1s 2s	2s ^3S	1	159,850
1s 2s	2s ^1S	0	166,272

Electron and Shell disposition of Zinc, Cadmium and Mercury

	K	L	M	N	O	P
	s	s p	s p d f	s p d f	s p d f	s p d f
Zn	2	2 6	2 6 10-	2		
Cd	2	2 6	2 6 10-	2 6 10-	2	
Hg	2	2 6	2 6 10-	2 6 10 14	2 6 10-	2

APPENDIX 5.1

Possible resonant energy combinations of the inert gases and Mercury, with suitable cathode material elements.

Coincidences giving possible transitions, (λ in nm) with:

He (2^3S) metastable level,

1. Aluminium ΔE = 0.16 eV, at 1,400.
2. Magnesium ΔE = 0.1 eV, at 2,400 then 800, lifetime ratio 27.

$He^+(^2S_{1/2})$ ion level.

1. Silver ΔE = 0.005 eV, triplet level excited giving 900 then 240 transitions.
2. Aluminium ΔE = 0.16 eV, many lines at 800.
3. Arsenic ΔE = 0.04 eV, transition at 560.
4. Copper ΔE = 0.04 eV, number of transitions, one at 820.
5. Phosphorous ΔE = 0.15 eV, transition at 784.5 which has isoelectronic laser transition in Argon IV.

   ΔE = 0.63 eV, giving most persistent laser transition PII at 604.3.
6. Selenium ΔE = 0.25 eV, transition at 509.7 in Se II which has lased.
7. Zinc ΔE = 0.5 eV, giving laser transition at 610.0 ($5d\ ^2D_{5/2} - 5p\ ^2P_{3/2}$), this laser line was predicted during this work.

   ΔE = 0.25 eV, giving transition from $6p\ ^2P_{3/2}$ level at 1,210 which has analogous laser transition 862.2 in HgII, this has yet to be reported.

Ne (1s) metastables

1. Manganese ΔE = 0.04 eV, transition at 320.
2. Zirconium Transition at 480.

Ne $^{+}(^{2}S_{3/2})$ ion level

1. Aluminium ΔE = 0.022 eV, transition at 247.5
   ΔE = 0.003 eV, " " 331.5
   (Duffendack and Thomson, (2.19)).

Argon - no coincidences found

Mercury (Hg $6\,^{3}P_{0}$, $6\,^{3}P_{2}$) metastables.

1. Aluminium ΔE = 0.005 eV, excitation of $5s\,^{2}S_{1/2}$ level, giving transition at 2000.
2. Bismuth ΔE = 50 cm^{-1}, excitation of $6d\,^{2}D$ level.
3. Calcium ΔE = - 100 cm^{-1}, excitation $4d\,^{3}D$ level.
   ΔE = 100 cm^{-1}, " $7s\,^{3}S_{1}$ "
4. Gallium ΔE = 70 cm^{-1} " $6s\,^{2}S$ "
   ΔE = 100 cm^{-1} " $4f\,^{3}F$ "
   possible transition at 600.
5. Barium ΔE = - 30 cm^{-1} excitation $6d'\,^{3}P$ "
6. Molybdenum ΔE = 60 cm^{-1} " $z\,^{5}D^{o}$ "
7. Niobium ΔE = 100 cm^{-1} " $t\,^{4}D$ "
   ΔE = - 20 cm^{-1} " $v\,^{2}P$ "
8. Osmium ΔE = - 30 cm^{-1} " $z\,^{7}F$ "
9. Platinum ΔE = 50 cm^{-1} " $6s\,^{1}D_{4}$ "

10.	Ruthenium	ΔE =	30 cm^{-1}	excitation	y ^3D_o
		ΔE =	50 cm^{-1}	"	$2^o(56^o)$
11.	Strontium	ΔE	1 cm^{-1}	"	11s $^3S_1$
12.	Technetium	ΔE	30 cm^{-1}	"	$^3S_{7/2}$
		ΔE	20 cm^{-1}	"	^6D
13.	Tungsten	ΔE	- 30 cm^{-1}	"	Z ^5P
		ΔE	20 cm^{-1}	"	^7D

APPENDIX 7.1

Measurement of small wave-length differences or intervals (Meissner, (7.20)).

Let us suppose that two very close lines λ_a and λ_b (ν_a and ν_b) produce overlapping interference patterns, the corresponding diameters being D_{a1}, D_{a2}, D_{a3} ... D_{b0}, D_{b1}, D_{b2} ... The central order number of λ_a and λ_b may be denoted by P_a and P_b. Then the fundamental formula $P = 2t/\lambda$ yields $P_a = p_a + \epsilon_a = 2t\nu_a$, and $P_b = p_b + \epsilon_b = 2t\nu_b$.

Thus, for the interval of the two lines we get:

$$\nu_a - \nu_b = (p_a - p_b)/2t + (\epsilon_a - \epsilon_b)/2t.$$

The fractional parts ϵ_a and ϵ_b have to be calculated. The value of $(p_a - p_b)$ will be a small integer or zero, but it remains undetermined until another photograph of the fringe system, taken with a different gap is at hand. From the change of the patterns then it is easy to determine whether the separation of the lines is smaller than the range of dispersion, or the orders overlap. In the first case, $(p_a - p_b)$ is zero, in the second 1 or 2, or even more. Using the expressions

$$P = 2t\nu \cos \phi = 2t\nu \, (1 - R^2/2f^2) = 2t\nu \, (1 - D^2/8f^2)$$

and $$(D_k^2 - D_i^2) / (k - i) = 4\lambda f^2/t = \Delta D^2,$$

for two consecutive rings of the a and b system we can write

$$\nu_a - \nu_b = (p_a - p_b)/2t + (D_{ak}^2/\Delta D_a^2 - D_{bk}^2/\Delta D_b^2)/2t.$$

As the lines are very close ΔD_a^2 and ΔD_b^2 will be the same ($= \Delta D^2 = 4f^2/\nu' t$). Therefore,

$$\nu_a - \nu_b = (p_a - p_b)/2t + (D^2_{ak} - D^2_{bk})/2t\ \Delta D^2.$$

From this relation we see that not only the values $(D^2_{a(k-1)} - D^2_{ak})$ and $(D_b^2{}_{(k+1)}$ in the single ring systems are constant but also the corresponding values $(D^2_{ak} - D^2{}_{bk})$ between two or more different systems. Thus, it is possible to arrange the observations of the D^2 in a rectangular scheme with constant horizontal (Δ H) and vertical (Δ V) differences. Sometimes, such a scheme will show, by discrepancies in the horizontal or vertical differences, that the one or the other D^2 value is far off and may be discarded.

The general scheme of an interference pattern, produced by three close components a, b, and c, can be arranged as follows:

ΔH	ΔH	ΔH	ΔH	ΔH		
D^2_{a0}	D^2_{a1}	D^2_{a2}	D^2_{a3}	D^2_{a4}	D^2_{a5}	
						ΔV_1
D^2_{b0}	D^2_{b1}	D^2_{b2}	D^2_{b3}	D^2_{b4}	D^2_{b5}	
						ΔV_2
D^2_{c0}	D^2_{c1}	D^2_{c2}	D^2_{c3}	D^2_{c4}	D^2_{c5}	

Supposing that the orders do not overlap, the intervals $\nu_a - \nu_b$ and $\nu_b - \nu_c$ are given as

$$(\nu_a - \nu_b) = (D^2_{ak} - D^2_{bk})/2t\ \Delta D^2 = \langle \overline{\Delta V_1} \rangle /2t\ \langle \overline{\Delta H} \rangle,$$

$$(\nu_b - \nu_c) = (D^2_{bk} - D^2_{ck}/2t\ \Delta D^2 = \langle \overline{\Delta V_2} \rangle /2t\ \langle \overline{\Delta H} \rangle\ ,$$

where the sign $\langle\ \rangle$ indicates the average values of the horizontal and vertical differences.

APPENDIX 7.2

Component identification on the 658.5nm line to illustrate D^2 array method.

A.

Component			ΔH		ΔH		ΔH		ΔH		ΔH	
	D^2_{oa}	46.2	74.8	121	75	196	73	269	69	338	78	416
	D^2_{ob}	67.	72.	139	74	213	76	289	72	361	77	438
	ΔV_1	20.8		18		17		20		23		22

$\langle \overline{\Delta V_1} \rangle = 20.13, \quad \langle \overline{\Delta H} \rangle = 74.1$

$(\tilde{\nu}_a - \tilde{\nu}_b) = 20.13/(74.1 \times 2.024)\text{cm}^{-1} = \underline{134 \times 10^{-3} \text{ cm}^{-1}}$

B.

Component			ΔH		ΔH		ΔH		ΔH		ΔH	
	D^2_{oa}	46.2	74.8	121	75	196	73	269	69	338	78	416
	D^2_{oc}	77.5	76.5	154	71	225	75	300	76	376	74	450
	ΔV_2	31.3		33		29		31		28		34

$\langle \overline{\Delta V_2} \rangle = 31.05, \quad \langle \overline{\Delta H} \rangle = 74.1$

$(\tilde{\nu}_a - \tilde{\nu}_c) = 31.05/(74.1 \times 2.024)\text{cm}^{-1} = \underline{207 \times 10^{-3} \text{ cm}^{-1}}$

Note:- All frequency differences are measured from the strongest component.

References - Chapter 1

1. Maiman, T. H., Nature, 187, 493, (1960).

2. Javan, A., Bennett, W. R., Jr., and Herriott, D. R.
Phys. Rev. Letters, 6, 106, (1961)

3. Schawlow, A. L., and Townes, C. H., Phys. Rev, 112, 1940, (1958).

4. Bennett, W. R. Jr., Appl. Optics, Supplement on Chemical Lasers, 3, (1965)

5. Mitchell, A. and Zemansky, M. W., Resonance radiation and excited atoms,
C.U.P., (1961).

6. Bennett, W. R., Jr., Kindlmann, P. J., Mercer, G. N., as reference (4),
pp. 34 - 58.

References - Chapter 2.

(1) Ward R. C., Aerospace Rept. T.D.R. - 930 (2250-20) TN - 1, (1961)

(2) Javan A., Quantum Electronics, ed. Townes C. H., (N. York, Col. Univ. Press, 1960).

(3) Fabrikant V. A., All Union Electr. Inst. 41, 236, (1940)

(4) Basov N. G., Krokin O. N., Appl. Opt., 1, 3, 213, (1962).

(5) Bennett W. R. Jr., Appl. Opt. Supplement Optical Masers, 35, (1962)

(6) Bates D. R. and Damgaard A., Phil. Trans. A242, 10, (1950)

(7) Massey H. S. W. and Burhop E. H. S., Electronic and Ionic Impact Phenomena, O.U.P., (1952).

(8) Townsend J. S., Electrons in gases, Hutchinson, (1948)

(9) Mott N. F. and Massey H. S. W., The Theory of Atomic Collisions, 2nd Editn., O.U.P., (1952).

(10) Bates D. R., Atomic and Molecular processes, N. York, Acad. Press, (1962)

(11) Hasted J. B., Physics of Atomic Collisions, Butterworths (1964).

(12) Hasted J. B., "Charge transfer and Collisional detachment", in (10)

(13) McDaniel W. W., Collision Phenomena in Ionized gases, Wiley, (1964)

(14) Massey H. S. W., Rept. Progress in Phys. 12, 248, (1948).

(15) Bates D. R. and McCarrol R., Phil. Mag. Suppl. 11, 39, (1962).

(16) Mitchell A. C. and Zemansky M., Resonance radiation and excited atoms, C.U.P., (1961).

(17) Page 513 ref. (7), and Page 420 ref. (11)

(18) Hasted J. B. and Lee A. R., Proc. Phys. Soc. (London) 79, 702, (1962).

(19) Duffendack O. S. and Thomson K., Phys. Rev. 40, 106, (1933).

(20) Gran, W. H. and Duffendack O. S., Phys. Rev. 51, 804, (1937).

(21) Lipeles M., Novick R. and Tolk N., Phys. Rev. Letters, 15, 21, 815 (1965).

(22) Bennett W. R., Jr., Appl. Opt., Suppl. Chemical Lasers 19, (1965).

(23) Shuler K. E., Carrington T., and Light J. C., Appl. Opt. Suppl. Chemical Lasers 8, (1965).

(24) Born M., Z. Physik, 38, 803, (1926).

(25) Kieffer L. J., and Dunn G. H., Revs. Mod. Phys. 38, 1, 1, (1966).

References - Chapter 3.

(1) Butayeva F. A. and Fabrikant V. A., J.E.T.P. 62, (1959).

(2) Soviet Gas Laser Research. A.D. 282253, 12, (1962)

(3) Sanders, J. H., Phys. Rev. Letters, 3, 86, (1959)

(4) Sanders J. H., Bell Telephone Labs. Case 38543 (1959).

(5) Javan A. Phys. Review Letters 3, 87, (1960)

(6) Javan A., Bennett W. R., Herriott D. R., Phys. Rev. Letters 6, 106, (1961)

(7) von Engel A., Ionised Gases, Clarendon Press, (1965)

(8) Francis O., Handbuch d. Physik XII, Springer-Verlag, Berlin

(9) Brown S. C., Basic data of Plasma Physics, Wiley, N. York, (1959).

(10) Parker P., Electronics, Arnold, (1953).

(11) Pringle D. H. and Farvis W. E., Phys. Rev. 96, 536, (1954)

(12) Udelson B. J., Burton and Creedon J. E., Phys. Rev. 88, 145, (1952)

(13) Brewer A. K. and Westhaver J. W., J. Appl. Phys. 8, 779, (1937)

(14) Hurt B. H., Univ. microfilms, 11803, (1964).

(15) Dorgelo H. B., Alting H. and Boers J., Physica, Haag, 2, 959, (1935)

(16) Wada J. W. and Heil H., I.E.E.E. J. Quant. Electr. 8, 327, (1965)

(17) Bochkova O. P., Razumovskaya L. P. and Frish, Opt. Spectry, 11, 376, (1961).

(18) Francis O., Ionisation Phenomena in Gases, Butterworth, London,(1955)

(19) Brown S. C., Handbuch do Physik, Band 22, p.34, Springer-Verlag, Berlin, (1956).

(20) Ward, R. C., Aerospace Report, T.D.R.-930, (2250-20) TN1 (1961).

(21) von Engel A. and Harris, W. L., Proc. Roy. Soc. A 222, 490, (1954).

(22) Paschen F., Ann. d. Physik 50, 901, (1916).

(23) Schuler H., High Resolution Spectroscopy, Tolansky S., Methuen, p.35, (1947).

(24) Tolansky S. as (23) p.48.

(25) Roessler F. L. and de Noyer L., Phys. Rev. Letters, 12, 14, 396, (1964).

(26) Little P. F. and von Engel A., Proc. Roy. Soc. A224, 209, (1954).

(27) Badareu E., Popescu I. and Iova I., Ann. Phys. 5, 508, (1960).

(28) Badareu E and Popescu I., J. Electr. and Control 503 (1958).

(29) Ciobotaru D., J. Electr. and Control, IV, 6, 529, (1958).

(30) Druyvesteyn M. J. and Penning F. M., Rev. Mod. Phys. 12, 87, (1940)

(31) White A. D., J. Appl. Phys. 30, 711, (1959).

(32) Musha T., Phys. Soc. Japan 17, 1440 and 1447, (1962).

(33) Davis W. D. and Vanderslice J. A., Phys. Rev. 131, 219, (1963)

(34) von Hippel A., Ann. Phys. 81, 1043, (1926).

(35) Honig R. E. Ionisation Phenomena in Gases, N. Holland, (1962) p.106 Munich Conf. (1961).

(36) Wehner O. K., Phys. Rev. 108, 35, (1957).

(37) Wehner O. K., Phys. Rev. 112, 1120, (1958).

(38) Laegreid N. and Wehner O. K., J. Appl. Phys. 32, 365, (1961).

(39) Wehner O. K., J. Appl. Phys. 33, 1842, (1962)

(40) Townes, C. H., Phys. Rev. 65, 11 and 12, 319, (1964)

(41) Sullivan J. V. and Walsh A. 'High Intensity Hollow Cathode Lamps' C.S.I.R.O., Report Melbourne.

(42) Stocker, B. J., B. J. Appl. Phys. 12, 9, 465, (1961).

(43) Sawyer, R. A., Phys. Rev. 36, 44, (1930).

(44) Mitchell K. B., J.O.S.A., 51, 8, 846, (1961)

(45) Boot H. A. and Clunie D. M., Nat. 197, 173, (1963)

(46) Cheo and Cooper, Appl. Phys. Letters 5, 3, 42, (1964)

(47) Breusava L. N., Rad. Eng. Electr. Phys. Oct. '65.

(48) Pakhomov, P. L., Reznikov G. P. and Fugal I. Opt. Spectry. 5, 20, (1966).

(49) Biondi M. A. and Holstein T., Phys. Rev. 82, 962, (1951); 83, 1078, (1951).

(50) Anderson J. M., Phys. Rev. 108, 898, (1957)

(51) Loeb L. B., Basic processes of Gaseous Electronics, Univ. of Cal. Press. Berkeley, (1955) p.567.

(52) Biondi M. A., 6th Conf. on Gaseous Electronics, Washington D.C., C4, (1953).

(53) Ferguson E. E., Fehsenfeld F. C., and Schmeltekopf, A. L., Phys. Rev. 138, 2A, A381, (1965).

(54) CollinsC. B. and Robertson W. W., J. Chem. Phys. 40, 8, 2202, (1964).

(55) Anderson J. M., Phys. Rev. 108, 898, (1957).

(56) Emeleus K. O. and Duffendack O. S., Phys. Rev. 47, 460, (1935).

(57) Collins C. B. and Hurt W. B., 3rd. Int. Conf. Phys. of Electr. and Atomic Collisions, London, (1963).

(58) Kerr D. E., Johns Hopkins Univ. (1960) Unpublished Rept.

(59) Hornbeck V. A. and Molnar J. P., Phys. Rev. 84, 621, (1951)

(60) Phelps A. V. and Brown, Phys. Rev. 86, 102, (1952).

References - Chapter 4

(1) Javan A., Bennett W. R. Jr., Herriott D. R., Phys. Rev. Letters 6, 106, (1961).

(2) Massey H. S. W. and Burhop E. H. S., Electronic and Ionic Impact Phenomena, (Clarendon Press, Oxford, 1952.

(3) Bennett W. R., Advances in Quantum Electronics, (Columbia Univ. Press, New York, (1961) pp. 28-43.

(4) Bennett W. R., Javan A. and Ballick E. A. Bull. Am. Phys. Soc. 5, 496, (1960).

(5) Klose, J. Z. Bull. Am. Phys. Soc. 9, 488, (1964).

(6) Ladenburg R., Rev. Mod. Phys. 5, 243, (1933).

(7) Griffiths J. H., Proc. Roy. Soc. (London) 143, 588, (1934).

(8) Bates D. R. and Damgaard A., Phil. Trans. A.242, 101, (1950).

(9) Bennett W. R., Bull. Am. Phys. Soc. 7, 15, (1962).

(10) Chebotayev, V. P., Rad. J., Eng. Electr. Phys. (U.S.A.) 10, 2, 316, (1965).

(11) Javan A., Phys. Rev. Letters 3, 87, (1959)

(12) Javan A., Quantum Electronics, Columbia Univ. Press, N. York (1960) pp. 564 - 571.

(13) Javan A., Bennett W. R., Herriott D. R., Advances in Quantum Electronics, Columbia Univ. Press, N. York, (1960) pp. 18-49.

(14) Bennett W. R., Appl. Opt. Supplement on Optical Masers (1962) pp. 24-61.

(15) Bennett W. R., (Priv. Communication with Gould) AD. 426961.

(16) Dorgelo, H.B., Alting H. and Boers J., Physica (Haag) 2, 959, (1935)

(17) Ladenburg R., and Dorgelo H. B., Physica, 5, 90, (1925)

(18) Benton E. E., Phys. Rev. 206, 128, (1962).

(19) Jesse, W. P., Sadauskis, J., Phys. Rev. 88, 417, (1952).

(20) Benton E. E. and Robertson W. W., Bull. Am. Phys. Soc. 7, 114, (1962)

(21) Rigden J. D. and White A. D., Proc. I.R.E. 50, 7, (1962)

(22) Suga T., Sci. Papers Inst. Phys. Chem. Res. Tokyo 34, 7, (1938).

(23) Suzuki N,Japan J. Appl. Phys. 3, 11, 705, (1964)

(24) Rigden J. D. and White A. D., Proc. I.E.E.E. 51, 943, (1963)

(25) Zarowin C. B., Schiff M. and White G. R., Proceedings Symp. on Opitcal Masers, Brooklyn. April (1963) pp. 425-434.

(26) Bloom A. L., Bell W. E. and Rempel R. C., Appl. Opt. 2, (1963).

(27) Patel C. K. N., McFarlane R. A. and Faust W. L., Quantum Electronics III, Columbia Univ. Press N. York 1964, pp. 561-572.

(28) McFarlane R. A., Faust W. L., and Patel C. K. N., Proc. I.E.E.E. 51, 468, (1963).

(29) Ablekov V. K., Pesin M. S. and Fabelinsky I. I., Soviet Phys. J.E.T.P. 12, 618, (1961).

(30) Dana L. and Laures P., Conf. (London) Sep. 1964, and Proc. I.E.E.E., 53, 78 (1965).

(31) Bridges W. B. and Chester A. N., Proc. I.E.E.E., 52, 843, (1964)

(32) Jenson R. C. and Fowles G. R., Proc. I.E.E.E., 52, 1350 (1964).

(33) Fowles R. C. and Jenson G. R., Appl. Opt. 3, 10, 1191, (1964)

(34) Bell W. E., Appl. Phys. Letters 4, 34, (1964).

(35) Bloom A. L. and Bell W. E. and Lopez F.O., Phys. Rev. 135a, 578, (1964).

(36) Heard H. G. and Peterson J., Proc. I.E.E.E. 52, 9, 1049, (1964)

(37) Gerritsen H. J. and Goedertier P. V., J. Appl. Phys. 35, 3060, (1964)

(38) Byer R. L., Bell W. E., Hodges E., Bloom A. L., J.O.S.A., 55, 12 1598, (1965).

(39) Bell W. E., Appl. Phys. Letters 7, 7, 190 (1965)

(40) Dyson D. J., Nature, 207, 361, 24 Jul. (1965).

(41) Suzuki N., Japan J. Appl. Phys. 4, 452, Jun (1965).

(42) Paschen F., Sitzungsber. Preuss Akad. Wissench 32, (1928)

(43) Hasted J. B., Physics of Atomic Collisions p.268 (Butterworths) (1964).

(44) Bridges W. B. and Chester A. N. (priv. comm.) I.E.E.E. Quantum Electr. 1 - 2, May (1965).

(45) Patel C. K. N., and Bennett W. R., Phys. Rev. Letters 6, 106, (1961)

(46) Patel C. K. N., and McFarlane R. A., Faust W. L., J.O.S.A., 53, 522,(1963)

(47) Patel C. K. N., Atomic Collisions Processes. (N. H. Publ. Press). Sep. (1963) pp. 1010 - 1054.

(48) Bennett W. R., Faust W. L. and McFarlane R. A. and Patel C. K. N. Phys. Rev. Letters 8, 470, (1962).

(49) Patel C. K. N. Patel, Faust W. L., McFarlane R. A. and Garrett C. G. B. Proc. I.E.E.E. 52, 713 (1964).

(50) Patel C. K. N., Bennett W. R., Faust W.L. and McFarlane R. A. Phys. Rev. Letter, 9, 102 (1962).

(51) Aisenburg S., Appl. Phys. Letters 2, 187, (1963).

(52) Bridges W. B., Appl. Phys. Letters 3, 3, 45, (1963).

(53) Bridges W. B., Appl. Phys. Letters 4, 128, (1964).

(54) G. Convert, M. Armand, P. Martinot-Lagarde, Compt. Rend. Acad. Sci. Paris 258, Mar 23, 3259, (1964).

(55) Ibid. 258, May; 4467, (1964).

(56) Bennett W. R., Knutson J. W., Mercer G. N. and Detch J. L., Appl. Phys. Letters 4, 180, (1964).

(57) Gordon E. I., Labuda E. F., and Bridges W.B., Appl. Phys. Letters 4, 178, (1964).

(58) Cheo P. K. and Cooper H. G., Bull. Am. Phys. Soc. 9, 6, 626, (1964)

(59) Bridges W. B. and Chester A. N., I.E.E.E. Quantum Electr. 66, May (1965).

(60) Gordon E. I., Labuda E. F. and Bridges W. B., Appl. Phys. Letters 4, 178, (1964).

(61) Cheo P. K. and Cooper H. G., Bull. Am. Phys. Soc 9, 6, 626, (1964).

(62) Bennett W. R. and Lichten W. (unpublished), Appl. Optics. Supplement on Chemical Lasers p.20. (1965).

(63) Fowles G. R. and Jenson R. C., Appl. Phys. Letters 6, 12,236 (1965).

(64) Piltch M., Walter W. T., Solimene N., and Gould G., Appl. Phys. Letters 7, 11, 309, (1965).

(65) Walter W. T., Solimene N., Piltch M., and Gould G., (priv. comm.) J. Quantum Electr. (in press).

References - Chapter 5.

(1) Schuler, H., Z. Phys., 35, 323, (1926)

(2) Tolansky, S., High Resolution Spectroscopy, Methuen, (1947).

(3) Roesler, F. L. and De Noyer, L., Phys. Rev. Letters 12, 14, 396 (1964)

(4) Heavens, O. S., Optical Masers, Ch. 4, Methuen, (1964)

(5) Badareu, E. and Wachter, Fr., J. Electr. Contr. 4, 1539, (1958)

(6) Francis, G. Handbuch der Physik, Band XXll, (1956)

(7) Popovici, C., and Somesan, M., Appl. Phys. Letters 8, 5, 103, (1966)

(8) Bell, W. E., Bloom, A. L. and Goldsborough, J. P., I.E.E.E. J. Quantum. Electr. 400, Dec. (1965).

(9) Piltch, M., Walter, W. T., Solimene, N., and Gould G. Appl. Phys. Letters, 7, 11, 309, (1965).

(10) Silfvast, W. T., Fowles, G. R. and Hopkins, B. D. Appl. Phys. Letters, 8, 12, 318, (1966).

(11) Hurt, Jr. W. B. Univ. microfilms 64 - 11803

(12) Birger-Persson, K., J. Appl. Phys. 36, 10, 3086, (1965).

(13) Mott, N. F. and Massey, E. H. S., The Theory of Atomic Collisions, O.U.P., (1952).

(14) Moore, C. E. Atomic Energy Levels, Vols. 1 - 3, Washington, D.C. Govt. Printing Office, (1952).

(15) Wehner, O. K., Phys. Rev. 112, 1120, (1958)

(16) Bogdanova, I. O. and Chen Gi - Tkek, Opt. i Spektr. 2, 681, (1957), (N.L.L. R.T.S. 2456)

(17) Ablekov, V. K., Pesin, M. S. and Fabelinsky, I. I., Sov. Phys. JeTP, 12, 618, (1961)

(18) Bell, W. E., Appl. Phys. Letters, 4, 2, 34, (1964).

(19) McLennon J, J., Mc.Lay, and Crawford, M., Proc. Roy. Soc. 134, 41,1937

(20) Naudé, S. M., Ann. d. Physik, 3, 1, 26, (1929)

(21) Mrozowski, S., Phys. Rev. 58, 332, (1940)

(22) Fowles, G. R. and Jenson, R. C. Appl. Optics, 3, 10, 1191 (1964)

(23) Berezin, I. A., and Yanovskaya, G. N., Opt. Spectr. 14, 1, 11, (1963)

(24) Bates, D. R. and Damgaard, A., Phil. Trans, A242, 10, (1950)

(25) Condon, E. U. and Shortley, G. H., Theory of Atomic Spectra, (Camb. Univ. Press) (1935).

(26) Le Grand Yves, Light, Colour and Viscon, Chapman-Hall, (1957).

(27) Moon, P., JOSA, 38, 3, 291, (1948)

(28) Walsh, J. T. W., Photometry, (Constable) (1958)

(29) Daughters, G. T., Fairchild Application Rept. APP - 47

(30) de Vos, J. C., Physica (Haag), 20, 690, (1954)

(31) Philips Electrical Ltd., "Tungsten Ribbon lamps for Optical measurements".

(32) Robertson, J. K. JOSA, 7, 983, (1923)

(33) Helmick, P. S. Phys. Rev, 17, 8, 135, (1921)

(34) Mitchell, K. B. JOSA, 51, 8, 846 (1961)

(35) Sawyer, R. A., Experimental Spectroscopy, Chapman Hall, (1951)

(36) Harrison, G. R., Lord, R. C. and Loofbourow, J. R. Practical Spectroscopy, Prentice-Hall, N. J. (1959)

(37) Bennett Jr., W. R., AD 426961

(38) Schawlow, A. L. and Townes, C. H., Phys. Rev. 112, 6, 1940, (1958)

(39) Cobine, J. D., Gaseous Conductors, McGraw-Hill, (1941).

(40) Mandel'stam, S. L., and Nedler, V. V. Opt. Spectr. 10, 196, (1961)

(41) Chebotayev, V. P., Rad. Engy. Electr. Phys (U.S.A.) 10, 2, 314, (1965)

(42) Zarowin, C. B., Schiff M. and White G. R. Brooklyn Symp. Opt. Masers, 425, (1963)

(43) Smith, J. J. Appl. Phys. 35, 3, 723, March (1964)

(44) Znamenskii, V. B., Buinov, G. N. and Bursakov, E. S.
Opt. Spectr., 20, 3, 292, (1966)

(45) Sturgess, D. J. and Oskam, H. J., J. Appl. Phys. 35, 10, 2887, (1964)

(46) von Engel, A., Ionised Gases, Clarendon Press, (1965).

(47) Parker, P., Electronics, Arnold, (1955)

(48) Chebotayev, V. P., Opt. Spectr. 20, 1, 10, (1966)

References - Chapter 6.

(1) Javan, A., Bennett W. R. Jr., and Herriott D. R. Phys. Rev. Letters 6, 106, (1961).

(2) White A. D., and Rigden J.D., Proc. 1.R.E. 50, 7, (1962)

(3) Basov N.G., and Krokhin O. N., Appl. Opt. 1, 213, (1962).

(4) Javan A., Phys. Rev. Letters 3, 87, (1959).

(5) V. A. Fabrikant, Sov. Phys. JETP 14, 375, (1962).

(6) Ward R.C., Aerospace Tech. Rept. TDR-930 (2250-20) TN-1.

(7) Bennett W. R. Jr., Appl. Opt. Supplement 1, 35, (1962).

(8) Bennett W. R. Jr., Bull. Am. Phys. Soc. 7, 15, (1962).

(9) Patel, C. K. N., Bennett W. R. Jr., Faust W. C. and McFarlane R.A. Phys. Rev. Letters 9, 102, (1962).

(10) Rigden J. D. and White A. D., Proc. I.E.E.E. 6 943, (1963).

(11) Bennett W. R. Jr., AD 426961, 1963.

(12) Engel A. von., Ionised Gases, (Clarendon Press, Oxford) 2nd Edit. Ch. 8 1965.

(13) Ibid, Ch. 3, p.63.

(14) Toyoda K. and Yamanaka C., Japan J. Appl. Phys. 4, 226 (1965).

(15) Wada J. W. and Heil H., I.E.E.E. J. Quantum Electr. 8, 327, (1965).

(16) Engel A. von and Steenbeck M., Electrische Gasentladungen, Band 2, (Springer-Verlag, Berlin 85, (1932).

(17) Dorgelo H. B., Alting H and Boers J. Physica Haag 2, 959, (1935).

(18) Young R. T., J. Appl. Phys. 36, 7, 2324, (1965).

(19) Labunda E. F., and Gordon E.I., J.Appl. Phys. 35, 1647 (1964).

(20) Korolev, F. A., Odintsov A. I. and Mitsai V. N. Opt. Spectry. 19, 1, 36, (1965).

(21) Mielenz K. D. and Nefflen K. Appl. Opt. 4, 565, (1965).

(22) White A. D. and Gordon E. I., Appl. Phys. Letters 3, 199 (1963).

(23) Bochkova O. P. and Razumovskaya L. P. Opt. Spectry, 17, 8, (1964).

(24) Bochkova O. P., Razumovskaya L. P. and Frisch S. E. Opt. Spectry 11, 376, (1961).

(25) Bochkova O. P. and Razumovskaya L. P., Opt. Spectry, 18, 5, 438, (1965).

(26) Bochkova O. P. and Razumovskaya L. P., Opt. Spectry, 18, 5, 389, (1965).

References - Chapter 7

(1) Jenson R. C., and Fowles G. R. Proc. I.E.E.E., 52, 1350 (1964)

(2) Fowles G. R. and Jenson R.C., Appl. Optics 3, 10, 1191, (1964).

(3) Dana L., and Laures P., Proc. I.E.E.E. 53, 78, (1965).

(4) Martin W. C. and Corliss, C. H., J. Res. Nat. Bur. Stds, 64A, 6, 433, Nov. - Dec., (1960).

(5) Keefe W. M. and Graham W. J., Phys. Letters 20, 6, 643, (1966).

(6) Bridges W. B., and Chester A. N., Nerem Record, 106, (1964)

(7) Berezin I. A. and Yanovskaya G. N., Opt. Spectr. 14, 1, 11, (1963)

(8) McFarlane R. A., Appl. Optics. 3, 1196, (1964)

(9) Principles of Radar, M.I.T., McGraw Hill, 2nd Edition (1964)

(10) Whitteman W. J., Q.E.C., 'Phoenix', April 1966, (M.S. 5065 report)

(11) White, A. D., Appl. Optics, 3, 3, 431, (1964)

(12) Taylor, U. S. Amer. Phys. Soc., reported by E. Paine. Conf. Lasers and Applications, I.E.E. London Sept. (1963).

(13) Ahmed, S. A. and Faith T., Qu. Electr. Conf. Phoenix Ariz. April 12 - 15, IB - 2, (1966).

(14) Heavens, O. S., and Willett, C. S. Opt. Acta, 13, 3, 271, (1966)

(15) Willett C. S. and Heavens O.S., Opt. Acta, 13, 4, (1966)

(16) Fowles G. R. and Jenson R. C., Phys. Rev. Letters, 14, 10, 347 (1965).

(17) Willett C. S., I.E.E.E., J. Quant. Electr., Jan. (1967)

(18) Tolansky S., Phil. Mag 35, 229, (1944)

(19) Candler C., Modern Interferometers, Hilger, (1951)

(20) Meissner, K. W., JOSA 31, 6, 405 (1941)

(21) Murakawa, K. Z. f. Phys. 109, 3, 162 (1938)

(22) Murakawa, K. Z. f. Phys. 112, 3, 234 (1939)

(23) Murakawa, K. Nature 137, 1030 (1936)

(24) Tolansky, S., Proc. Phys. Soc. 48, 49, (1936)

(25) Tolansky, S., and Forrester G. O., Proc. Roy. Soc. A168, 78, (1938)

(26) Kopfermann H., Nuclear Moments, Academic Press Inc., N.Y., (1958).

(27) Murakawa, K. J., Phys. Soc. (Japan) 19, 9, 1539, (1964)

(28) Kuhn, H. G., Atomic Spectra, Longmans, (1962)

(29) White, H. E., Intro. to Atomic Spectra, McGraw-Hill N. York, (1934).

(30) Dorgelo, H. B., Z. Phys. 26, 756, (1925)

(31) Orstein, L. S., and Burger, H. C. Z. Phys. 40, 403, (1926)

(32) Schuler, H. and Jones, E., Z. Phys. 77, 801, (1932)

(33) Shenstone A. G. and Russell H. N., Phys. Rev. 39, 415, (1932)

(34) Turkin, Y. I., Opt. Spectry, 7, 5, (1959)

(35) Schrammen A., Ann. Phys. 87, 638, (1928)

(36) Schuler, H., and Keyston, J. E. Z. Phys. 67,433, (1931)

(37) Turkin, Y. I., Opt. Spectry 20, 4, 411, (1966)

(38) Byer R. L., Bell W. E., Hodges E., and Bloom A. L. JOSA, 55, 12, 1598 (1965)

(39) Bridges, W. B. and Chester, A. N., I.E.E.E. J. Quant. Electr. QE-1, 2, 66, (1965).

References, Appendices and Future work.

Appendix 4.1

1. Fowles G. R., and Silfvast, W. T. I.E.E.E. J. Quant. Electr., Q.E. - 1, 3, 1 (1965)

2. Silvast, W. T., Fowles G. R. and Hopkins, B. D. Appl. Phys. Letters, 8, 12, 318, (1966)

3. Bloom, A. L., Bell W. E. and Lopez F. O., Phys. Rev., 135, A578, (1964)

Future work

1. Bell, W. E. and Bloom A. I.E.E.E. J. Quant. Electr. 400, Dec., (1965).

2. Assagoe, K., Japan. J. Phys. 4, 85, (1927).

3. Bennett, W. R. and Knutsen, J. W. Proc. I.E.E.E. 52, 861, 1964.

4. Dworetsky, S. H, Novick, R., Smith W. W. and Tolk N. 19th Ann. Gaseous Electr. Conf. Oct. 12-14, (1966) Atlanta.

5. Deheer, F. J., Muller, L. W., Geballe, R. Physica, 31, 1745, (1965).

6. Froome, K. D., Proc. Roy. Soc., A223, 195, (1954).

APPENDIX A.

Reprint from
JOURNAL OF APPLIED MATHEMATICS AND PHYSICS (ZAMP)
Vol. 16, Fasc. 1 (1965) BIRKHÄUSER VERLAG BASEL Page 87
Received: October 14, 1964

Possibility of the Use of a Hollow Cathode Discharge as an Amplifying Medium

By O. S. HEAVENS, University of York, Heslington, York and C. S. WILLETT, Royal Holloway College, University of London, London, Great Britain

The hollow-cathode discharge has long been used as a source of sharp, intense spectral lines. The mechanisms of this type of discharge have not been extensively studied, although it is known that the current in the discharge is predominantly electronic. The source of the very high electron current is that of photo-emission from the cathode surface, produced by the high intensity of ultraviolet radiation present in the discharge. Such discharges contain a large concentration of ions and atoms of the cathode material, produced by sputtering action of the carrier gas. Under some conditions, the intensities of the metallic lines is very high and may be comparable with those from the carrier gas.

In recent work on lasers using ion spectra (e.g. A, Kr, Xe) very high intensities and large gains have been reported. Although the detailed mechanisms of these systems are not yet fully understood, a contributing feature is the fact that the lower levels of the laser transitions are connected to the ion ground state by ultraviolet transitions, of very high transition probability.

In the system under consideration, use is made of the fact that there exists a near coincidence in energy between an excited level of Al II ($3\,p^2\,{}^1D$) and one of the metastable (or quasi-metastable) levels of the 1s (PASCHEN) group of neon. By a similar mechanism to that used in the He-Ne laser, excitation to the ${}^1D$ level of Al II by collision with metastables appears promising. From the ${}^1D$ level under consideration, return to the ground state of the ion occurs by radiative transitions via the $3\,p\,{}^1P$ level. Calculation of the transition probabilities, using a central field approximation, suggests that population inversion is possible. Limited experimental work so far has established the conditions under which the Al II ($3\,p^2\,{}^1D \rightarrow 3\,p\,{}^1P$) line (at 3900 Å) is obtained. The present system has an uncooled cathode and cannot be operated continuously at a high enough power to give a sufficiently high density of Al II for laser action to be possible. A water-cooled system is now under construction.

OPTICA ACTA, 1966, VOL. 13, NO. 3, 271-274 APPENDIX B.

Correspondence

Laser transition at 651·6 nm in ionized iodine

C. S. WILLET and O. S. HEAVENS

Department of Physics, University of York, England

(*Received* 20 *May* 1966)

Laser action has been observed on an intercombination line of the spectrum of singly ionized iodine, in a pulsed, positive column discharge in a mixture of helium and iodine.

Oscillation was observed on the six lines of wavelength 703·299, 658·521, 612·749, 576·072, 567·808 and 540·736 nm, which have been previously observed by Fowles and Jenson [1, 2]. In addition laser action was obtained at a wavelength of 651·6 nm. This line corresponds to the intercombination transition $6p'\,^3F_2$–$5p^5\,^1P_1$, in the notation of Martin and Corless [3].

The discharge tube incorporating internal electrodes was of 7 mm bore and the plasma length 88 cm. It was excited by means of a pulse modulator, discharging a 0·0033 μF capacitor through a 4:1 pulse transformer at an input voltage of approximately 2–4 kv, at 1 kc/s. The laser output pulse was insensitive to the value of the discharge capacitor and was of approximately 20 μsec duration. The gain on the 576·0 nm line was greater than 5 per cent per metre. The optical resonator consisted of dielectric-coated concave mirrors, one of which had a radius of 2 m and with a reflecting coating centred at a wavelength of 540 nm, whilst the other was of radius 1m and centred on $\lambda = 632{\cdot}8$ nm.

The vapour pressure of the iodine was similar to that used by Jenson and Fowles [1, 2], although the optimum helium pressure was found to be approximately 10 torr. As shown in the figure the newly reported line, in common with the other iodine laser transitions, has a terminal ultra-violet transition ($5p^5\,^1P_1$–$5p^4\,^3P_2$) to the iodine ion ground state.

As is seen from the figure laser action is observed in the ($6p'\,^3D_2$–$6s'\,^3D_2$) line at 540·7 nm in the I II spectrum but not in the 533·8 nm line ($6p'\,^3F_3$–$6s'\,^3D_2$). This is surprising in view of the fact that the $6p'\,^3F_3$ level lies closer to the He^+ ground state level than does the $6p'\,^3D_2$ level. Moreover, the corresponding transition in ionized chlorine at $\lambda = 490{\cdot}47$ nm ($4p'\,^3F_3$–$4s'\,^3D_2$) is known to show laser action under comparable conditions [4]. Also, the intensities of the 533·8 nm and the 540·7 nm lines are observed to be of the same order in the experiments of Berezin and Yanovskaya [5].

The 533·8 nm line would appear to be similar to the 606·89 nm line ($6p'\,^3F_2$–$6s'\,^3D_1$), which has an upper level from which laser transitions are observed (567·8, 703·2, 651·6 nm), and a lower level common to the other laser transitions (576·0 and 658·5 nm), and yet does not show laser action.

Both 533·8 nm and 606·9 nm lines have been shown by Tolansky [6] to possess two almost equal intensity components in their wide hyperfine structure. Jenson and Fowles [7] have reported laser action on only the strongest component

of the many hyperfine components of the lines they have examined (540·7, 567·8, 576·0, 612·7, 658·5 and 703·2 nm).

Other I II levels close to the He^+ ground state level possess direct (ultra-violet) transitions to the iodine ion ground state, so large populations would not be expected in these levels.

Although it is probable that the helium ion plays a part in populating the upper levels of ionized iodine, just as it does in the helium-mercury ion laser [8], it is likely that direct electronic excitation plays an important role. Thus laser action occurs at 562·5 nm ($6p\,^3P_2$–$6s\,^3S_1$) and at 690·4 nm [9] in neon–iodine mixtures.

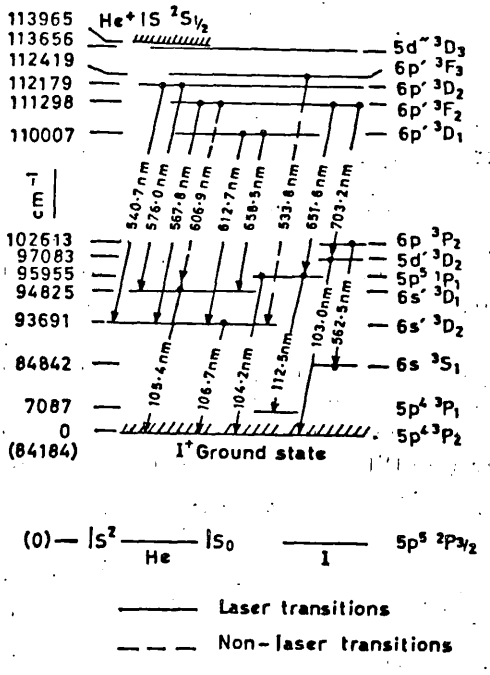

Partial energy level diagram showing laser transitions in ionized iodine.

The 562·5 nm line of ionized iodine corresponds to the isoelectronic laser transition in Xe III at 378·0 nm, and to analogous laser transitions in argon, fluorine and bromine together with the 521·8 nm ($4p\,^3P_2$–$4s\,^3S_1$) transition (cw) in ionized chlorine.

The regularity with which these p–s transitions occur arises from the high probability of electron collision excitation from the ground state to p-levels, from which direct transitions to the ion ground state are forbidden, and the low probability of direct excitation to the s-levels.

Work is currently in progress to determine the large cross section occurring in the helium ion-atom resonant collision process, in which energy discrepancies of more than the accepted few kT are involved [10].

References

[1] Fowles, G. R., and Jenson, R. C., 1964, *Appl. Optics*, **3**, 10, 1191.
[2] Fowles, G. R., and Jenson, R. C., 1964, *Proc. IEEE*, **52**, 851.
[3] Martin, W. C., and Corliss, C. H., 1960, *J. Res. nat. Bur. Stand.* A, **54**, 443.
[4] McFarlane, R. A., 1964, *Appl. Optics*, **3**, 1196.
[5] Berezin, I. A., and Yanovskaya, G. N., 1963, *Opt. Spectrosc.*, **14**, 1, 11.
[6] Tolansky, S., 1935, *Proc. roy. Soc.* A, **149**, 269.
[7] Fowles, G. R., and Jenson, R. C., 1965, *Phys. Rev. Letters*, **14**, 10, 347.
[8] Dyson, D. J., 1965, *Nature, Lond.*, **207**, 361.
[9] Jenson, R. C., and Fowles, G. R., 1964, *Proc. IEEE*, **52**, 1350.
[10] Mott, N. R., and Massey, H. S. W., 1952, *The Theory of Atomic Collisions* (Oxford University Press).

APPENDIX C.

OPTICA ACTA, 1966, VOL. 13, NO. 3, 0-000

Laser oscillation on hyperfine transitions in ionized iodine

C. S. WILLETT and O. S. HEAVENS

Department of Physics, University of York, York, England

(*Received* 4 *July* 1966)

In previous studies of laser action in ionized iodine [1], oscillation has been observed on only one component of a set of hyperfine transitions. In the experiments reported here, simultaneous oscillation on several hyperfine components was obtained. The following transitions were examined:

Transition	*Wavelength* (nm)
$5d\,^3D_1$–$6p'\,^3F_2$	521·6
$6s'\,^3D_2$–$6p'\,^3D_2$	540·7
$6s'\,^3D_2$–$6p'\,^3F_2$	567·8
$6s'\,^3D_1$–$6p'\,^3D_2$	576·0
$6s'\,^3D_1$–$6p'\,^3F_2$	606·9
$6s'\,^3D_2$–$6p'\,^3D_1$	612·7
$5p^5\,^1P_1$–$6p'\,^3F_2$	651·6
$6s'\,^3D_1$–$6p'\,^3D_1$	658·5

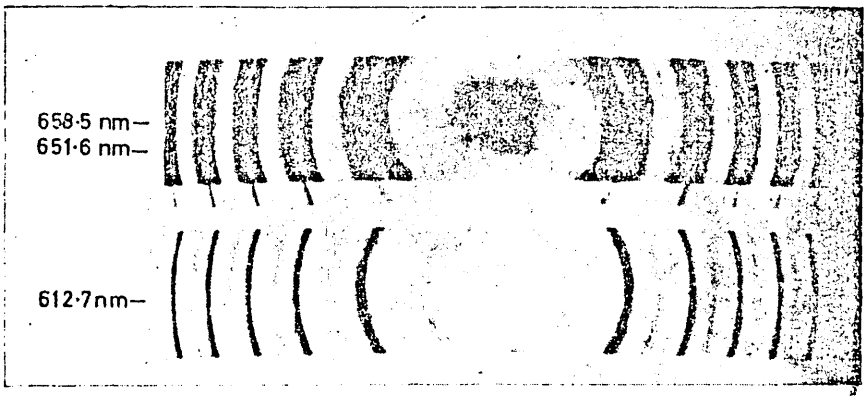

Figure 1. Fabry–Perot fringes on dispersed part-spectrum of ionized iodine laser lines. Etalon spacer 10·12 mm.

Laser oscillation was observed in a cavity supporting multi-wavelength oscillation on the two strongest hyperfine components, classified by Murakawa [2] and Tolansky [3], of the lines 567·8, 576·0, 612·7 nm, whilst oscillation occurred on three hyperfine transitions at 658·5 nm.

The laser was operated in a near confocal arrangement using pairs of dielectric-coated mirrors of 1m radius of curvature, (reflectivity peaked at 632·8 and 500·0 nm), at a separation of 140 cm.

The active plasma length was approximately 1 m, and the bore of the discharge tube was 2 cm. The discharge was excited by means of a pulse modulator discharging a 0·0033 μF capacitor through a 4 : 1 pulse transformer, at an input voltage of about 3 kv as previously described [4]. The initial vapour pressure of iodine, prior to close-off of the discharge tube was 0·1–0·2 torr, with helium added to about 5 torr. To obtain laser action on the hyperfine components it was found necessary to maintain the initial iodine vapour pressure, and to maintain a discharge having a part molecular spectrum appearance.

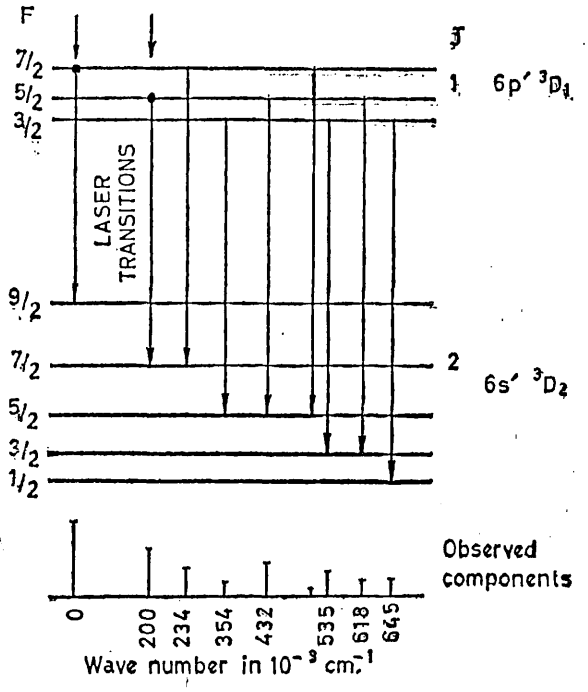

Figure 2. Transition diagram for the iodine line at 612·7 nm. The height of a line indicates its relative intensity.

Laser oscillation was observed on the following hyperfine components of the lines:

(1) 567·8 nm (i) F 9/2–9/2 strongest component.
(ii) F 5/2–3/2, with a separation of 324×10^{-3} cm^{-1}.

(2) 576·0 nm On two components having a separation of 100×10^{-3} cm^{-1}.

(3) 612·7 nm (i) F 7/2–9/2 strongest component.
(ii) F 5/2–7/2, with a separation of 200×10^{-3} cm^{-1}.

(4) 658·5 nm On three components, with separation from the strongest, of 130×10^{-3} cm^{-1}, and 210×10^{-3} cm^{-1}.

Figure 1 shows the dispersed laser lines 658·5, 651·6 and 612·7 nm crossed with Fabry–Perot fringes. Laser oscillation on hyperfine components is made evident by the clear doubling of the fringes at 612·7 nm; and three components at 658·5 nm by the triple structure. Also partly shown is the doubly forbidden laser transition 651·6 nm ($5p^5\,{}^1P_1$–$6p'\,{}^3F_2$).

Figure 2 gives the transition diagram for the line 612·7 nm, showing the laser and non laser transitions, together with observed relative intensities [3].

Figure 3 shows a similar transition diagram for the line 567·8 nm (after Murakawa [5]).

The use of the prism wavelength selection technique for suppressing transitions competing for upper level population, [6] resulted in no further hyperfine transitions, but enabled laser oscillation at 606·9 nm ($6s'^3D_1$–$6p'^3F_2$), previously unreported, to be obtained. This line has both upper and lower levels common to other laser transitions.

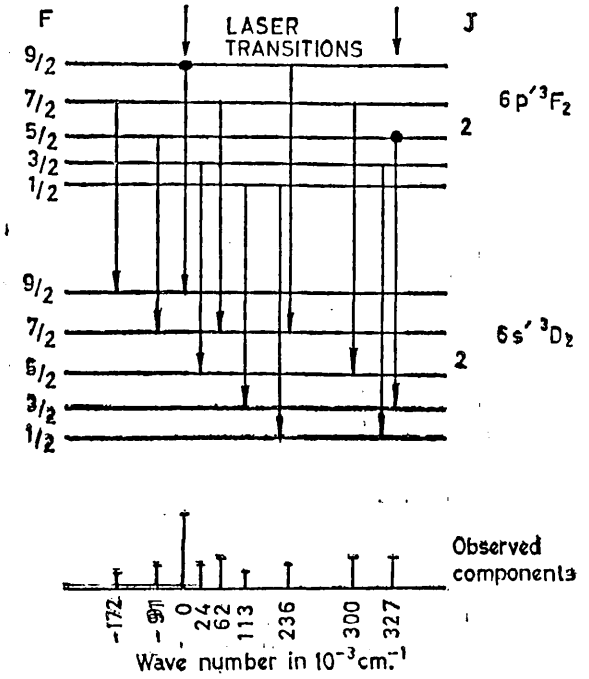

Figure 3. Transition diagram for the iodine line at 567·8 nm. (after Murakawa [5]).

ACKNOWLEDGMENTS

It is a pleasure to acknowledge the competent technical assistance given by J. Clarke in this work, and the provision of excellent silica/glass blowing services by B. Davis and S. Moehr of this University.

REFERENCES

[1] FOWLES, G. R., and JENSON, R. C., 1965, *Phys. Rev. Letters*, **14**, 10, 347.
[2] MURAKAWA, K., 1938, *Z. Physik.*, **109**, 162.
[3] TOLANSKY, S., 1936, *Proc. phys. Soc. Lond.*, **48**, 49.
[4] HEAVENS, O. S., and WILLETT, C. S., 0000, *Opt. Acta* (In press).
[5] MURAKAWA, K., 1936, *Nature, Lond.*, **137**, 1030.
[6] WHITE, A. D., 1964, *Appl. Optics*, **3**, 431.

APPENDIX D.

"Notes and Lines" (I.E.E.E. J. Quantum Electronics, Jan. 1967)

"New laser oscillations in singly ionised iodine"

In addition to lines previously reported, (1), (2), further oscillation has been observed at:- 7138.97 Å ($5d'\ ^3D_3 - 6p'\ ^3D_2$) and at 6825.23 Å ($6s'\ ^3D_3 - 6p'\ ^3F_2$) in singly ionised iodine in a pulsed helium-iodine mixture using prism wavelength selection.

Laser oscillation on hyperfine transitions at 7033.0 Å ($5d'\ ^3D_2 - 6p'\ ^3F_2$) and 6068.9 Å ($6s'\ ^3D_1 - 6p'\ ^3F_2$) in addition to those reported earlier (2) have now also been observed.

Excitation was by means of a pulse modulator discharging a 0.0066μF capacitor through a 4:1 pulse transformer giving pulses up to 16 KV at a few amperes. The optimum pressures in a plasma tube of 1.8 - 2.0 cm bore were: helium, 5 - 6 torr; vapour pressure of iodine approximately 0.2 - 0.5 torr. Higher output was found to result from using wide bore plasma tubes and short, low current pulses as in the helium-mercury laser (3), giving gains on the strong laser lines of the order of 10 per cent/metre.

C. S. Willett
Department of Physics,
University of York, England.

(1) R. C. Jenson and G. R. Fowles; "New Laser Transitions in iodine - Inert Gas Mixtures", Proc. I.E.E.E., Vol. 52, p.1350, (1964).

(2) C. S. Willett and O. S. Heavens; "Laser oscillation on hyperfine transitions in ionised iodine", Optica Acta, Vol. 13, No. 3, (in Press), (1966).

(3) D. J. Dyson; "Mechanism of population inversion at 6149 Å in the mercury ion laser" Nature, Vol. 207, pp. 361-363, 24 July, (1965).